이학박사학위논문

The Sea-Air CO_2 Fluxes in the Korean Marginal Seas and the Western North Pacific

한반도 주변해와 북서태평양의 해양-대기 이산화탄소 교환량에 관한 연구

2012 년 8월

서울대학교 대학원

지구환경과학부

최 상 화

The Sea-Air CO_2 Fluxes in the Korean Marginal Seas and the Western North Pacific

한반도 주변해와 북서태평양의 해양-대기
이산화탄소 교환량에 관한 연구

지도교수 김 경 렬

이 논문을 이학박사학위논문으로 제출함
2012년 4월

서울대학교 대학원
지구환경과학부
최 상 화

최상화의 박사학위논문을 인준함
2012 년 6월

위 원 장 허 여 욱 (인)
부 위 원 장 김 경 렬 (인)
위 원 이 동 섭 (인)
위 원 김 동 선 (인)
위 원 강 동 진 (인)

Abstract

To elucidate the distribution of surface fCO_2, its controlling factors and sea-air CO_2 fluxes in the marginal sea and open ocean, surface fCO_2 data were analyzed in the Ulleung Basin (UB) of the East Sea (ES), northern East China Sea (ECS), and western North Pacific (NP).

Temperature, salinity, chlorophyll *a* (Chl-*a*), and surface CO_2 fugacity (fCO_2) were extensively investigated in the UB of the ES during four cruises. In spring, surface fCO_2 showed large variations ranging from 260 to 356 μatm, which were considerably lower than the atmospheric CO_2 levels. Surface fCO_2 was highest (316 to 409 μatm) in summer. The central part of the study area was undersaturated with respect to atmospheric CO_2, while the coastal and easternmost regions were oversaturated. In autumn, the entire study area was fairly undersaturated with respect to atmospheric CO_2. In winter, surface fCO_2 ranged from 303 to 371 μatm, similar to that in autumn, despite the much lower sea surface temperature. The seasonal variation in surface fCO_2 could not be explained solely by seasonal changes in sea surface temperature and salinity. The vertical mixing, lateral transport, and sea-air CO_2 exchange considerably influenced the seasonal variation in surface fCO_2. The UB of the ES was a sink of atmospheric CO_2 in spring, autumn, and winter, but a weak source of CO_2 to the atmosphere in summer. The annual integrated sea-air CO_2 flux in the UB of the ES was -2.47 ± 1.26 mol C m^{-2}

yr^{-1}, quite similar to a previous estimate (-2.2 mol C m^{-2} yr^{-1}) in the south ES. This indicates that the UB of the ES acts as a strong sink of atmospheric CO_2.

Temperature, salinity, chlorophyll *a*, nitrate, and sea-air differences of CO_2 fugacity (ΔfCO_2) were extensively investigated in the northern ECS during seven research cruises from 2003 to 2009. The ΔfCO_2 showed large intraseasonal variation in spring and summer. In spring, the areal mean ΔfCO_2 was almost two times lower in April 2008 than in May 2004, probably associated with differences in sea surface temperature (SST). In summer, the areal mean ΔfCO_2 in August 2003 was also twice as large as that in July 2006. In addition, ΔfCO_2 exhibited large seasonal variation with positive values in autumn and negative values in other seasons. The positive ΔfCO_2 in autumn was ascribed to vertical mixing with CO_2-enriched subsurface waters and relatively high SST in this season. The annually integrated sea-air CO_2 flux in the northern ECS was -2.2 ± 2.1 mol C m^{-2} yr^{-1}, indicating CO_2 absorption from atmosphere to the sea. The CO_2 influx in the ECS was twice that estimated for continental shelves worldwide, suggesting that the ECS acts as a strong sink of atmospheric CO_2 compared to other continental shelves.

Temperature, salinity, and surface fCO_2 were measured in the western NP during five research cruises from 2006 to 2010. Temporal SST variations were heavily associated with Oceanic Nino Index (ONI). However, ONI was not the immediate cause of temporal variations of surface fCO_2. Up to 65~80% of temporal variations of surface fCO_2 could be explain by thermodynamic changes from SST

and sea surface salinity (SSS) variability in half of all the observations. Biological activity might affect to reduce the surface fCO_2 in May 2010, while it might rarely in September 2006 and June 2009. Though mixed layer depth (MLD) was deepening with reversal ONI, deep MLD could not lead to increase surface fCO_2. Sea-air CO_2 flux (over 0.5 mmol C m^{-2} day^{-1}) induced decrements the variability of surface fCO_2. The North Equatorial Current (NEC), southern area, acted as a source of CO_2 to the atmosphere from May to September. In October, the NEC acted as a CO_2 sink. The subtropical gyre, northern area, acted as a CO_2 source from June to September. While it acted as a CO_2 sink in May and October.

The annual CO_2 uptake rate would be 3.15 x 10^{-3} Pg C yr^{-1} and 2.96 x 10^{-3} Pg C yr^{-1} in the UB of the ES and the northern ECS, respectively. Those were 0.22% and 0.21% of annual global carbon uptake rate, while those were 0.033% and 0.034% of global ocean area. In the western NP, the annual CO_2 uptake rate would be 8.03 x 10^{-2} Pg C yr^{-1}, 5.6% of global carbon uptake rate whereas 8.1% of area (Takahashi *et al*., 2009). The Korean marginal seas, the UB of the ES and northern ECS, are powerful atmospheric CO_2 sinks about seven times as strong as open ocean, the western NP.

Keywords: surface fCO_2, sea-air CO_2 flux, seasonal variations, marginal sea, East Sea, East China Sea, North Pacific

Contents

List of Tables

List of Figures

Chapter 1 Introduction

Ocean is one of the biggest reservoirs in the global carbon cycle (Sarmiento and Gruber, 2002; Sabine *et al*., 2004). Ocean is the largest mobile carbon inventory and also absorbs about one third of anthropogenic carbon emitted to the atmosphere by human activities (IPCC, 2007). IPCC (2007) reports that anthropogenic carbon emissions by human activities were 5.4 Pg C yr^{-1} in 1980s, 6.4 ± 0.4 Pg C yr^{-1} in 1990s, and 7.2 ± 0.3 Pg C yr^{-1} from 2000 to 2005. CO_2 emitted to the atmosphere from 2000 to 2005 4.1 ± 0.1 Pg C yr^{-1} contributed to increase the atmospheric CO_2 concentrations, and then 2.2 ± 0.5 Pg C yr^{-1}, about 30% of the emitted anthropogenic CO_2, was absorbed to the ocean. Ocean exchanges carbon with other carbon reservoirs through broad variety of interfaces and ways. Though ocean is described as a simple box in the illustrations of global carbon cycle (Fig. 1.1), it exists as diverse sizes and depths in various locations from equatorial to polar region. CO_2 in the atmosphere penetrates the sea-air interface through gas exchange and it dissolves and forms carbonate species in seawater. The amount of CO_2 dissolved in seawater was determined by the difference of CO_2 concentration, i.e. partial pressure, between overlying atmosphere and surface seawater, solubility of CO_2, and gas exchange coefficient of CO_2. The solubility of CO_2 in seawater is a function of seawater temperature and gas exchange coefficient of CO_2 is that of seawater temperature and wind speed. While atmosphere, i.e.

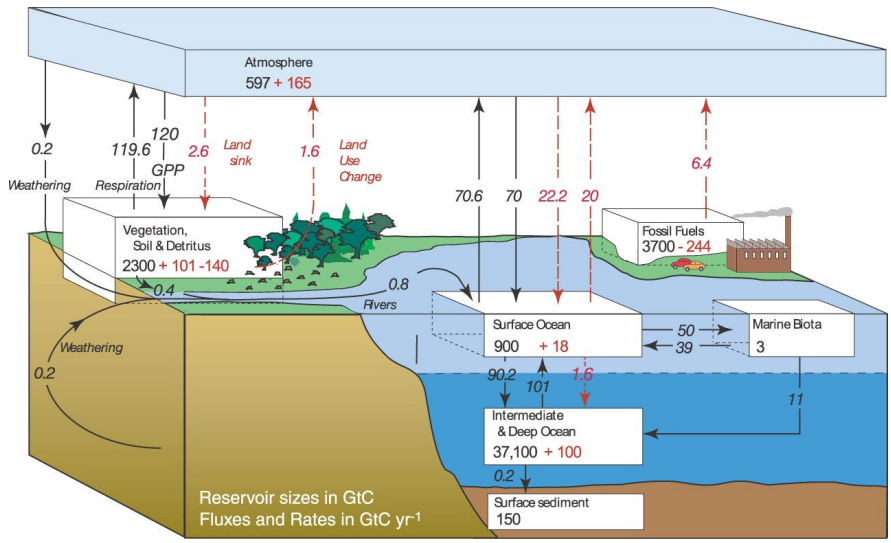

Figure 1.1. The global carbon cycle for the 1990s, showing the main annual fluxes in Gt C yr^{-1}: pre-industrial 'natural' fluxes in solid line and 'anthropogenic' fluxes in dashed line (from IPCC, 2007).

troposphere, is relatively well-mixed, partial pressure of CO_2 in surface seawater, surface pCO_2, shows various temporal and spatial variability (Fushimi, 1987; Watson *et al*., 1991; Takahashi *et al*., 1993; Inoue *et al*., 1995; Landrum *et al*., 1996; Goyet and Peltzer, 1997; Watai *et al*., 1999; Ishii *et al*., 2001). The variations of sea-air CO_2 exchanges were originated from the spatial distribution of surface pCO_2. Oceanic environments determined distributions of carbon and fluxes through the interface.

Marginal seas play important roles in the global carbon cycle, with those having high biological activities serving as annual net sinks (Borges *et al*., 2005; Omar *et al*., 2007; Chen and Borges, 2009). However, while marginal seas at temperate and high latitudes act as net sinks, those at tropical and subtropical latitudes may act as net sources (Borges *et al*., 2005; Chen and Borges, 2009). Previous studies on the sea-air CO_2 fluxes of marginal seas have reported large variability ranging from 0.1~0.45 Pg C yr^{-1}, which is attributable to the complex and heterogeneous ecosystems and hydrodynamics of these seas (Liu *et al*., 2000; Thomas *et al*., 2004; Borges *et al*., 2005; Chen and Borges, 2009). For the same reason, estimates of sea-air CO_2 flux for marginal seas still contain much uncertainty. Therefore, spatially and temporally high-resolution CO_2 measurements in marginal seas are essential for improving estimates of global sea-air CO_2 fluxes.

In case of Korean waters, relatively few studies have investigated sea-air CO_2 fluxes in the southwestern part of the East Sea (ES), the Ulleung Basin (UB) (Oh, 1998; Kang, 1999; Choi *et al*., 2011). Oh (1998) and Kang (1999) estimated

daily and monthly averaged sea-air CO_2 flux in the ES using a multifactor mathematical model tuned by observational data in summer and winter. Choi *et al*. (2011) reported the surface pCO_2 distribution and sea-air CO_2 flux in the UB of the ES in the summer of 2005. Until now, however, seasonal observations of sea-air CO_2 fluxes have not been performed in the ES.

The spatial distribution and seasonal variations of surface pCO_2 in the UB of the ES were investigated based on data obtained in April 2006, August 2007, and February and October 2008. Here we evaluate the major physical and biological factors controlling the distribution of surface pCO_2 in the study area, and estimate the sea-air CO_2 fluxes for four seasonal surveys.

Although continental margins cover only about 7% of the world's ocean surface area, they play a major role in oceanic carbon cycling, receiving larger nutrient supplies from river and sustaining higher biological production because of coastal upwelling (Chen and Borges, 2009). The complex and dynamic nature of the continental margin produces highly variable sea-air CO_2 fluxes. Recently, Chen and Borges (2009) synthesized worldwide measurements of pCO_2 at the continental shelves and suggested that the temperate and high-latitude shelves are undersaturated with respect to atmospheric CO_2 in all seasons, while low-latitude shelves are oversaturated. On the basis of pCO_2 data obtained at 60 continental shelves around the world, they also concluded that continental shelves indeed act as a sink for atmospheric CO_2. However, large ranges of error are involved in estimating the role of coastal carbon uptake in the global carbon cycle due to the

complexity of coastal ecosystems and hydrodynamics (Zhai *et al*., 2005; Shim *et al*., 2007; Chen and Borges, 2009; Zhai and Dai, 2009). Therefore, spatially and temporally high-resolution pCO_2 measurements are needed to obtain precise estimates of sea-air CO_2 fluxes at the continental margin.

Measurements of the surface pCO_2 and other carbon parameters have been carried out in the East China Sea (ECS) since the late 1990s (Tsunogai *et al*., 1997, 1999; Peng *et al*., 1999; Wang *et al*., 2000; Shim *et al*., 2007; Chou *et al*., 2009; Zhai and Dai, 2009). Tsunogai *et al*. (1999) measured the surface CO_2 fugacity in the central ECS during five cruises in various seasons and suggested that the ECS absorbed atmospheric CO_2 at a rate of 2.9 mol C m^{-2} yr^{-1}. Shim *et al*. (2007) observed the surface pCO_2 in the northern ECS during four cruises in three seasons and estimated sea-air CO_2 flux to be -0.87 mol C m^{-2} yr^{-1} based on Wanninkhof's (1992) equation; this estimate was more than three times lower than the estimate of Tsunogai *et al*. (1999). In addition, Zhai and Dai (2009) examined surface pCO_2 and dissolved oxygen in the outer Changjiang Estuary during seven field surveys and estimated the integrated sea-air CO_2 flux to be -1.9 mol C m^{-2} yr^{-1}, with CO_2 influx more than double the estimate of Shim *et al*. (2007). The results of previous studies suggest that sea-air CO_2 fluxes are fairly variable in the different regimes of the ECS. Because the ECS is hydraulically dynamic and complex due to influences of the Kuroshio and large river discharge from the Changjiang, high-resolution temporal and spatial measurements are essential to obtain unbiased estimates of sea-air CO_2 fluxes in the ECS.

Surface pCO_2 was measured during seven research cruises in the northern ECS in various seasons from 2003 to 2009. The obtained data may provide a better estimate of sea-air CO_2 fluxes than previous estimates. The goals of this study were to monitor sea-air differences of pCO_2 (ΔpCO_2), to elucidate intra- and interseasonal variations of ΔpCO_2, and to provide an unbiased estimate of sea-air CO_2 fluxes in the northern ECS.

Measurements of oceanic CO_2 in the North Pacific (NP) started in late 1960s (Keeling, 1968). In the western NP, observations actively carried out from 1980s, then it was reported that low-latitude tropic areas acted as a weak CO_2 source to the atmosphere with small seasonal variations of sea surface temperature (SST) and sea surface salinity (SSS) (Fushimi, 1987; Inoue *et al*., 1995; Ishii *et al*., 2001). While mid-latitude temperate areas where include the Kuroshio were reported that it acted as CO_2 sinks in winter and sources in summer due to the large seasonality on SST and SSS (Inoue *et al*., 1995; Watai *et al*., 1999; Ishii *et al*., 2001). Though lots of research results such as variations of surface pCO_2 and its controlling processes, sea-air CO_2 fluxes, etc. have been reported through various observations, our understandings about the nature is still incomplete because the nature is in a state of flux. Sarmiento and Gruber (2002) reported that carbon uptake rates by ocean were reduced during ENSO event from 1960s to 1990s and vice versa after 1990s (Fig. 1.2). Yeh *et al*. (2009) reported that CP-El Nino (the central Pacific El Nino) has become more frequent rather than EP-El Nino (the canonical eastern Pacific El Nino) during the late twentieth century. The carbon uptake rates by

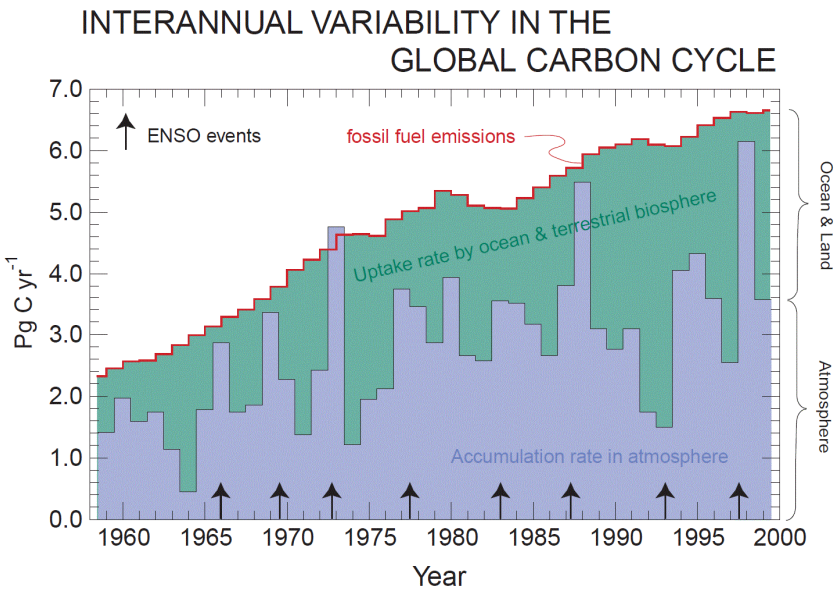

Figure 1.2. Growth rate of carbon reservoirs. The blue area represents the yearly accumulation rate of atmospheric carbon dioxide. Over the same period, the red line represents fossil-fuel emissions. Net uptake by the ocean or terrestrial biosphere (green area) must account for the difference. Higher growth rates generally appear to be associated with El Nino episodes (arrow), the exception being since the early 1990s (from Sarmiento and Gruber, 2002).

ocean might be changed in response to the shift of the El Nino mode. Successive observations on the sea-air CO_2 fluxes were needed in the North Pacific to follow up the natural variability.

Surface pCO_2, SST and SSS were measured during five research cruises in the western NP from 2006 to 2010. The obtained data may provide a better understanding of temporal variations of surface pCO_2 in the western NP. The purposes of these investigations were to elucidate the major factors controlling the surface pCO_2 in the western NP, and to estimate the sea-air CO_2 fluxes for five observations.

As previously mentioned above, oceanic environments are various and then distributions of surface pCO_2 and sea-air CO_2 fluxes also show wide variability according to its environments. The ECS is one of the most productive continental shelf seas. The ES is one of typical marginal seas called “miniature ocean”. The NP is a part of the largest open ocean on earth. This study provides an overview of seasonal or temporal variation of surface pCO_2, its controlling processes and sea-air CO_2 fluxes in three different types of seas; the UB of ES, the northern ECS, and the western NP.

Chapter 2 Materials and methods

2.1 Study area

2.1.1 The Ulleung Basin of the East Sea

The ES is a semi-enclosed marginal sea surrounded by Korea, Japan, and Russia. It consists of three major basins: the Japan, Yamato, and Ulleung Basins. The average depth of the ES is 1,740 m, and it connects to the western NP through four shallow straits with depths less than 140 m. Because of these strait depths, subsurface waters cannot be directly exchanged between the ES and NP. Deep cold water forms below the thermocline (located at 100~200 m) in the ES and has relatively uniform hydrographic properties. The thermohaline circulation and biogeochemical cycle of the ES are independent of those in the open ocean, and the sea has thus been called a "miniature ocean." The ES offers good opportunities to investigate oceanic processes because of its relatively small spatial scale, as well as its relatively short turnover time, estimated to be less than 100 years (Min *et al*., 2002; Hahm and Kim, 2008). Due to high biological productivity and accumulation of anthropogenic CO_2 (Yamada *et al*., 2005; Park *et al*., 2006; Yoo and Park 2009), the ES could be an important marginal sea in which to study oceanic carbon cycles.

2.1.2 The northern East China Sea

The ECS is the first and third largest marginal sea in the western NP and world, respectively, and includes a large area of shallow continental shelf about 0.5×10^6 km^2 with enormous inputs of freshwater and terrestrial nutrients. The ECS is bounded to the east by the Kuroshio, and there is extensive exchange between the ECS and the Kuroshio through frontal processes (Chern *et al*., 1990; Chen *et al*., 1995). The sea is bounded to the west by continental China and receives tremendous river runoff from the Changjiang, which has an annual mean discharge of 920 km^3 yr^{-1} (Yang *et al*., 2006). An imaginary east-west line connecting Jeju Island with the mainland of China separates the East China sea from the Yellow Sea to its north. The runoff from the Changjiang shows large seasonal variation, with a maximum in summer and a minimum in winter (Bearsley *et al*., 1985). The river discharge forms the Changjiang Diluted Water (CDW) by mixing with saline ambient water. In winter, the CDW flows southward along the Chinese coast in a narrow band because of the low river discharge and the prevailing northeasterly wind. In summer, however, the CDW propagates across the shelf because of the combined effect of high discharge and the prevailing southerly wind. During this time, the CDW covers most of the northern part of the ECS (Le, 1988; Hu, 1994; Su and Weng, 1994). The ECS is one of the most productive marginal seas in the world due to the large nutrient supply from the Changjiang and coastal mixing

(Wong *et al*., 2000; Gong *et al*., 2003). In the Chinese coastal areas near the Changjiang, surface waters are nutrient rich and therefore have high concentrations of chlorophyll *a* (Chl-*a*) and high primary production rates. Farther from the coastal area, Chl-*a* and primary production levels gradually decrease because of limited nutrient supplies.

2.1.3 The western North Pacific

The Pacific is the deepest (average depth 3,940 m; cf., Atlantic, 3,310 m; Indian 3,840 m), the coldest (average temperature 3.14^{o}C; cf., Atlantic 3.99^{o}C; Indian 3.88^{o}C), and by far the largest (180x10^{6} km^{2}; cf., Atlantic 107x10^{6} km^{2}; Indian 74x10^{6} km^{2}) of the oceans (Sverdrup and Armbrust, 2008). NP affects the Korean waters by warm Kuroshio originated from the NP, flows through the southern part of Korea Peninsula. In the NP, the ocean surface in equatorial region is dominated by the westerly flow of water in the North Equatorial Current (NEC), caused primarily by the Trades. The NEC separated by a narrow current flowing eastward, a countercurrent, the Subtropical Countercurrent (STCC). Associated with NEC is a current gyre, i.e. subtropical gyre. Subtropical gyre is elongated east-west and lie primarily in the subtropical regions, centered around 30^{o}N. In addition to equatorial currents, the current gyre includes a major east-west current flowing in a direction opposite to the equatorial current. The extension of NP subtropical gyre current is

the Kuroshio. In the subpolar and polar regions there is small current gyre, circulated opposite to the subtropical gyres. NP is one of oligotrophic regions with low productivity (about 50 g C m^{-2} yr^{-1}; Gregg *et al*., 2003) because of the nutrients limitation, except continental boundaries.

2.2 Observations

2.2.1 The Ulleung Basin of the East Sea

The study area was the UB of the ES (35°~37°N, 129°~132°E, Fig. 2.1). The data were obtained during four seasonal cruises on board the R/V *Eardo* in spring (15~16 April 2006), summer (5~9 August 2007), autumn (9~14 October 2008), and winter (20~23 February 2008).

2.2.2 The northern East China Sea

Measurements for this area were performed during seven cruises of the R/V *Eardo* in spring (29 April~8 May 2004, 14~24 April 2008), summer (26 August~3 September 2003, 19~25 July 2006), autumn (3~8 October 2004, 1~8 November 2005), and winter (16~22 February 2009). The study area was the northern ECS

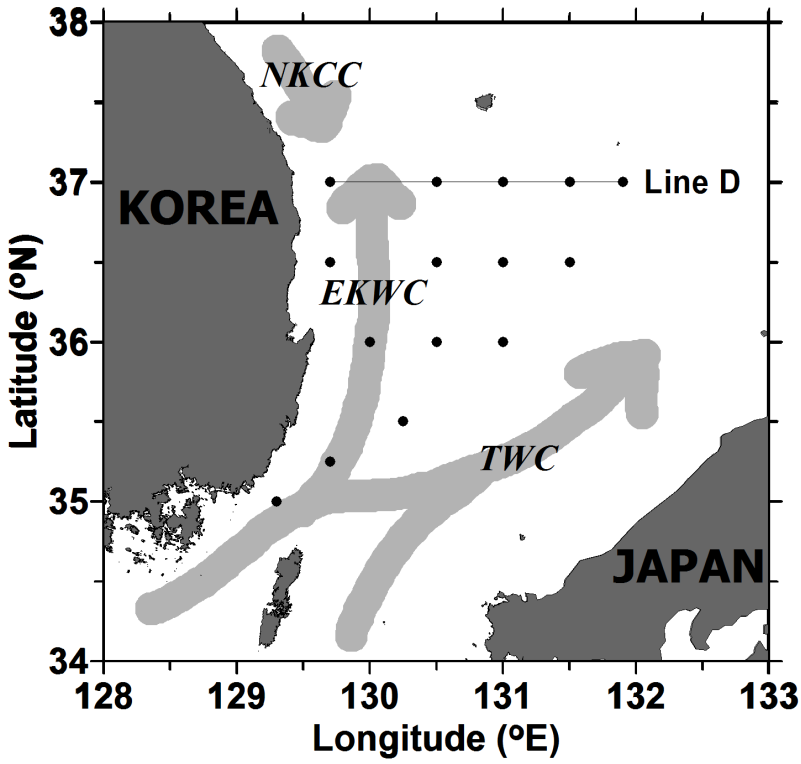

Figure 2.1. Study area and locations of sampling stations in the Ulleung Basin of the East Sea. TWC indicates the Tsushima Warm Current, EKWC East Korea Warm Current, and NKCC North Korea Cold Current.

surrounding Cheju Island (31°30′~34°0′N, 124°0′~127°30′E) and was divided into eastern and western parts on the basis of the thermohaline front located around 125~126.5°E (Fig. 2.2), which formed between the TWC water and coastal water (Hickox *et al*., 2000). The eastern part of the study area with properties of the TWC had warmer temperatures and higher salinities than the western part.

2.2.3 The western North Pacific

Measurements for this area were performed during five cruises of the R/V *Onnuri* in May-June (10~20 June 2008, 25 June~2 July 2009 and 26 May~7 June 2010) and September-October (12~26 September 2006, 28 September~12 October 2007). The study area was the western NP (10°~25°N, 124°0′~151°15′E) and was divided into southern and northern parts on the basis of surface currents, NEC and STCC, the boundaries of these were located around 16~20°N (Fig. 2.3).

2.3 Analytical methods

2.3.1 Underway system

Continuous measurements were made of pCO_2, temperature, and salinity in the

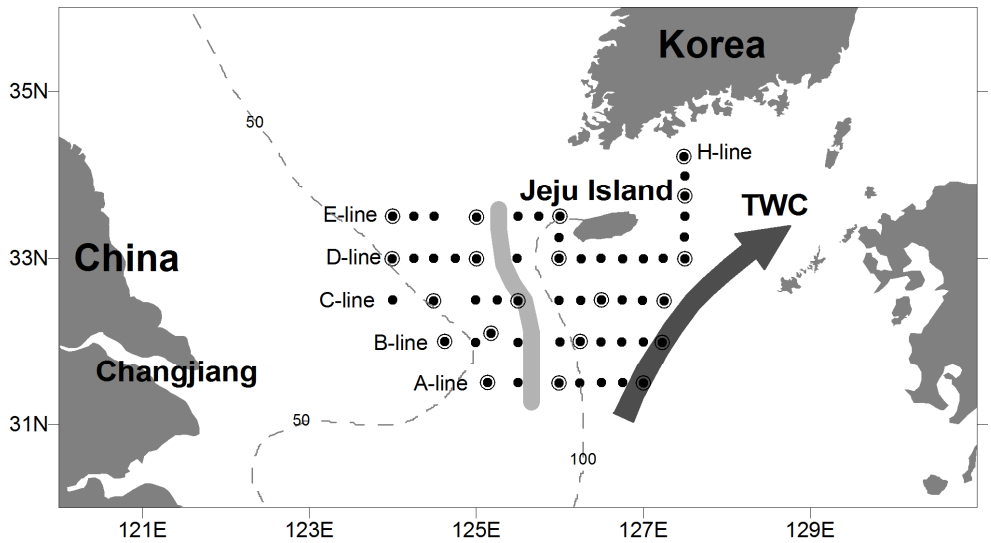

Figure 2.2. Study area and locations of sampling stations in the northern East China Sea. The thick gray line indicates a thermohaline front. TWC: Tsushima Warm Current.

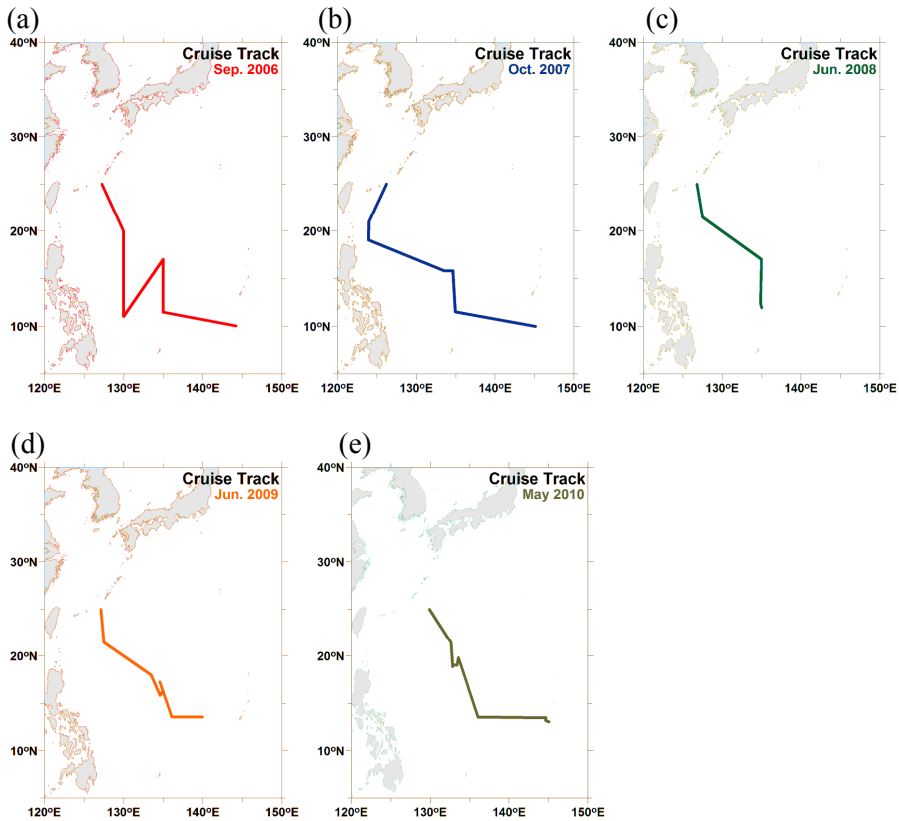

Figure 2.3. Study area and cruise tracks in the western North Pacific. In (a) September 2006, (b) October 2007, (c) June 2008, (d) June 2009, and (e) May 2010.

surface seawater, which was pumped aboard from a 5-m depth during the surveys. Surface pCO_2 and atmospheric CO_2 were determined every minute and every hour, respectively, using an underway CO_2 measurement system consisting of a flowing pCO_2 system (Fig. 2.4) similar to those designed by Wanninkhof and Toning (1993) and Weiss (1981), and a spiral spray-type equilibrator (Ho *et al*., 1997). The seawater pumped into ca. 4 L equilibrator, an upper half of which was headspace, with a flow rate of 6 L min^{-1}. The equilibrated air in the headspace circulated with a flow rate of 50 mL min^{-1}, which were same rates with all measurements, i.e. equilibrated air, marine air and standard gases, in a closed loop between equilibrator and detector. A non-dispersive infrared CO_2 and H_2O analyzer (model 6262, LI-COR, Lincoln, NE, USA) measured the fraction of CO_2 (pCO_2) in the equilibrated air sample. CO_2 mole fraction in dry air at 1-atm pressure were provided by LI-COR instrument through internal processes to correct the moisture interferences using measurements from the water channel of the LI-COR instrument and a connected pressure sensor. Because partial pressure is a concept appropriate for ideal gases and CO_2 is not an ideal gas, pCO_2 value was converted to fugacity of CO_2, fCO_2, by Weiss (1974). The system was calibrated every 12 hours with working standard gases (~250, 380, and 450 ppm CO_2 in the air, Korea Industrial Gases, Ltd., Shihung City, Korea), which were subsequently calibrated with the National Oceanic and Atmospheric Administration (NOAA) and World Meteorological Organization (WMO). Consistency between pre- and post-cruise analyses for the working standard gases was 1 μatm. Repeated analyses also

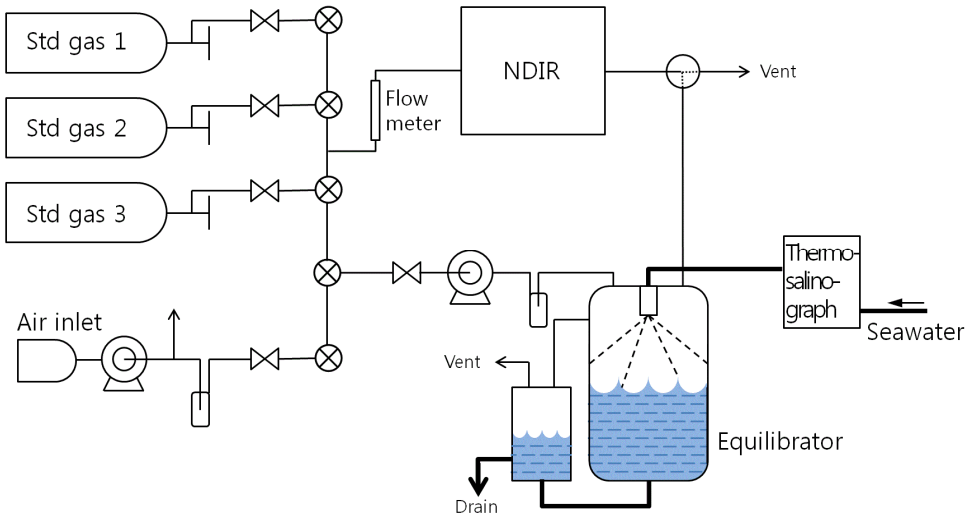

Figure 2.4. The schematic diagram of CO_2 measurements underway system. fCO_2 of surface seawater and marine air is measured with NDIR, LI-6262, and sea surface temperature and salinity are measured with thermosalinograph, SBE45.

indicated that the fCO_2 measurement had a precision of ± 1 μatm. Water temperatures in the equilibrator were warmer by 0.3~1.0°C than surface water temperatures measured by conductivity–temperature–depth (CTD) sensors at hydrocasting stations. The temperature difference between the equilibrator and the *in situ* temperatures was corrected using the following equation proposed by Takahashi *et al*. (1993): $(\delta pCO_2/\delta T)/pCO_2=0.0423\ °C^{-1}$.

2.3.2 Water sampling and analyses

Vertical profiles of temperature, salinity, and density were measured with a SeaBird conductivity-temperature-depth profiler (CTD; SBE 9/11 plus, SeaBird Inc., Bellevue, WA, USA). Seawater samples for nitrate and Chl-*a* analyses were collected using a Rosette sampler with 10-L Niskin bottles. Water samples for nitrate analysis were filtered through GF/F filter paper (25 mm, Whatman, Middlesex, U.K.), placed in acid-cleaned polyethylene bottles, and poisoned with $HgCl_2$, which did not have any effect on the determination of nitrate concentration (Kattner, 1999). Nitrate concentrations were measured using a flow injection autoanalyzer (model QuikChem AE, Lachat, Loveland, CO, USA) and standard colorimetric procedures (Strickland and Parsons, 1972) and calibrated using brine standard solutions (CSK Standard Solutions, Wako Pure Chemical Industries, Osaka, Japan). Duplicate analyses suggested that the precision of the nitrate

measurements was 3%. Water samples for Chl-*a* analysis were filtered through GF/F filter paper (47 mm, Whatman); the filters were then immediately frozen using liquid nitrogen. The Chl-*a* concentration in the extracted filtrate mixed with 90% acetone for 24 h was determined using a Turner-designed fluorometer (10-006R, Turner BioSystems, Sunnyvale, CA, USA).

2.4 Calculation of the thermodynamic effect of T, S changes on fCO_2

CO_2 is exchanged between atmosphere and ocean via equilibration of CO_2 gas and dissolved CO_2. Dissolved CO_2 is part of the carbonate system in seawater that includes bicarbonate, HCO_3^-, and carbonate ion, CO_3^{2-}. Proportions among carbon species in seawater were determined by thermodynamic equilibria such as Henry's law with solubility coefficient of CO_2 in seawater and carbonic acid dissociation with first and second dissociation constants. Solubility coefficient and equilibrium constants depend on temperature, pressure and salinity. Surface fCO_2 can change in two ways: first, thermodynamic change by variations of temperature and salinity within a same total amount of carbon dioxide and second, actual changes in total amount of carbon dioxide by seawater mixing, gas exchange, and biological uptake, etc. Thus surface fCO_2 determined as a function of thermodynamic factors (temperature and salinity) and non-thermodynamic factors (dissolved inorganic

carbon (DIC), total alkalinity (TA), vertical mixing, lateral mixing, biological uptake, and sea-air CO_2 exchange, etc.). fCO_2 is expressed approximately as

$$fCO_2 \approx NfCO_{2ave}(T_{ave}, S_{ave}) + \Delta fCO_2 (T_{obs}-T_{ave}) + \Delta fCO_2 (S_{obs}-S_{ave}) + \Delta NfCO_2 (T_{ave}, S_{ave})$$

where $NfCO_{2ave}$ (T_{ave}, S_{ave}) represents the mean temperature- and salinity-normalized fCO_2, ΔfCO_2 (T_{obs}-T_{ave}) the thermodynamic effect of SST change on fCO_2, ΔfCO_2 (S_{obs}-S_{ave}) the thermodynamic effect of salinity change on fCO_2, and $\Delta NfCO_2$ (T_{ave}, S_{ave}) the change in the normalized fCO_2 due to the changes in non-thermodynamic effect of changes in DIC, TA, vertical mixing, lateral mixing, biological uptake, and sea-air CO_2 exchange, etc (Choi *et al*, 2012). The value of $\Delta NfCO_2$ (T_{ave}, S_{ave}) is thus obtained from

$$\Delta NfCO_2 (T_{ave}, S_{ave}) \approx fCO_2 - NfCO_{2ave}(T_{ave}, S_{ave}) - \Delta fCO_2 (T_{obs}-T_{ave}) - \Delta fCO_2 (S_{obs}-S_{ave})$$

For the normalization of SST and SSS, we used the fCO_2-SST and fCO_2-SSS relationships of Takahashi *et al*. (1993): $(dfCO_2/dT)/fCO_2 = 0.0423^{o}C^{-1}$, $(dfCO_2/dS)(S/fCO_2) = 0.94$. Thermodynamic effect ratio for spatial distribution ($TER_{spatial}$) of each season is a ratio of sheer fCO_2 change by a thermodynamic effect of SST and SSS variations to total fCO_2 change by thermodynamic and non-thermodynamic effect ($[|\Delta fCO_2 (T_{obs}-T_{ave})| + |\Delta fCO_2 (S_{obs}-S_{ave})|] / [|\Delta fCO_2 (T_{obs}-T_{ave})| + |\Delta fCO_2 (S_{obs}-S_{ave})| + |\Delta NfCO_2 (T_{ave}, S_{ave})|]$) using a seasonal mean of SST

and SSS. The thermodynamic effect ratio for seasonal change ($TER_{seasonal}$) is the same as above using annual mean of SST and SSS instead of seasonal mean.

2.5 Calculation of the sea-air CO_2 flux

The sea-air CO_2 fluxes across the sea-air interface can be calculated based on the equation,

$$F = k \times s \times \Delta fCO_2,$$

where k is the gas transfer velocity (cm h^{-1}), s is the solubility of CO_2 gas in seawater (mol kg^{-1} atm^{-1}; Weiss, 1974), and ΔfCO_2 is the sea-air difference of CO_2 fugacity. A positive flux indicates that the sea is acting as a CO_2 source; a negative flux means that the sea is acting as a CO_2 sink. We adapted the formula for k and the wind speed relationships from Wanninkhof (1992), which is as follows,

$$k = 0.31\ u^2\ (Sc/660)^{-1/2}$$

where u is a wind speed (m sec^{-1}), Sc is a Schmidt number of CO_2, and 660 is the Schmidt number of CO_2 in seawater at 20°C.

Wind speed is the key force driving gas exchange at the sea-air interface.

Here, we used the QuikSCAT wind speed data for the cruise dates, obtained from the Physical Oceanography Distributed Active Archive Center of the Jet Propulsion Laboratory, U.S. National Aeronautics and Space Administration (PO.DAAC, JPL, NASA: http://podaac.jpl.nasa.gov).

Chapter 3 Results

3.1 Distributions of surface fCO_2 in the Ulleung Basin of the East Sea

3.1.1 Surface currents

The UB is located in the southwestern part of the ES. Although the Korea Strait is the only entrance to the UB, several surface currents occur in the basin. The TWC branches from the Kuroshio into the UB and then splits into two or three branches (Chang *et al*., 2002). Especially in summer, because of wet season in this area, the TWC carries both warm, low salinity water originating from the shelf of the ECS and high salinity water of Kuroshio origin (Chang *et al*., 2004). The northward branch along the east coast of Korea is called the East Korean Warm Current (EKWC; Uda, 1934).

HYCOM is a Hybrid Coordinate Ocean Model which provides data-assimilative hybrid isopycnal-sigma-pressure (generalized) ocean modeling results. HYCOM well reproduces past ocean circulations through data-assimilation. Figure 3.1 shows the surface temperature and salinity overlaid with currents for the four survey periods from HYCOM (http://www.hycom.org/dataserver/glb-analysis). In

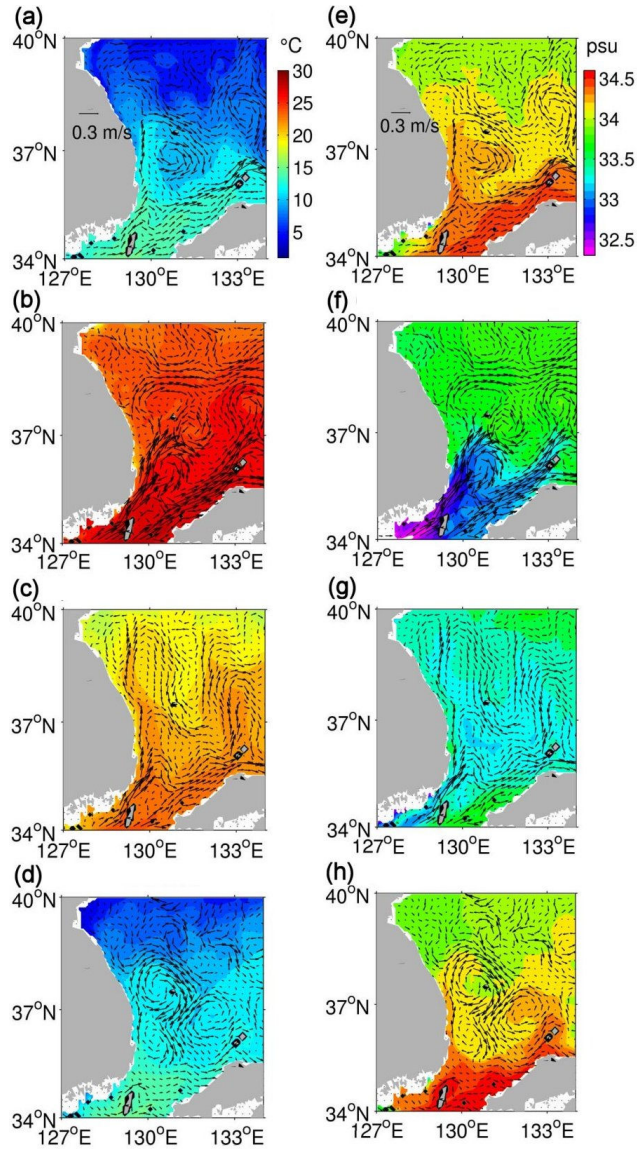

Figure 3.1. Surface distributions of temperature overlaid with surface currents in (a) April 2006, (b) August 2007, (c) October 2008, and (d) February 2008 and salinity overlaid with surface currents in (e) April 2006, (f) August 2007, (g) October 2008, and (h) February 2008 in the Ulleung Basin of the East Sea from HYCOM (HYbrid Coordinate Ocean Model, http://www.hycom.org/dataserver/glb-analysis).

spring (April 2006), the TWC, which had salinity higher than 34.4, passed along the Japanese coast, and there was a distinct anticyclonic eddy with 10°C core temperature and 34.2 salinity in the center of the UB (Figs. 3.1a and e). In summer (August 2007), the TWC transported warm (> 25°C) and less saline (< 33.2) water into the UB through both channels in the Korea/Tsushima Strait (Figs. 3.1b and f). In autumn (October 2008), the TWC became weaker than in summer, and an anticyclonic eddy also became weaker (Figs. 3.1c and g). In winter (February 2008), the surface current through the Korea/Tsushima Strait was the weakest, but an anticyclonic eddy was well developed compared to other seasons (Figs. 3.1d and h). The surface temperature in the UB was warmer in winter than in spring.

3.1.2 Spring observation

The surface distributions of temperature, salinity, fCO_2, and Chl-*a* for the spring cruise are shown in Figure 3.2. In spring (April 2006), surface measurements were conducted in a narrow area covering from 129.5 to 131.5°E along 37°N. Due to the narrow coverage, the SST and SSS were confined to within a narrow range from 9.4 to 11.7°C and from 34.2 to 34.5, respectively (Figs. 3.2a and b). However, surface fCO_2 showed large variations, ranging from 260 to 356 μatm, which were considerably lower than atmospheric CO_2 (376.6 μatm). The thermodynamic effect of SST change on fCO_2, ΔfCO_2 (T_{obs}-T_{ave}), the thermodynamic effect of SSS change

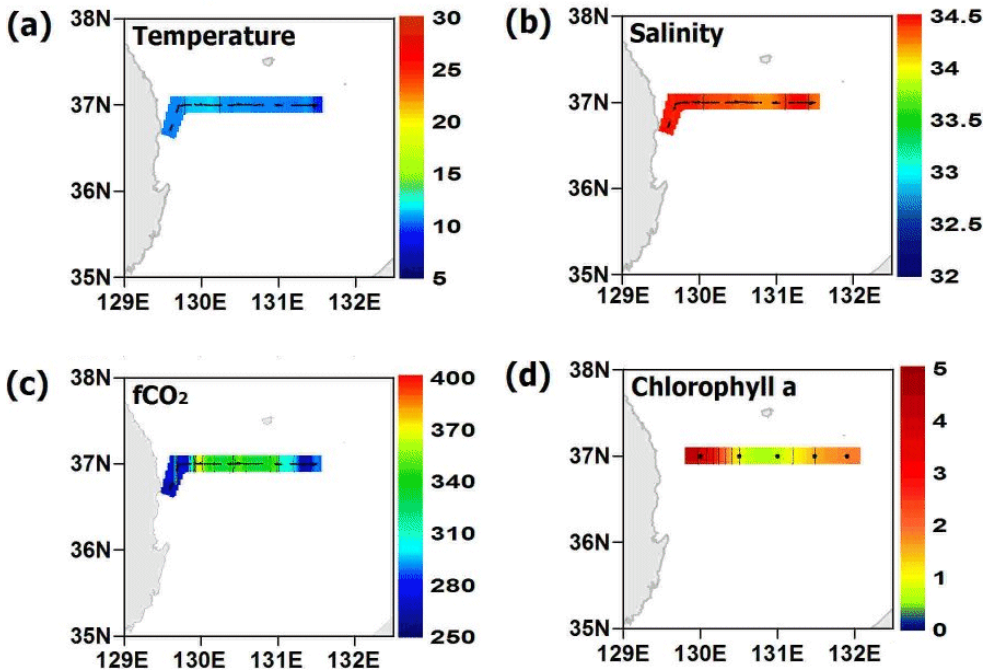

Figure 3.2. Surface distributions of (a) temperature, (b) salinity, (c) fCO_2, and (d) chlorophyll *a* in the Ulleung Basin of the East Sea in April 2006.

on fCO_2, ΔfCO_2 (S_{obs}-S_{ave}), the change in the normalized fCO_2 due to the changes in non-thermodynamic effect of changes in DIC and TA, $\Delta Nf CO_2$ (T_{ave}, S_{ave}), thermodynamic effect ratio for spatial distribution, $TER_{spatial}$, and thermodynamic effect ratio for seasonal distribution, $TER_{seasonal}$ for the spring cruise are shown in Figure 3.3 (Terms are defined in 2.4). ΔfCO_2 (T_{obs}-T_{ave}) and ΔfCO_2 (S_{obs}-S_{ave}) were in small ranges, from -17 to 13 μatm and from -2 to 1 μatm, respectively, whereas $\Delta Nf CO_2$ (T_{ave}, S_{ave}) was a large range, from -57 to 59 μatm (Figs. 3.3a, b and c). Thus, $TER_{spatial}$ was as low as 0.22 ± 0.20, implying that SST and SSS were not the major factors in controlling the spatial distribution of surface fCO_2 in spring (Fig. 3.3d). Among non- thermodynamic factors controlling surface fCO_2, vertical and lateral mixing, and sea-air CO_2 exchange will be discussed in Section 4.1. Lower surface fCO_2 (less than 300 μatm) was observed in the area where Chl-*a* concentrations in the surface waters were relatively high (Figs. 3.2c and d). Figure 3.6 shows the relationship between $\Delta Nf CO_2$ (T_{ave}, S_{ave}) and surface Chl-*a* for the four surveys. The changes of normalized fCO_2 by non-thermodynamic factors showed a strong negative correlation with Chl-*a* only in spring (r^2=0.75). It suggested that spatial distribution of surface fCO_2 is largely influenced by biological activities in spring.

3.1.3 Summer observation

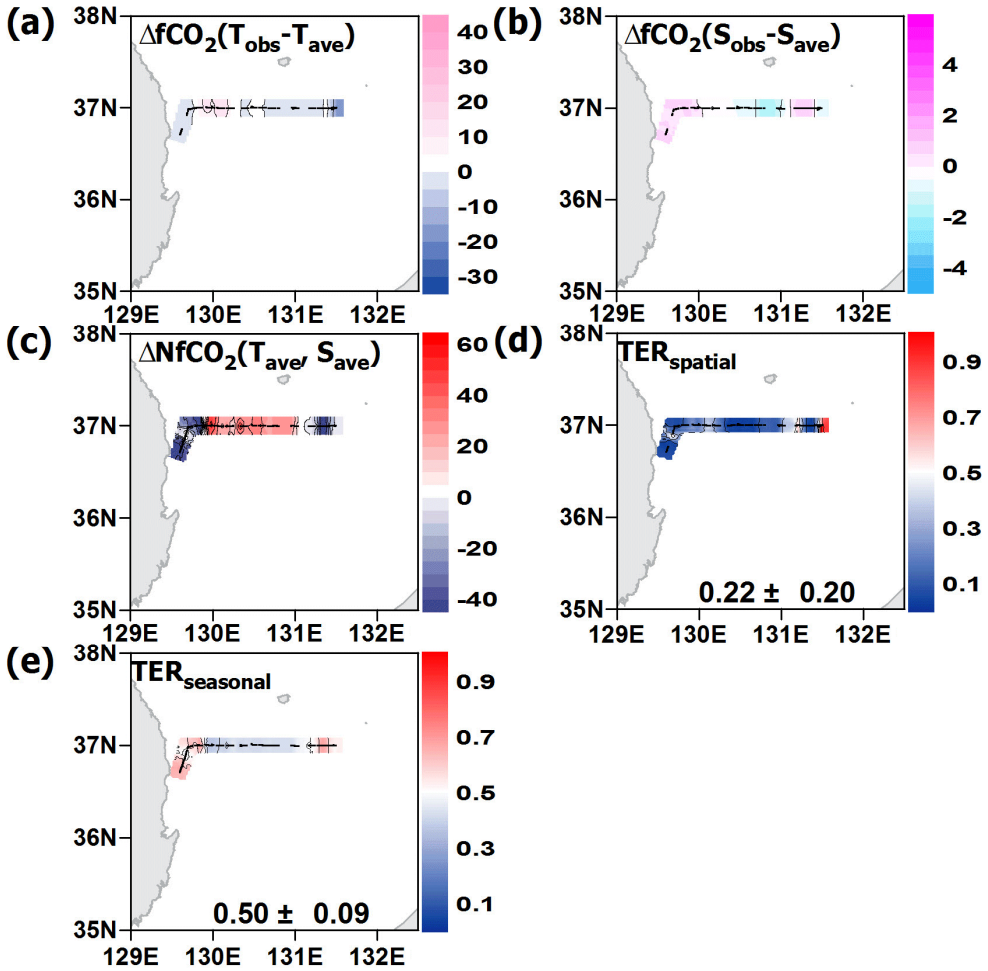

Figure 3.3. Surface distributions of (a) ΔfCO_2 (T_{obs}-T_{ave}), (b) ΔfCO_2 (S_{obs}-S_{ave}), (c) $\Delta NfCO_2$ (T_{ave}, S_{ave}), (d) $TER_{spatial}$, and (e) $TER_{seasonal}$ in the Ulleung Basin of the East Sea in April 2006. The figures in (d) and (e) represent the mean ± standard deviation (S.D.) (Terms are defined in 2.4).

In summer (August 2007), SST showed a wide range from 21.4 to 26.2°C, and SSS varied from 32.8 to 33.8 (Figs. 3.4a and b). Surface fCO_2 had a wide range from 316 to 409 μatm, the highest among the four seasons (Fig. 3.4c). Lower surface fCO_2 was observed in the central part of the study area where SSS was also relatively low (< 33.0). Despite that a variation of ΔfCO_2 (T_{obs}-T_{ave}) became larger than that in spring, ranging from -36 to 38 μatm, spatial distribution of surface fCO_2 was much more similar to ΔfCO_2 (S_{obs}-S_{ave}) (Figs. 3.5a and b). Spatial distribution of $\Delta NfCO_2$ (T_{ave}, S_{ave}) corresponded with that of ΔfCO_2 (S_{obs}-S_{ave}) (Figs. 3.5b and c). Moreover, $\Delta NfCO_2$ (T_{ave}, S_{ave}) showed a larger range from -48 to 62 μatm than both ΔfCO_2 (T_{obs}-T_{ave}), from -36 to 38 μatm and ΔfCO_2 (S_{obs}-S_{ave}), from -5 to 5 μatm. Thus, $TER_{spatial}$ was 0.45 ± 0.18, representing SST and SSS were not the primary factors to determine the spatial distribution of surface fCO_2 in summer (Fig. 3.5d). The TWC became less saline in summer because it included low salinity shelf water from the ECS. Furthermore, the CDW could reach the ES through the Korea Strait in summer (Chen *et al*., 2003). Wang and Chen (1996) reported that the normalized alkalinity (NTA = TA x 35 / S) and salinity had a linear relationship with NTA shooting up (up to 2480 μmol kg^{-1}; normal range of surface NTA in the ECS and ES was 2320 ~ 2360 μmol kg^{-1}) at lower salinity by riverine alkalinity input in the shelf area of the ECS. High NTA and low DIC of surface water might be the major non-thermodynamic factors to diminish the surface fCO_2 in summer. The central part of the study area was undersaturated with

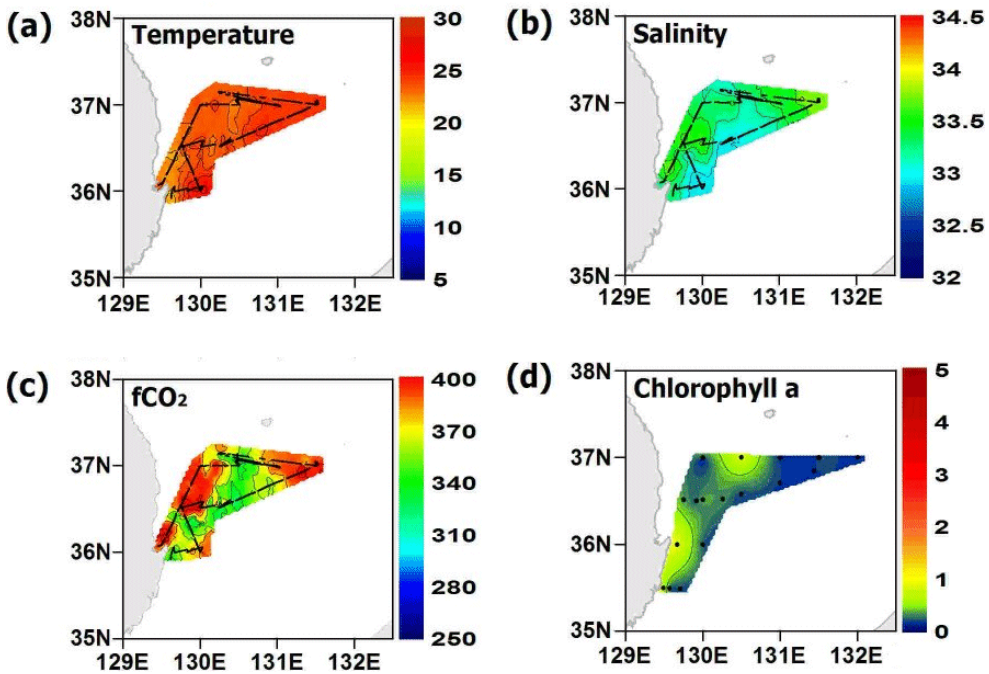

Figure 3.4. Surface distributions of (a) temperature, (b) salinity, (c) fCO_2, and (d) chlorophyll *a* in the Ulleung Basin of the East Sea in August 2007.

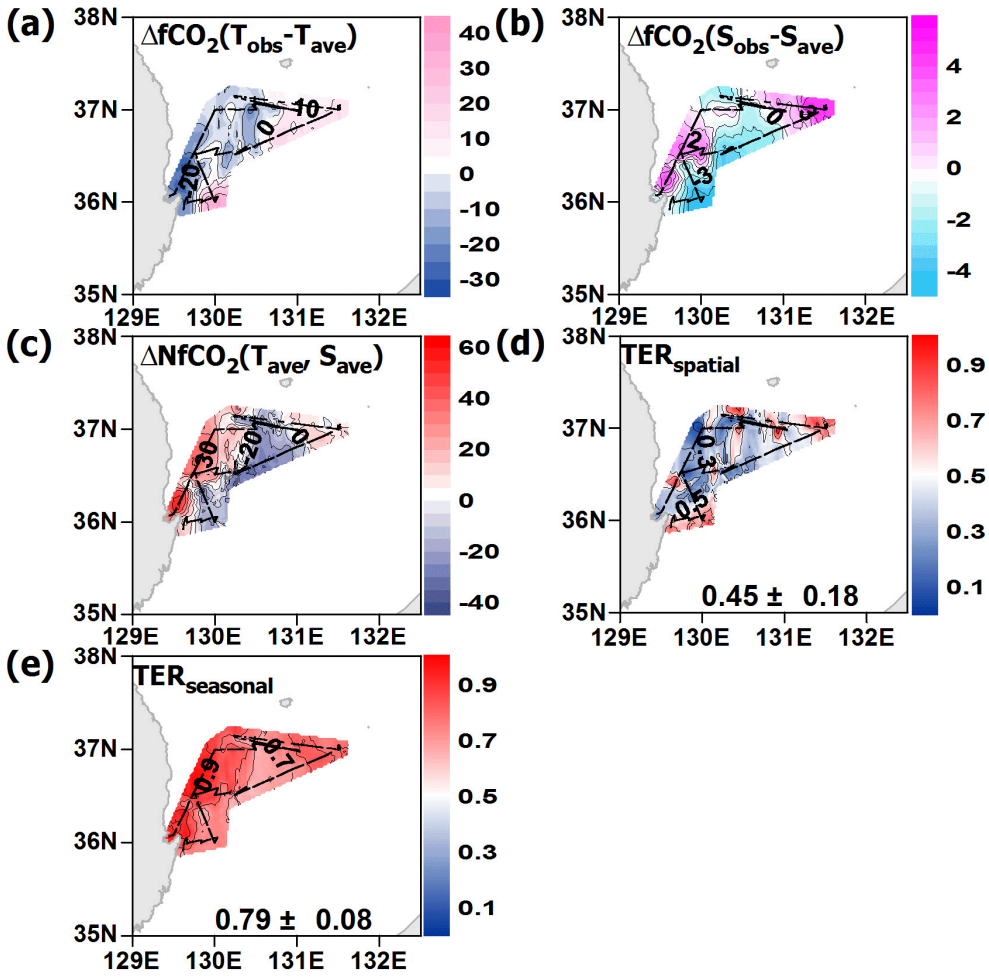

Figure 3.5. Surface distributions of (a) ΔfCO_2 (T_{obs}-T_{ave}), (b) ΔfCO_2 (S_{obs}-S_{ave}), (c) $\Delta NfCO_2$ (T_{ave}, S_{ave}), (d) $TER_{spatial}$, and (e) $TER_{seasonal}$ in the Ulleung Basin of the East Sea in August 2007. The figures in (d) and (e) represent the mean ± standard deviation (S.D.) (Terms are defined in 2.4).

respect to atmospheric CO_2 (371.0 μatm), whereas oversaturation was observed in coastal regions and in the far east of the study area. Oversaturation was found only in summer. Choi *et al*. (2011) measured surface fCO_2 in the UB of the ES on July 2005 and reported that the western and eastern parts of the UB were oversaturated with respect to atmospheric CO_2, while the central part was undersaturated. They suggested that the undersaturation resulted from low SSS and high biological activity. In this study, relatively high surface Chl-*a* concentrations were also observed in the central region (Fig. 3.4d). A rough anti-correlation showed between $\Delta NfCO_2$ (T_{ave}, S_{ave}) and surface Chl-*a* (Fig. 3.6), indicating that biological activity slightly influenced the spatial variability of surface fCO_2 in summer.

3.1.4 Autumn observation

In autumn (October 2008), SST ranged from 20.4 to 23.8°C, somewhat lower than in summer, and SSS varied from 32.3 to 33.6, rather similar to that in summer (Figs. 3.7a and b). Less saline waters were observed in the coastal regions; these waters were probably associated with the EKWC that branches from the TWC (Chang *et al*., 2004). Surface fCO_2 ranged from 298 to 355 μatm, a somewhat small variation than in summer (Fig. 3.7c). In autumn, the study area was fairly undersaturated with respect to atmospheric CO_2 (376.6 μatm). Lower surface fCO_2 was observed in the central part of the study area, which was characterized by moderate SST, SSS, and surface Chl-*a*. $\Delta NfCO_2$ (T_{ave}, S_{ave}) showed a smallest range from -20 to 40

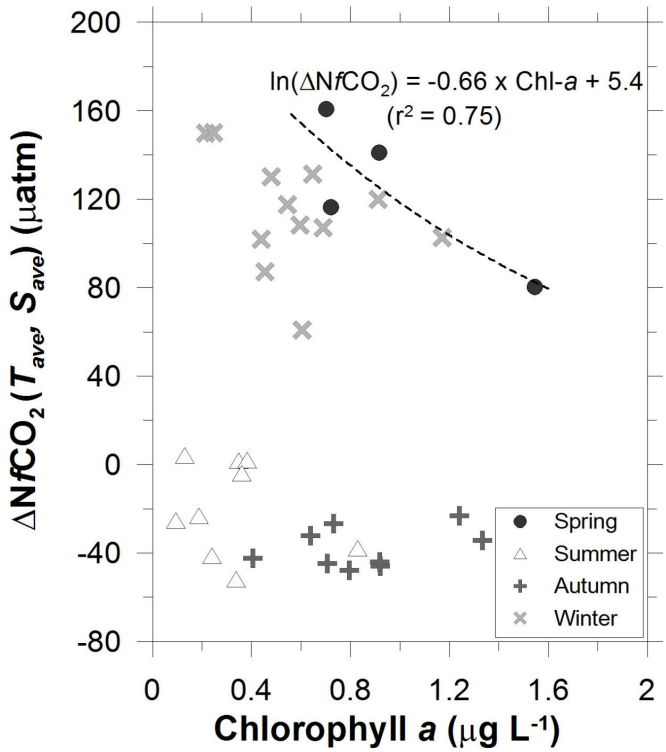

Figure 3.6. Relationship between $\Delta NfCO_2$ (T_{ave}, S_{ave}) and surface chlorophyll *a* in the Ulleung Basin of the East Sea for the four seasonal surveys.

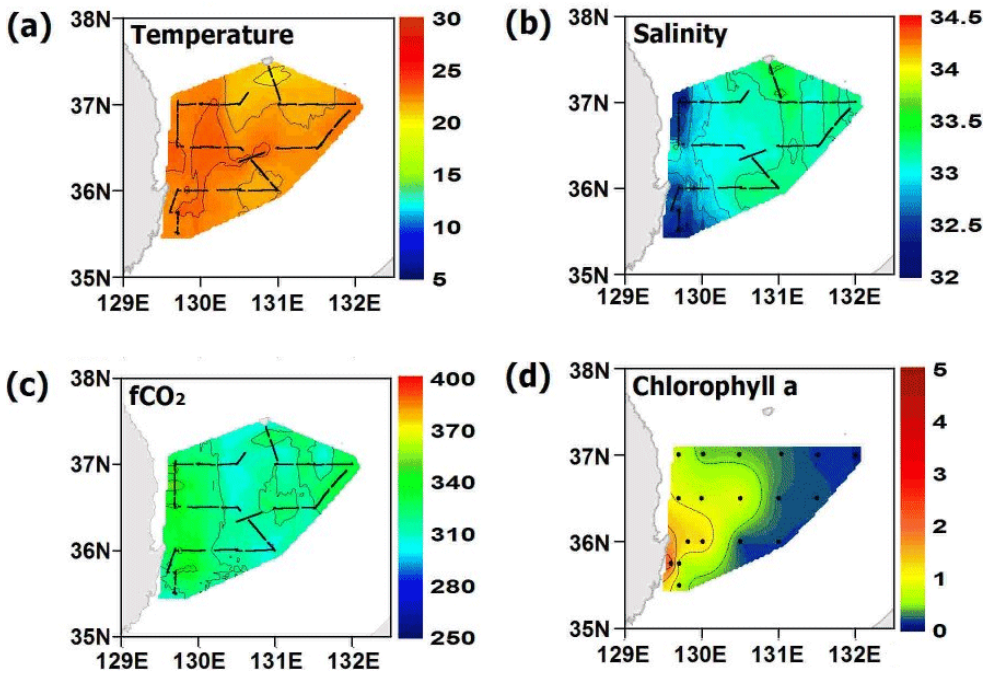

Figure 3.7. Surface distributions of (a) temperature, (b) salinity, (c) fCO_2, and (d) chlorophyll *a* in the Ulleung Basin of the East Sea in October 2008.

μatm among 4 seasonal observations (Fig. 3.8c). $TER_{spatial}$ was 0.58 ± 0.16, which was the highest value (Fig. 3.8d). It meant that SST and SSS were the major factors to control the surface fCO_2 in autumn. Distributions of ΔfCO_2 (T_{obs}-T_{ave}) and ΔfCO_2 (S_{obs}-S_{ave}) were almost opposite in phase, thus the variations of surface fCO_2 by SST and SSS changes were canceled out (Figs. 3.8a and b). Due to both a compensation of surface fCO_2 variation by SST and SSS changes, and small amount of non-thermodynamic effect on surface fCO_2, surface fCO_2 in the central part of the study area was low. Surface fCO_2 was relatively high in the coastal areas, where SSS was relatively low and surface Chl-*a* concentrations were high (Figs. 3.7b, c and d). In summer, low SSS and high Chl-*a* led to a decrease in surface fCO_2, but these two factors were less important for controlling surface fCO_2 in autumn. $\Delta Nf CO_2$ (T_{ave}, S_{ave}) was high in the coastal area where SSS was low (Figs. 3.7b and 3.8d). In the coastal areas where the water's depth was shallow, vertical mixing actively occurred in autumn when the surface stratification was weakened by the decrease in SST. In this study, the mixed layer depth increased from 10 m in summer to 25 m in autumn. It was deeper in the coastal areas than offshore (Fig. 3.9). Thus, the high surface fCO_2 in coastal areas was ascribed to vertical mixing, which brought CO_2-rich subsurface waters to the surface. Shim *et al*. (2007) suggested that the high surface fCO_2 in the northern ECS in autumn was the result of vertical mixing with deep waters rich in CO_2.

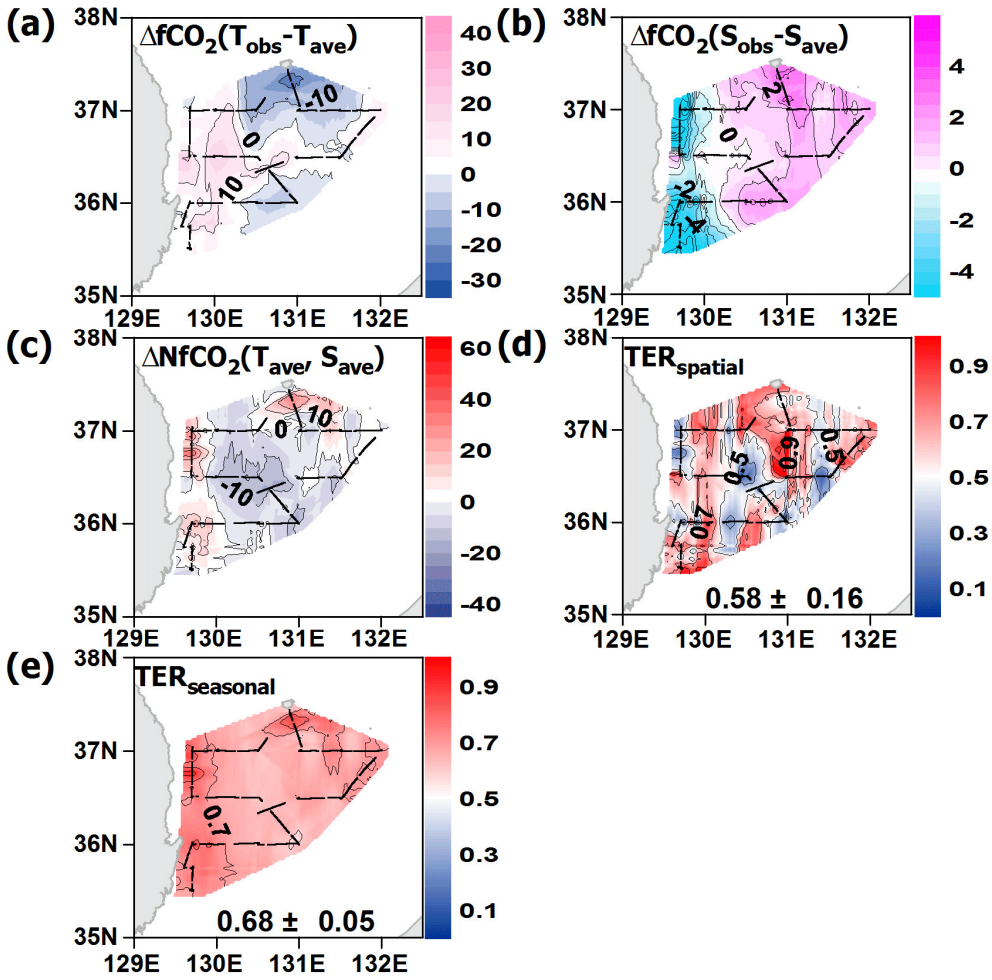

Figure 3.8. Surface distributions of (a) ΔfCO_2 (T_{obs}-T_{ave}), (b) ΔfCO_2 (S_{obs}-S_{ave}), (c) $\Delta NfCO_2$ (T_{ave}, S_{ave}), (d) $TER_{spatial}$, and (e) $TER_{seasonal}$ in the Ulleung Basin of the East Sea in October 2008. The figures in (d) and (e) represent the mean ± standard deviation (S.D.) (Terms are defined in 2.4).

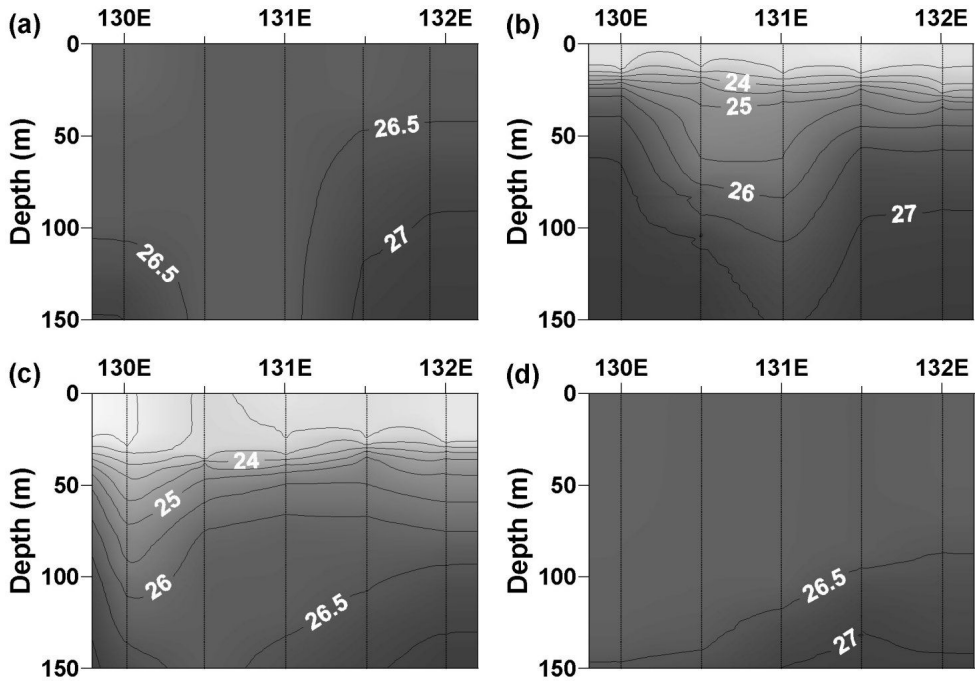

Figure 3.9. Vertical distributions of density (σ_θ) from the surface to 150 m depth along Line D (37°N) from 130°E to 132°E in the Ulleung Basin of the East Sea in (a) April 2006, (b) August 2007, (c) October 2008 and (d) February 2008.

3.1.5 Winter observation

In winter (February 2008), the SST ranged from 10.1 to 14.4°C, about 10°C lower than in autumn, and SSS varied from 34.0 to 34.4, somewhat higher than in autumn (Figs. 3.10a and b). Surface fCO_2 in winter ranged from 303 to 371 μatm, quite similar to that in autumn, despite the much lower SST (Fig. 3.10c). ΔfCO_2 (S_{obs}-S_{ave}) varied in a small range (Fig. 3.11b). ΔfCO_2 (T_{obs}-T_{ave}) and $\Delta NfCO_2$ (T_{ave}, S_{ave}) showed reversed distributions (Figs. 3.11a and c). Due to the anti-correlation between ΔfCO_2 (T_{obs}-T_{ave}) and $\Delta NfCO_2$ (T_{ave}, S_{ave}), surface fCO_2 range was similar with that in autumn in spite of the much lower SST. $TER_{spatial}$ in winter was 0.45 ± 0.18 (Fig. 3.11d), showing SST and SSS were not the primary factors to control the spatial distribution of surface fCO_2 like in summer. In winter, the surface mixed layer was deeper than 100 m in the study area (Fig. 3.9), implying active vertical mixing within the upper 100 m. Active mixing might have led to an increase in surface fCO_2, which could have offset the decrease due to lower SST. Higher surface fCO_2 was observed in the northwestern part of the study region, where the surface mixed layer was deeper than in other areas and surface Chl-*a* concentrations were lowest. Highest $\Delta NfCO_2$ (T_{ave}, S_{ave}) in the northwestern part implied strong vertical mixing and/or weak biological activity. Lower surface fCO_2 was found at the southern and eastern parts of the study area, where surface Chl-*a* concentrations were relatively high. $\Delta NfCO_2$ (T_{ave}, S_{ave}) in the southern and eastern parts were negative, representing relatively high biological activity. $\Delta NfCO_2$ (T_{ave},

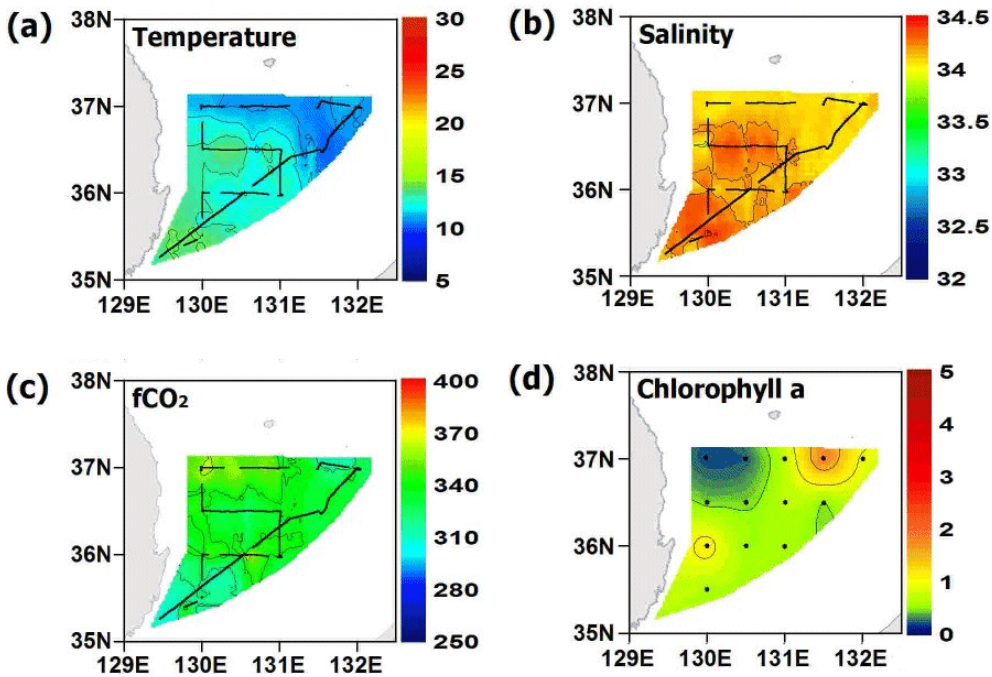

Figure 3.10. Surface distributions of (a) temperature, (b) salinity, (c) fCO_2, and (d) chlorophyll *a* in the Ulleung Basin of the East Sea in February 2008.

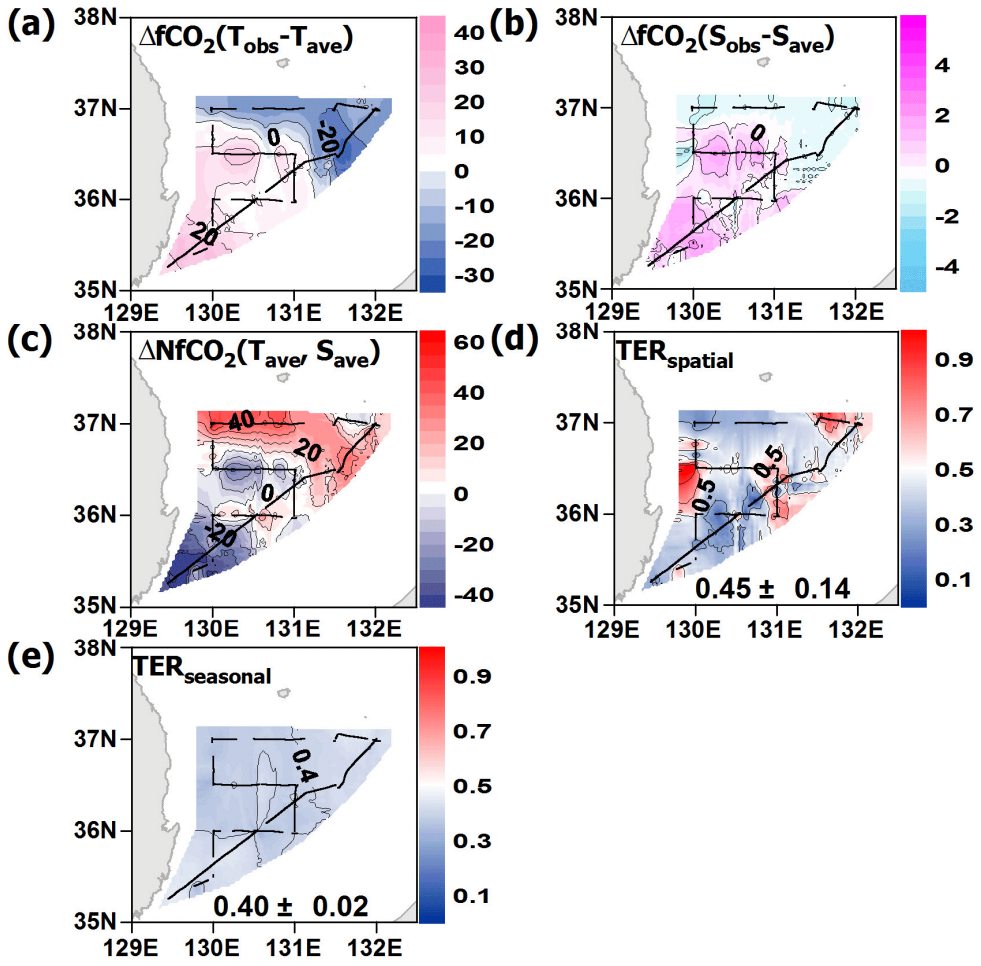

Figure 3.11 Surface distributions of (a) ΔfCO_2 (T_{obs}-T_{ave}), (b) ΔfCO_2 (S_{obs}-S_{ave}), (c) $\Delta NfCO_2$ (T_{ave}, S_{ave}), (d) $TER_{spatial}$, and (e) $TER_{seasonal}$ in the Ulleung Basin of the East Sea in February 2008. The figures in (d) and (e) represent the mean ± standard deviation (S.D.) (Terms are defined in 2.4).

S_{ave}) was vaguely correlated with surface Chl-*a* (Fig. 3.6). In winter, surface fCO_2 was influenced, to some degree, by biological activity.

3.2 Distributions of surface fCO_2 in the northern East China Sea

3.2.1 Spring observations

Spring observations were conducted in May 2004 and April 2008. In May 2004, SSTs ranged from 13.6 to 23.4°C, with an increasing gradient from west to east across the study area; these temperatures were slightly higher than those in April 2008, which ranged from 11.1 to 18.1°C (Fig. 3.12). SSSs also showed an increasing gradient from west to east and did not exhibit a considerable difference between May 2005 and April 2008. In spring, the thermohaline front was located around 126°E. Average atmospheric fCO_2 was 378.0±6.3 and 382.5±3.3 μatm in May 2004 and April 2008, respectively (Table 3.1 and Fig. 3.13). In May 2004, the sea-air ΔfCO_2 had negative values in most parts of the study area, with a minimum of -126 μatm, and positive values west of 125°E, with a maximum of 54 μatm (Fig. 3.12). In April 2008, however, the values for ΔfCO_2 were negative across the entire study area, with a range of approximately -152 to -13 μatm. The highest negative ΔfCO_2 was observed at the frontal area located at 126°E. The areal mean ΔfCO_2

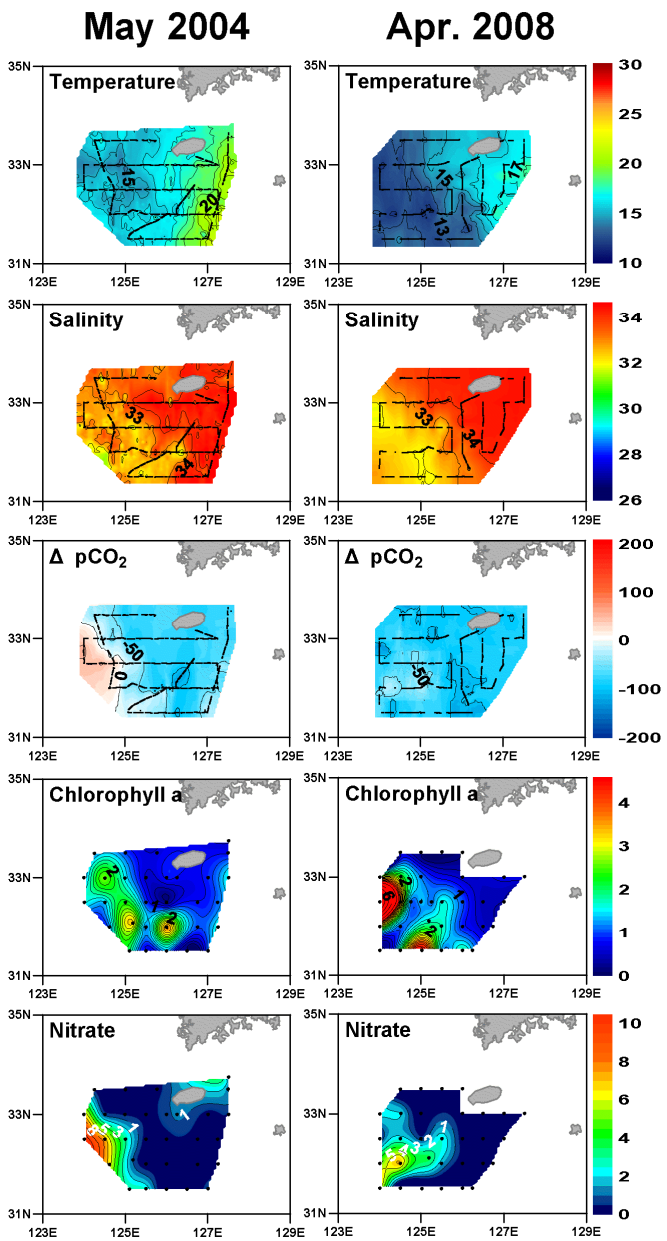

Figure 3.12. Surface distributions of temperature, salinity, sea-air differences of CO_2 fugacity (ΔfCO_2), chlorophyll *a*, and nitrate in the northern East China Sea in spring, May 2004 and April 2008. Data obtained in May 2004 are from Shim *et al*. (2007).

Table 3.1. Averaged atmospheric fCO_2 for the seven surveys in the northern East China Sea

Periods	Atmospheric fCO_2 (μatm)[a]
Aug. 2003	368.8±3.5
May 2004	378.0±6.3
Oct. 2004	365.4±3.0
Nov. 2005	376.8±3.8
Jul. 2006	368.0±6.6
Apr. 2008	382.5±3.3
Feb. 2009	384.7±3.1

[a] Averaged atmospheric fCO_2 along cruise tracks expressed as mean±S.D.

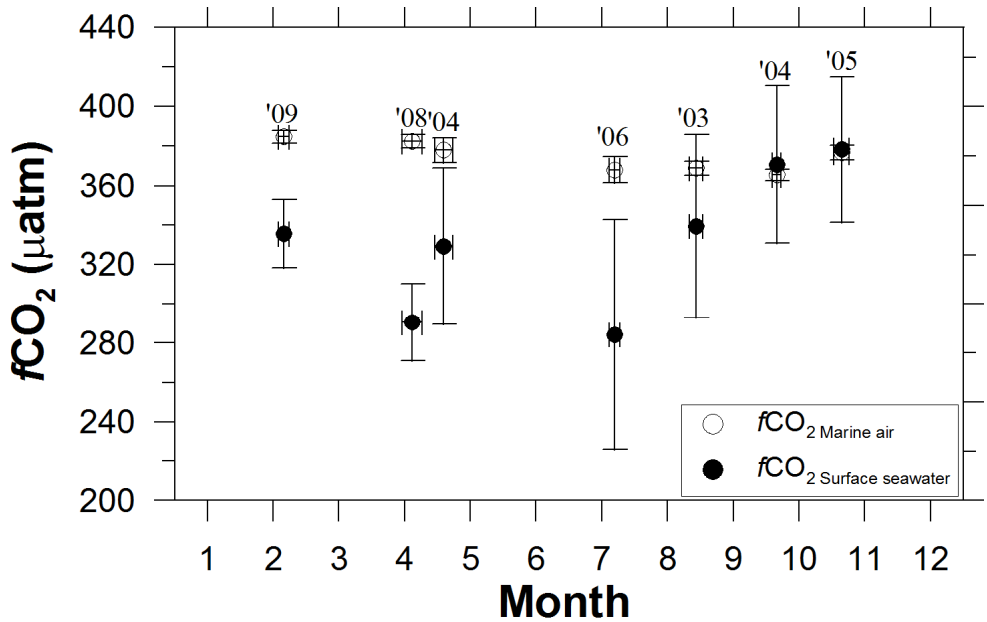

Figure 3.13. Monthly data ranges of fCO_2 in surface seawater and marine air during the seven observations in the northern East China Sea. The circles represent mean fCO_2 in surface seawater (●) and marine air (○). The vertical and horizontal bars represent 1 S.D. of each fCO_2 data and observation periods, respectively.

was -48 ± 41 μatm in May 2004 and -87 ± 20 μatm in April 2008 (Table 3.2). In spring, high surface Chl-*a* concentrations were observed in the western part of the study area, with maximum values of 3.7 and 8.1 mg m^{-3} in May 2004 and April 2008, respectively (Fig. 3.12). Noh *et al*. (2005) reported that spring bloom started in April in the northern ECS. Surface nitrate concentrations were highest in the westernmost part of the study area, and decreased gradually eastward; concentrations in the eastern part of the study area were lower than 1.0 μmol L^{-1} (Fig. 3.12). Kim *et al.* (2009) suggested that the high surface nitrate concentrations in the northern ECS during spring resulted from vertical mixing, which brought large supplies of nitrate from deeper water. ΔfCO_2 (T_{obs}-T_{ave}), ΔfCO_2 (S_{obs}-S_{ave}), $\Delta Nf CO_2$ (T_{ave}, S_{ave}), $TER_{spatial}$, and $TER_{seasonal}$ for the spring cruises are shown in Figure 3.14. In May 2004, ΔfCO_2 (T_{obs}-T_{ave}) and ΔfCO_2 (S_{obs}-S_{ave}) varied in wider ranges than those in April 2008 (Fig. 3.14). $\Delta Nf CO_2$ (T_{ave}, S_{ave}) in both May 2004 and April 2008 showed large values in the westernmost part of the study area where high surface nitrate concentrations were observed (Fig. 3.14). $TER_{spatial}$ of the eastern part of thermohaline front was 0.70±0.17 which represented that SST and SSS might be the major factors to control the spatial distribution of this region (Fig. 3.14).

3.2.2 Summer observations

Table 3.2. Areal mean sea-air differences of CO_2 fugacity (ΔfCO_2), mean wind speed, and mean sea-air CO_2 flux in the northern East China Sea during the four seasons.

Season	Observation time	ΔfCO_2[a] (μatm)	Wind speed[b] (m sec^{-1})	CO_2 flux[c] (mmol C m^{-2} day^{-1})	
				Survey average	Seasonal average
Spring	May 2004	-48±41	6.5±3.5	-5.1±4.3	-6.8±4.3
	Apr. 2008	-87±20	6.2±2.7	-8.4±1.9	
Summer	Aug. 2003	-41±47	7.4±2.5	-6.0±6.8	-6.6±8.5
	Jul. 2006	-85±59	5.8±1.8	-7.2±5.1	
Autumn	Oct. 2004	7.9±40	9.1±2.1	1.6±8.2	0.81±7.3
	Nov. 2005	0.1±34	6.4±2.5	0.02±3.5	
Winter	Feb. 2009	-50±17	10±3.5	-12±4.1	-12±4.1

[a] Mean ΔfCO_2 along cruise tracks expressed as mean±S.D.

[b] Mean wind speed of study area (31.5~34°N, 124~127.5°E) from QuikSCAT satellite data during each observation period expressed as mean±S.D.

[c] Mean sea-air CO_2 fluxes based on the transfer coefficient by Wanninkhof (1992) expressed as mean±S.D. A positive value represents CO_2 emission from the sea to the atmosphere and a negative value refers to CO_2 absorption from atmosphere to the sea.

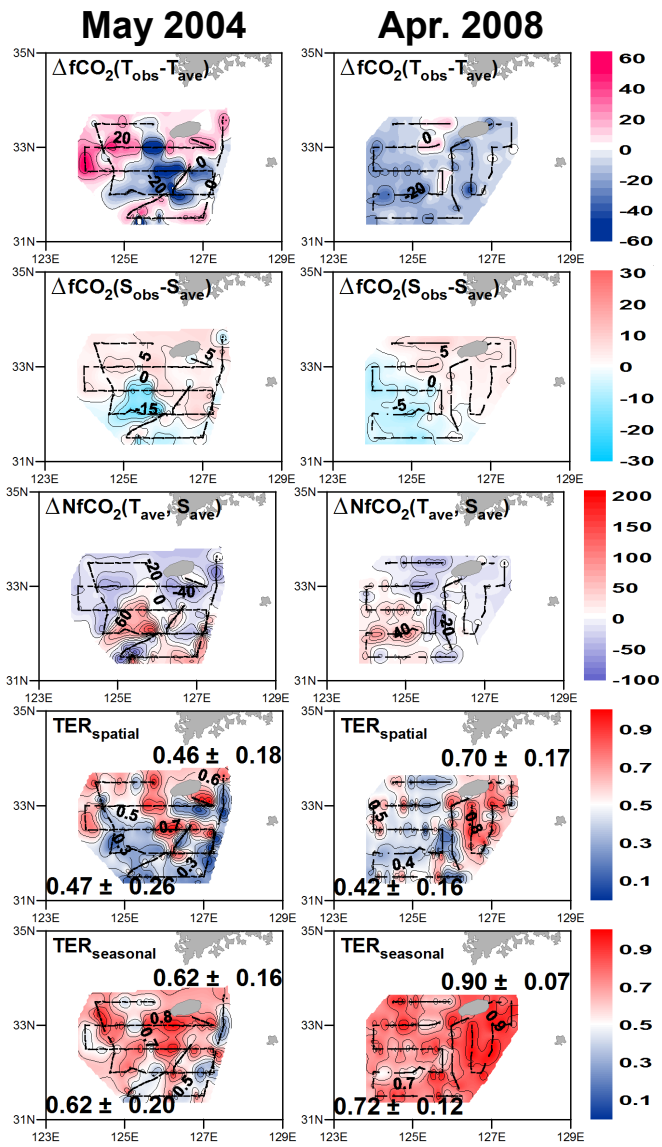

Figure 3.14. Surface distributions of ΔfCO_2 (T_{obs}-T_{ave}), ΔfCO_2 (S_{obs}-S_{ave}), $\Delta NfCO_2$ (T_{ave}, S_{ave}), $TER_{spatial}$, and $TER_{seasonal}$ in the northern East China Sea in May 2004 and April 2008. The figures in $TER_{spatial}$ and $TER_{seasonal}$ represent the mean ± standard deviation (S.D.), lower one for western region and upper one for eastern (Terms are defined in 2.4).

Summer data consists of two expeditions conducted in August 2003 and July 2006. In August 2003, SSTs showed a high, narrow range between 25.4 and 29.5°C, without a distinct spatial pattern, and were somewhat higher than SSTs in July 2006, which ranged from 22.5~27.2°C and had a decreasing gradient from west to east (Fig. 3.15). Low SSSs (<29.0) were observed in the western part of the study area during the two summer expeditions (Fig. 3.15), suggesting large summer inputs of freshwater from the Changjiang. The thermohaline front was located around 126.5°E in August 2003 and 126°E in July 2006. Average atmospheric fCO_2 was 368.8±3.5 and 368.0±6.6 μatm in August 2003 and July 2006, respectively (Table 3.1). In August 2003, the sea-air ΔfCO_2 showed positive values in the eastern part with a maximum of 67 μatm and negative values in the western part with a minimum of -142 μatm (Fig. 3.15). In July 2006, the sea-air ΔfCO_2 values were negative across the entire study area with a minimum of -198 μatm, except for the frontal area where fCO_2 was slightly oversaturated. The CO_2 sink in the eastern part was not as strong as that in the western part. The areal mean ΔfCO_2 was -41 ± 47 μatm in August 2003 and -85 ± 59 μatm in July 2006 (Table 3.2), rather similar to values for spring. Surface Chl-*a* concentrations were much lower in summer than in spring (Fig. 3.15); in August 2003, surface Chl-*a* concentrations were much lower in summer than in spring (Fig. 3.15); in August 2003, surface Chl-*a* concentrations ranged from 0.2 to 1.3 mg m^{-3}, lower than the range of 0.4~2.9 mg m^{-3} for July 2006. As in spring, summer surface Chl-*a* concentrations were somewhat higher in the western part than in the eastern part of the study area.

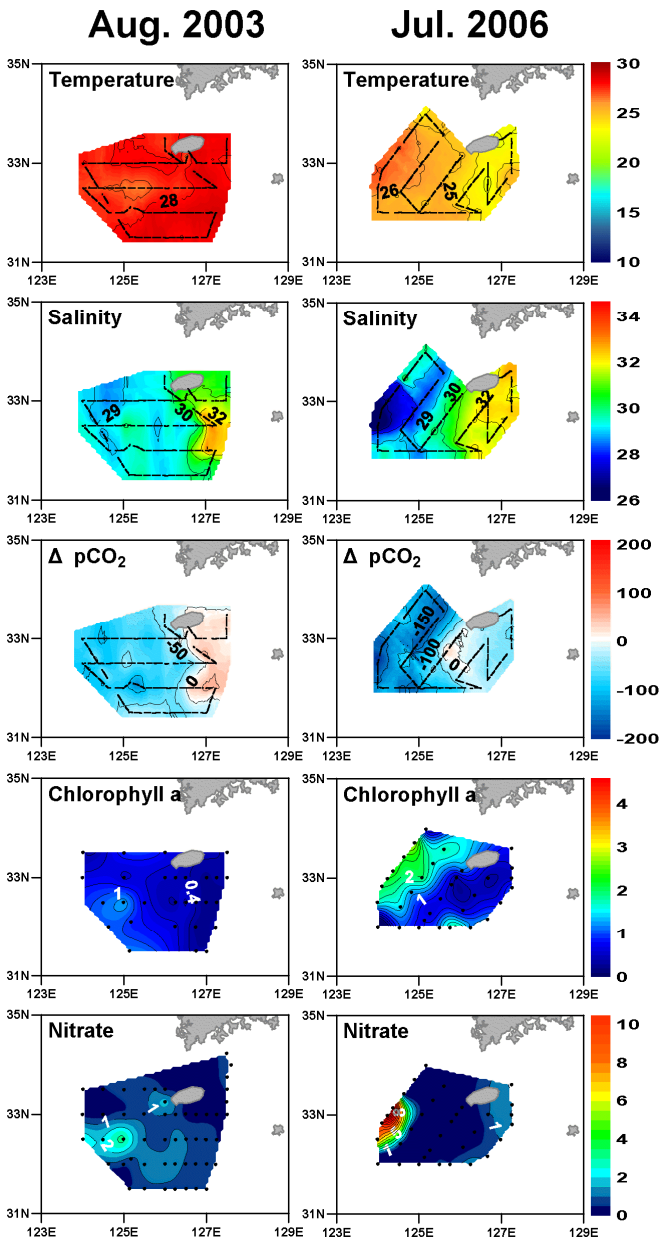

Figure 3.15. Surface distributions of temperature, salinity, sea-air differences of CO_2 fugacity (ΔfCO_2), chlorophyll *a*, and nitrate in the northern East China Sea in summer, August 2003 and July 2006. Data obtained in August 2003 are from Shim *et al*. (2007).

In summer, high surface nitrate concentrations were confined to a small region of the western part, with all other areas showing very low nitrate concentrations of less than 1.0 μmol L^{-1} (Fig. 3.15). Kim *et al*. (2009) suggested that the inflow of the Changjiang plume in summer caused the high surface nitrate concentrations in the northern ECS. While ΔfCO_2 (S_{obs}-S_{ave}) varied in small ranges in both August 2003 and July 2007, ΔfCO_2 (T_{obs}-T_{ave}) showed conflicting variabilities in large ranges (Fig. 3.16). $\Delta Nf CO_2$ (T_{ave}, S_{ave}) in both August 2003 and July 2006 showed negative values in the westernmost part of the study area where less saline surface water by freshwater inputs were expected (Fig. 3.16). The higher $TER_{spatial}$, which were 0.55±0.17, 0.85±0.10 and 0.70±0.22 in western and eastern part in August 2003 and eastern part in July 2006, respectively, represented that SST and SSS might be the major factors to control the spatial distributions except in the western part in July 2007 where large freshwater intrusion was observed (Fig. 3.16).

3.2.3 Autumn observations

Autumn observations were carried out in October 2004 and November 2005. In October 2004, SSTs varied from 22.2 to 25.7°C, with an increasing gradient from west to east. In November 2005, the range was somewhat lower at 18.7~24.5°C (Fig. 3.17). In the eastern part of the study area, SSSs were relatively high at around 34 and generally similar for the two observations. However, in the western part, SSSs were somewhat lower in November 2005 than in October 2004 (Fig.

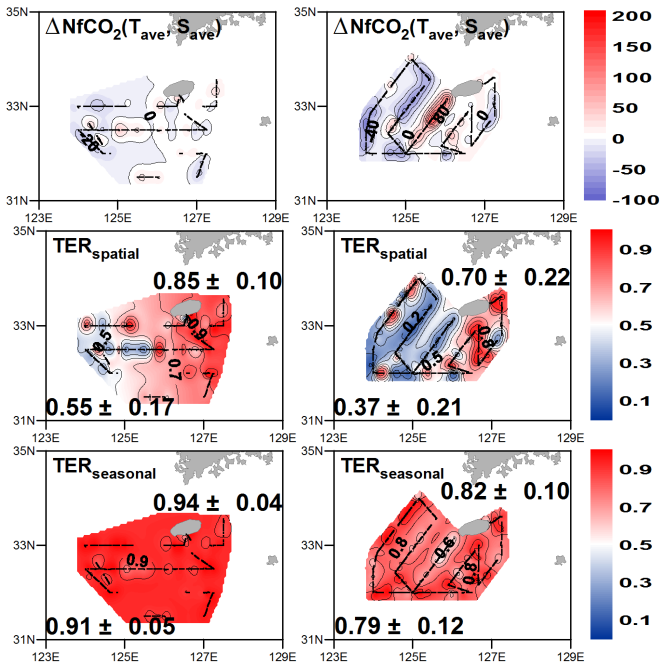

Figure 3.16. Surface distributions of ΔfCO_2 (T_{obs}-T_{ave}), ΔfCO_2 (S_{obs}-S_{ave}), $\Delta NfCO_2$ (T_{ave}, S_{ave}), $TER_{spatial}$, and $TER_{seasonal}$ in the northern East China Sea in August 2003 and July 2006. The figures in $TER_{spatial}$ and $TER_{seasonal}$ represent the mean ± standard deviation (S.D.), lower one for western region and upper one for eastern (Terms are defined in 2.4).

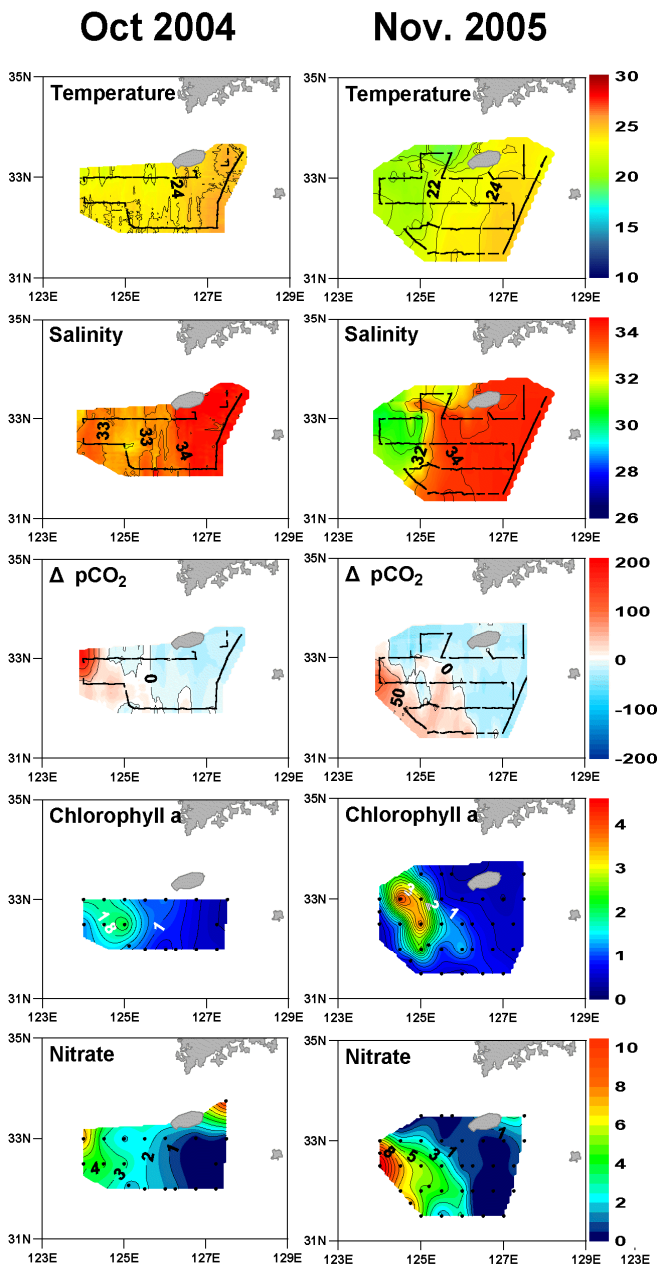

Figure 3.17. Surface distributions of temperature, salinity, sea-air differences of CO_2 fugacity (ΔfCO_2), chlorophyll *a*, and nitrate in the northern East China Sea in autumn. Data obtained in October 2004 and November 2005 are from Shim *et al*. (2007).

3.17). The thermohaline front was located around 126.5°E in October 2004 and 125°E in November 2005. Average atmospheric fCO_2 was 365.4±3.0 and 376.8±3.8 μatm in October 2004 and November 2005, respectively (Table 3.1). In October 2004, sea-air ΔfCO_2 was positive in the western part with a maximum of 202 μatm, but negative in the eastern part with a minimum of -40 μatm (Fig. 3.17). Maximum ΔfCO_2 was observed in the westernmost part, and it gradually decreased eastward. In November 2005, ΔfCO_2 also showed positive values in the western part with a maximum of 118 μatm and negative values in the eastern part with a minimum of -58 μatm. In autumn, the western part acted as a source of CO_2, and the eastern part as a sink. The areal mean ΔfCO_2 values were 7.9 ± 40 and 0.1 ± 34 μatm in October 2004 and November 2005, respectively (Table 3.2), implying that the study area was a source of CO_2 in autumn, unlike in other seasons. In autumn, high surface Chl-*a* concentrations were observed in the western part, with maximum values of 2.2 and 4.1 mg m^{-3} in October 2004 and November 2005, respectively (Fig. 3.17), which were somewhat lower than maximum values in spring. High surface nitrate concentrations were also found in the western part, with maximum values of 4.2 and 12.4 μmol L^{-1} in October 2004 and November 2005, respectively (Fig. 3.17), which were rather similar to those in spring. In the eastern part, however, surface nitrate concentrations were lower than 1.0 μmol L^{-1}, as in spring. In November 2005, ΔfCO_2 (T_{obs}-T_{ave}), ΔfCO_2 (S_{obs}-S_{ave}) as well as $\Delta Nf CO_2$ (T_{ave}, S_{ave}) varied in wide ranges, while those showed quite small variations in October 2004

(Fig. 3.18). Thus, $TER_{spatial}$ both in October 2004 were 0.56±0.20 and 0.65±0.18 in western and eastern part, respectively, that meant SST and SSS might be the major factors to control the spatial distributions, and vice versa in November 2005 (Fig. 3.18).

3.2.4 Winter observation

The winter data were based on a single expedition carried out in February 2009. SSTs ranged from 9.6 to 17.1°C, with an increasing gradient from west to east across the study area (Fig. 3.19). SSSs also showed an increasing gradient from west to east, with a range of 32.1 to 34.5 (Fig. 3.19). In winter, the thermohaline front was located around 126°E. Average atmospheric fCO_2 was 384.7±3.1 μatm in February 2009 (Table 3.1). The sea-air ΔfCO_2 values were negative across the entire study area, with a minimum of -77 μatm. The areal mean ΔfCO_2 was -50 ± 17 μatm (Table 3.2), implying that the study area was a CO_2 sink in winter. The CO_2 sink in the western part was not as strong as that in the eastern part. Surface Chl-*a* concentrations were very low, less than 0.6 mg m^{-3}, across the entire study area (Fig. 3.19). High surface nitrate concentrations were found in the westernmost part, with a maximum value of 13.8 μmol L^{-1}, and decreased gradually eastward (Fig. 3.19). While ΔfCO_2 (T_{obs}-T_{ave}) and ΔfCO_2 (S_{obs}-S_{ave}) showed increasing gradients from west to east across the study area, $\Delta NfCO_2$ (T_{ave}, S_{ave}) showed decreasing one in a wide variations rather than ΔfCO_2 (T_{obs}-T_{ave}) and ΔfCO_2 (S_{obs}-S_{ave}) (Fig. 3.20). Thus, $TER_{spatial}$ were 0.36±0.11 and 0.41±0.17 in western and

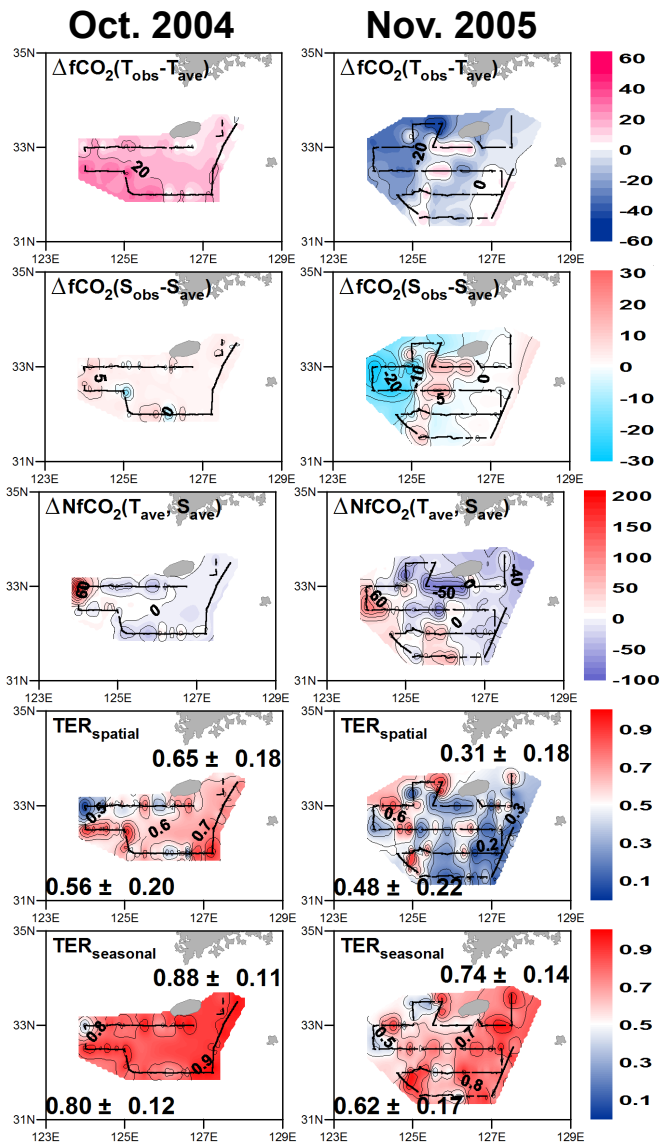

Figure 3.18. Surface distributions of ΔfCO_2 (T_{obs}-T_{ave}), ΔfCO_2 (S_{obs}-S_{ave}), $\Delta NfCO_2$ (T_{ave}, S_{ave}), $TER_{spatial}$, and $TER_{seasonal}$ in the northern East China Sea in October 2004 and November 2005. The figures in $TER_{spatial}$ and $TER_{seasonal}$ represent the mean ± standard deviation (S.D.), lower one for western region and upper one for eastern (Terms are defined in 2.4).

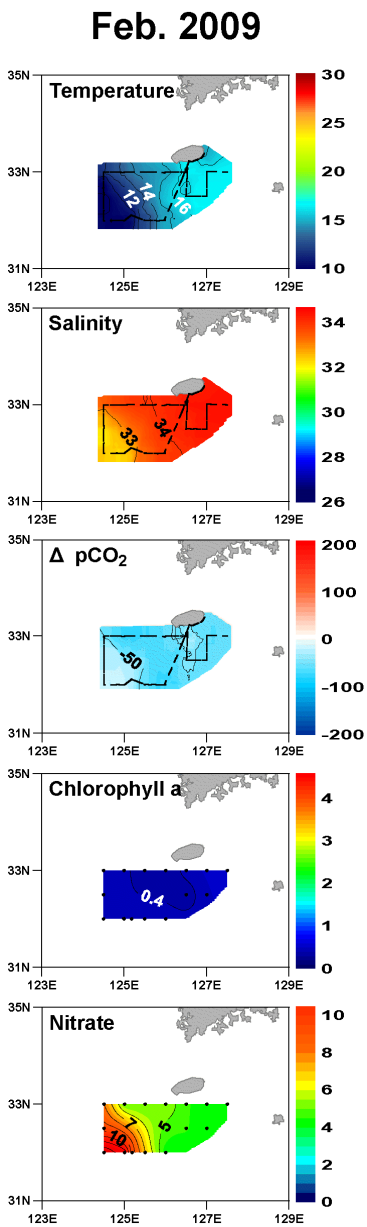

Figure 3.19. Surface distributions of temperature, salinity, sea-air differences of CO_2 fugacity (ΔfCO_2), chlorophyll *a*, and nitrate in the northern East China Sea in winter.

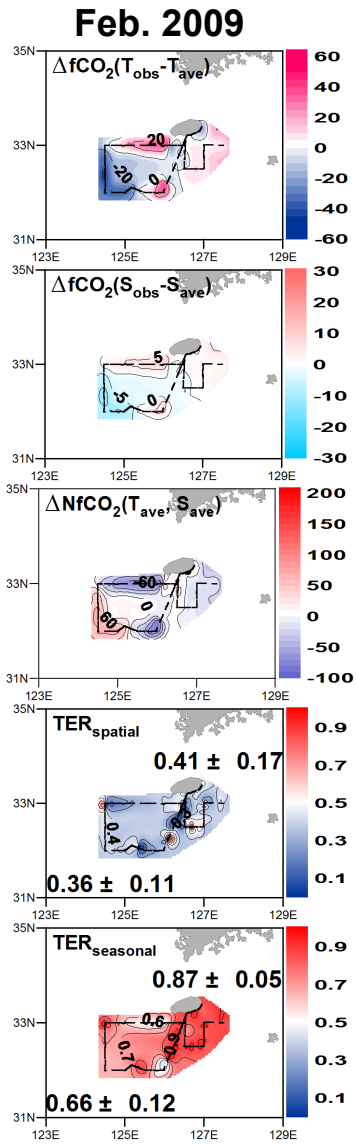

Figure 3.20. Surface distributions of ΔfCO_2 (T_{obs}-T_{ave}), ΔfCO_2 (S_{obs}-S_{ave}), $\Delta NfCO_2$ (T_{ave}, S_{ave}), $TER_{spatial}$, and $TER_{seasonal}$ in the northern East China Sea in February 2009. The figures in $TER_{spatial}$ and $TER_{seasonal}$ represent the mean ± standard deviation (S.D.), lower one for western region and upper one for eastern (Terms are defined in 2.4).

eastern part, respectively, that meant SST and SSS would not be the major factors to control the spatial distributions in February 2009 (Fig. 3.20).

3.3 Distributions of surface fCO_2 in the western North Pacific

3.3.1 May-June observations

May-June observations were conducted in June 2008 and 2009, and May 2010. In June 2008, SSTs ranged from 27.6 to 29.8°C. SST generally showed an increasing gradient from north to south across the study area, except the southern area lower than 15°N (Fig. 3.21a). These temperatures were lower than those of another June observation in 2009 (Figs. 3.21a and b). SSSs ranged in slightly narrow ranges from 33.8 to 34.4 with high SSSs around 20°N; these SSSs were also lower than those of both June 2009 and May 2010 (Fig. 3.21b and c). NEC is the major surface current in this study area. NEC and the northern subtropical gyre had different hydrographic characteristics such as temperature and salinity. The location of NEC boundary varied yearly. In June 2008, the northern boundary of NEC seemed to be on around 20°N. Surface fCO_2 showed ranges from 361.7 to 396.5 μatm; these were lower than those of June 2009 and May 2010 (Fig. 3.21b and c). Surface fCO_2 values between 15 and 20°N were slightly higher than atmospheric CO_2, whereas those of the other areas were similar with that of atmosphere. In June

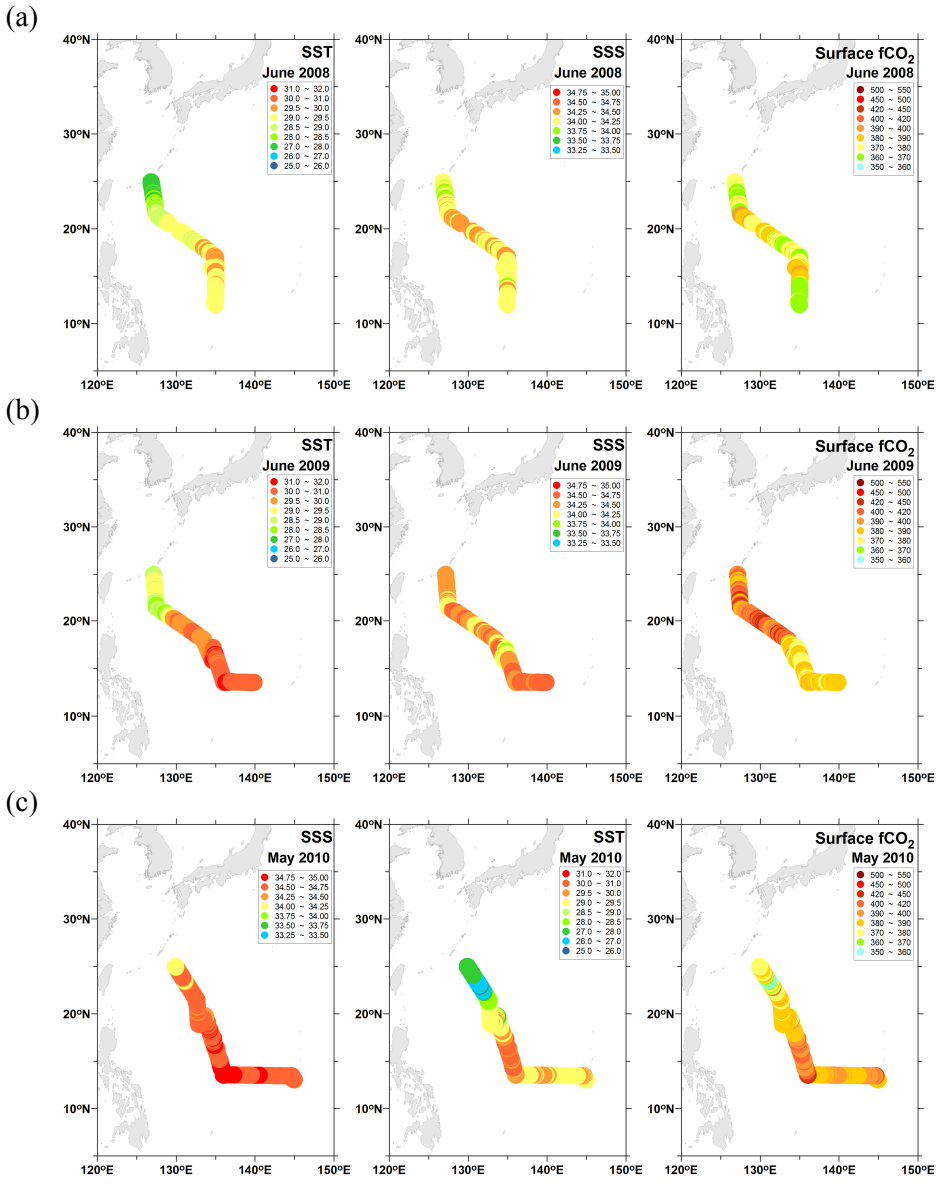

Figure 3.21. Surface distributions of temperature, salinity, and fCO_2 in the western North Pacific in (a) June 2008, (b) June 2009, and (c) May 2010.

2009, SSTs ranged from 28.2 to 31.4°C. SSTs consistently increased from north to south along the cruise track except around 21°N where SSTs declined about 1°C. SSSs ranged from 33.6 to 34.7. SSSs did not show any trend which is increasing or decreasing in the entire study area. The northern boundary of NEC seemed to locate on 17°N. Surface fCO_2 ranged from 365.0 to 448.6 μatm. Surface fCO_2 between 17 and 25°N was much higher than those of between 10 and 17°N. Mean surface fCO_2 of the northern area was 397.0±16.4 μatm which was the highest areal mean among the areal mean during five observations in the western NP, whereas that of the southern area was 380.0±4.5 μatm. In May 2010, SSTs ranged 25.8 to 30.7°C. SSTs of the northern area over 20°N were the lowest among all May-June observations, but those of the southern area were not. SSSs ranged from 33.7 to 34.9. SSSs showed the highest values among all periods. The northern boundary of NEC seemed to locate on 17.5°N. Surface fCO_2 showed the widest ranges from 357.1 to 528.2 μatm. Surface fCO_2 of the southern area between 10 and 17.5°N was higher than those of the northern area between 17.5 and 25°N. Mean surface fCO_2 of the southern area was 396.5±12.5 μatm, 386.0±6.5 μatm in the northern area. In the middle of the northern area, surface fCO_2 showed somewhat lower value than that of atmosphere. ΔfCO_2 (T_{obs}-T_{ave}), ΔfCO_2 (S_{obs}-S_{ave}), $\Delta N fCO_2$ (T_{ave}, S_{ave}), $TER_{spatial}$, and $TER_{temporal}$ for the May-June cruises are shown in Figure 3.22. ΔfCO_2 (S_{obs}-S_{ave}) varied in smaller ranges rather than ΔfCO_2 (T_{obs}-T_{ave}) and $\Delta N fCO_2$ (T_{ave}, S_{ave}) in all observation periods, while ΔfCO_2 (T_{obs}-T_{ave}) and $\Delta N fCO_2$ (T_{ave}, S_{ave}) varied within similar ranges (Fig. 3.22). The higher $TER_{spatial}$, which were

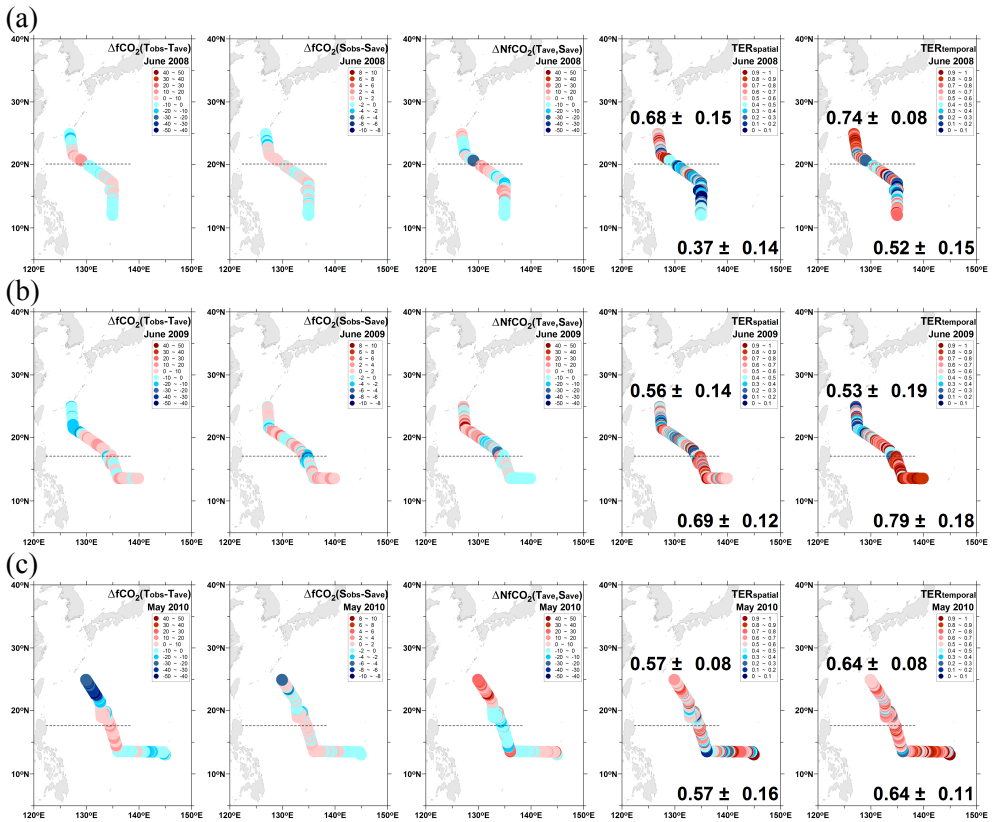

Figure 3.22. Surface distributions of ΔfCO_2 (T_{obs}-T_{ave}), ΔfCO_2 (S_{obs}-S_{ave}), $\Delta NfCO_2$ (T_{ave}, S_{ave}), $TER_{spatial}$, and $TER_{seasonal}$ in the western North Pacific in (a) June 2008, (b) June 2009, and (c) May 2010. The figures in $TER_{spatial}$ and $TER_{temporal}$ represent the mean ± standard deviation (S.D.), lower one for southern area (North Equatorial Current, NEC) and upper one for subtropical gyre (Terms are defined in 2.4). Dashed lines represent the boundary between North Equatorial Current (NEC) and subtropical gyre in each observation period.

0.68±0.15, 0.56±0.14, 0.57±0.08, 0.69±0.12, and 0.57±0.16 in subtropical gyre in June 2008, June 2009, and May 2010 and the NEC in June 2009, and May 2010, respectively, represented that SST and SSS might be the major factors to control the spatial distributions except in the NEC in June 2008 (Fig. 3.22).

3.3.2 September-October observations

September-October observations were conducted in September 2006 and October 2007. In September 2006, SSTs ranged from 28.6 to 31.6°C (Fig. 3.23a). These temperatures were higher than those of October 2007 (Fig. 3.23a). SSSs showed slightly wide ranges with lower minimum value with respect to May-June observations from 33.5 to 34.8; these salinity ranges were similar with those of October 2007 (Fig. 3.23b). The northern boundary of NEC seemed to locate on 20°N. Surface fCO_2 ranged from 350.7 to 393.3 μatm; these ranges were similar with those of June 2008, and slightly higher than those of October 2007 (Fig. 3.23b). Surface fCO_2 in lower latitudes between 10 and 19°N varied in wide ranges, from 350.7 to 393.3 μatm, than those in higher latitudes, from 359.8 to 390.0 μatm. In October 2007, SSTs ranged from 27.6 to 30.6°C. Low SSTs under 29°C were widespread from north to about 15°N. SSSs ranged from 33.6 to 34.6. The northern boundary of NEC seemed to locate on 16°N. Surface fCO_2 ranged from 355.2 to 394.7 μatm; these ranges were the lowest among all of five western NP observations. Most of surface fCO_2 was lower than the atmospheric CO_2. In

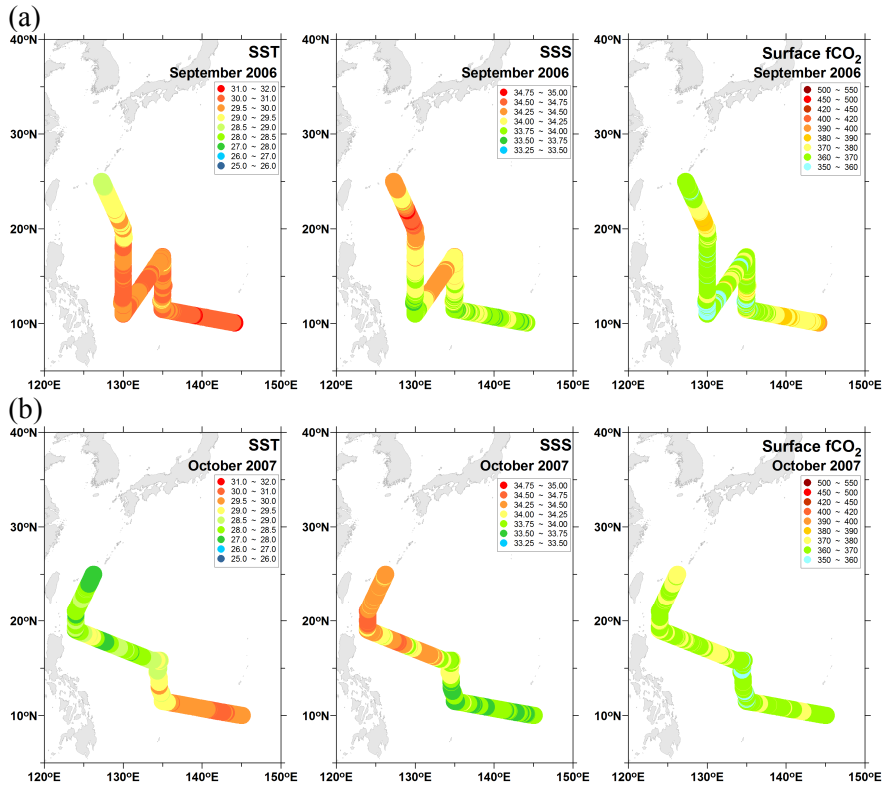

Figure 3.23. Surface distributions of temperature, salinity, and fCO_2 in the western North Pacific in (a) September 2006 and (b) October 2007.

September-October observations, ΔfCO_2 (T_{obs}-T_{ave}), ΔfCO_2 (S_{obs}-S_{ave}), and $\Delta NfCO_2$ (T_{ave}, S_{ave}) varied in smaller ranges rather than those in May-June observations (Fig. 3.24). All of $TER_{spatial}$ exceeded 0.5, from 0.53 to 0.69, and then SST and SSS would be the major factors to control the spatial distributions in the western North Pacific in September 2006 and October 2007 (Fig. 3.24).

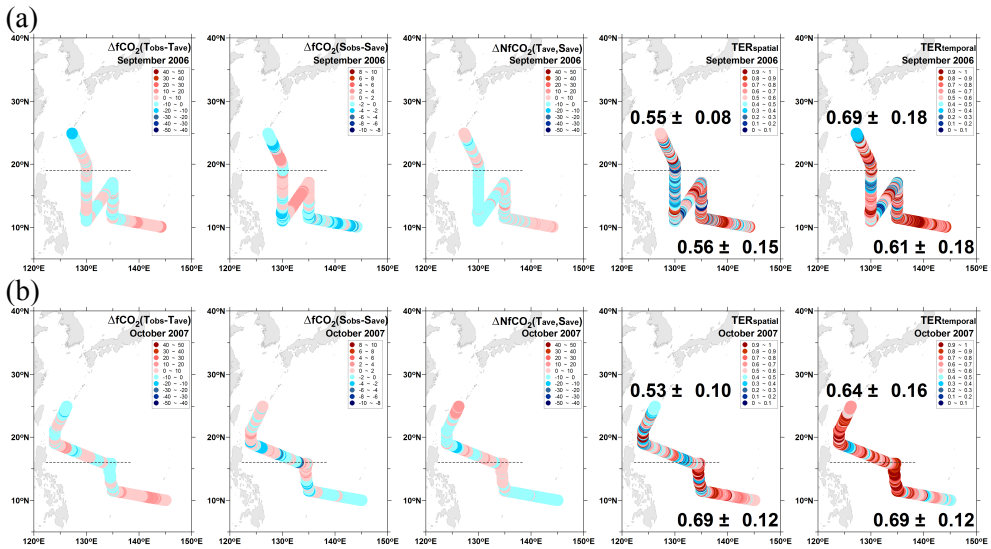

Figure 3.24. Surface distributions of ΔfCO_2 (T_{obs}-T_{ave}), ΔfCO_2 (S_{obs}-S_{ave}), $\Delta NfCO_2$ (T_{ave}, S_{ave}), $TER_{spatial}$, and $TER_{seasonal}$ in the western North Pacific in (a) September 2006, and (b) October 2007. The figures in $TER_{spatial}$ and $TER_{temporal}$ represent the mean ± standard deviation (S.D.), lower one for southern area (North Equatorial Current, NEC) and upper one for subtropical gyre (Terms are defined in 2.4). Dashed lines represent the boundary between North Equatorial Current (NEC) and subtropical gyre in each observation period.

Chapter 4 Discussions

4.1 The Ulleung Basin of the East Sea

- Factors influencing the seasonal variability of surface fCO_2

During the four seasonal surveys, the spatial mean SST showed a large variation of 13.2°C, while the spatial mean SSS showed a variation of 1.32 (Table 4.1). To validate the major influences of SST and SSS on surface fCO_2, we plotted the $TER_{seasonal}$ for the four seasonal surveys (Figs. 3.3e, 3.5e, 3.8e, and 3.11e). $TER_{seasonal}$ were 0.50 ± 0.09, 0.79 ± 0.08, 0.68 ± 0.05, and 0.40 ± 0.02 in the spring, summer, autumn, and winter, respectively. SST and SSS played major roles to control surface fCO_2 in autumn and especially in summer. In the northern reaches of the South China Sea, however, the seasonal variations of surface fCO_2 were mainly influenced by the seasonal variations of SST (Zhai *et al*., 2005). In the northern ECS, where the Kuroshio passed through, the seasonal variations in surface fCO_2 were affected by the seasonal changes in SST (Shim *et al*., 2007).

The measured surface fCO_2 values in spring and winter were not significantly different from those in summer and autumn, despite the large differences in SST (Table 4.1). Considering only the temperature effect of 4.23% $^{o}C^{-1}$ (Takahashi *et al*., 1993), the surface fCO_2 would show a difference of about 200 μatm between winter and summer. However, the seasonal variation of surface

Table 4.1. Seasonal surface water properties of the Ulleung Basin of the East Sea. Potential Energy Anomaly (PEA) represents the degree of stratification in the water column. Higher PEA indicates more stable water column by well-stratification.

Seasons	**SST (℃)**	**SSS (psu)**	**Surface fCO_2 (μatm)**	**PEA (J m^{-2})**
Spring	10.73±0.44	34.38±0.08	309.4±29.7	0.25±0.28
Summer	23.87±0.93	33.33±0.27	371.5±26.3	4.22±0.31
Autumn	22.26±0.67	33.06±0.26	320.3±10.5	3.85±0.71
Winter	11.90±1.12	34.15±0.11	333.3±13.4	0.18±0.22

fCO_2 was attenuated to 62 μatm (Table 4.1). The damped seasonal variability of surface fCO_2 resulted from several processes, such as vertical and lateral mixing, biological activity, and sea-air CO_2 exchange (Murata and Takizawa, 2003; Shim *et al*., 2006). We plotted the relationships among $\Delta N fCO_2$ (T_{ave}, S_{ave}), SST, and SSS obtained during the four seasonal surveys (Fig. 4.1). A good inverse relationship between $\Delta N fCO_2$ (T_{ave}, S_{ave}) and SST in winter represented non-thermodynamic increment of surface fCO_2 by vertical mixing.

To elucidate the effects of vertical mixing on the surface fCO_2, the degree of stratification in the water column was calculated using the potential energy anomaly (PEA; Simpson *et al*., 1977; Shim *et al*., 2007). The low PEA indicated that the water column was unstable and well mixed. PEA was an order of magnitude higher in summer and autumn than in winter and spring (Table 4.1), indicating that the water column was unstable and well mixed in winter and spring. Low $TER_{seasoal}$ in winter and spring were consistent with low PEA. In winter and spring, therefore, the active vertical mixing brought CO_2-rich subsurface waters to the surface, and thus caused the high surface fCO_2. Shim *et al*. (2007) explained the high surface fCO_2 observed in the ECS during spring and autumn by vertical mixing with CO_2-rich water masses. Consequently, the small seasonal variability of surface fCO_2 was ascribed to the high surface fCO_2 due to active vertical mixing in winter and spring.

The TWC entered the ES through the Korea Strait, transporting warm and salty water into the study area (Chang *et al*., 2004). The TWC branched from the

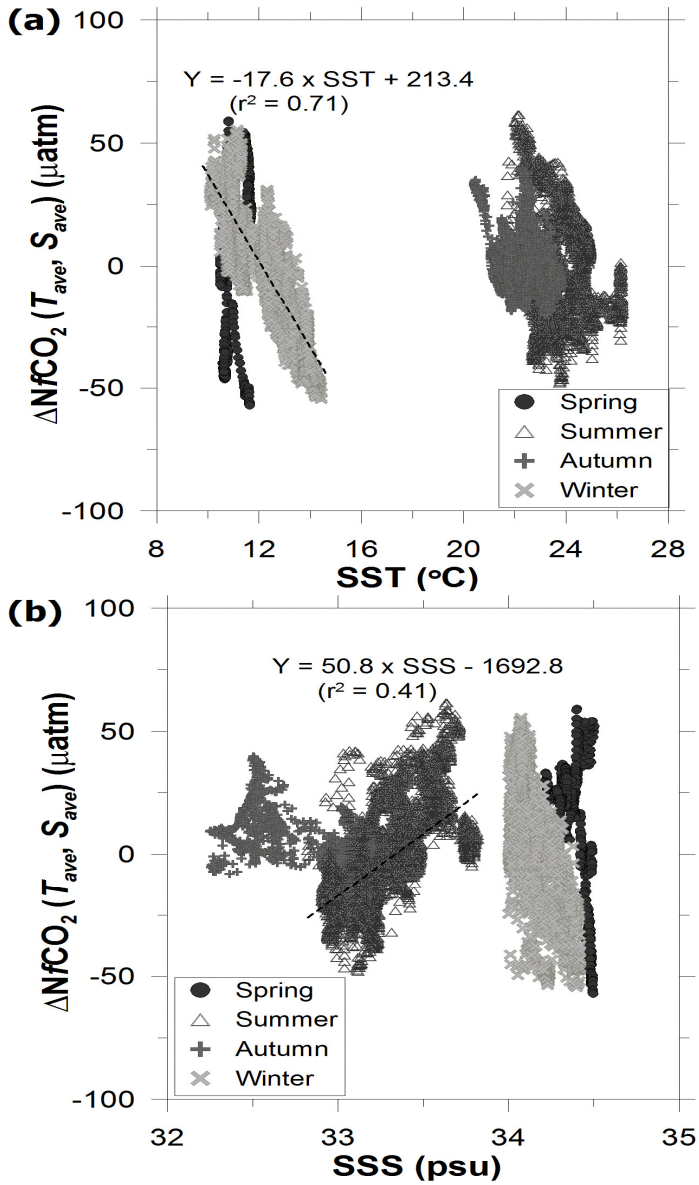

Figure 4.1. Relationships between $\Delta NfCO_2$ (T_{ave}, S_{ave}) and (a) SST and (b) SSS in the Ulleung Basin of the East Sea during the four seasonal surveys.

Kuroshio and passed through the ECS before entering the study area. Kim *et al*. (2012) measured the surface fCO_2 in the northern ECS during four seasons; the spatial mean fCO_2 values were 311±31 μatm in spring, 309±53 μatm in summer, 376±37 μatm in autumn, and 335±17 μatm in winter. To identify the effects of lateral advection on the surface fCO_2, the spatial mean surface fCO_2 values measured in the study area were compared with those in the ECS during four seasons (Table 4.1). In winter and spring, the surface fCO_2 values measured in the study area were rather similar to those in the ECS. However, they were somewhat higher in summer and lower in autumn than those in the ECS. In summer, the TWC Water with lower surface fCO_2 was transported into the study area. A relationship between $\Delta N fCO_2$ (T_{ave}, S_{ave}) and SSS in summer represented decline of non-thermodynamic changes on surface fCO_2 by intrusion of low-salinity and low-fCO_2 waters into the study area. Therefore, the small seasonal variability of surface fCO_2 resulted from the lateral transport of water masses with lower surface fCO_2 in summer.

In Figure 3.4, the relationship of what was random, indicating that the seasonal variation of the surface fCO_2 was not affected by biological activities. The primary production estimated in the study area also showed little seasonal variation (Noh, personal communication). Therefore, the small seasonal variability of surface fCO_2 was not related to the biological activity.

Surface fCO_2 is also influenced by the sea-air CO_2 exchange. The changes in surface fCO_2 due to sea-air CO_2 exchange were quantitatively estimated from the

mean seasonal mixed layer depths (MLD; 70, 25, 50, and 92 m in spring, summer, autumn, and winter, respectively; the estimates were calculated from hydrocasting CTD data in each observation), surface mean DIC (2000 μmole kg^{-1}; from Park *et al*, 2006), and the Revelle factor (10; the global mean value). Values of 20.7, -1.7, 11.0, and 21.7 μatm were found for spring, summer, autumn, and winter, respectively. The increase in surface fCO_2 due to sea-air CO_2 exchange was largest in winter, the season with the highest CO_2 influx (Table 4.2). In summer, however, the surface fCO_2 decreased slightly by CO_2 outflux. Therefore, the small seasonal variability of surface fCO_2 was influenced, to some extent, by the sea-air CO_2 exchange.

4.2 The northern East China Sea

4.2.1 Interannual variation of sea-air ΔfCO_2

Sea-air ΔfCO_2 showed a slight difference between the two spring observations; ΔfCO_2 values were negative across the entire study area in April 2008, but positive values were found in the western part in May 2004 (Fig. 3.12). Shim *et al.* (2007) suggested that high surface fCO_2 in the northern ECS during spring resulted from vertical mixing with CO_2-enriched subsurface waters. Thus, the positive ΔfCO_2 in May 2004 was attributed to vertical mixing. In April 2008, the western part showed

Table 4.2. Sea-air differences of CO_2 fugacity (ΔfCO_2), wind speeds, and sea-air CO_2 flux in the Ulleung Basin of the East Sea during the four seasonal observations

Seasons	**ΔfCO_2 [a] (μatm)**	**Wind Speed [b] (m sec^{-1})**	**Sea-air CO_2 Flux [c] (mmol C m^{-2} day^{-1})**
Spring	-62.3 ± 32.4	8.10 ± 1.70	-10.4 ± 5.43
Summer	2.51 ± 22.1	6.50 ± 2.88	0.26 ± 2.29
Autumn	-55.0 ± 9.96	5.31 ± 2.34	-3.83 ± 0.70
Winter	-48.9 ± 13.4	10.3 ± 5.04	-13.3 ± 3.62
Annual mean			-6.83 ± 5.03[d] (-2.49 ± 1.84 mol C m^{-2} yr^{-1})

[a] Mean ΔfCO_2 along the cruise tracks expressed as the mean ± standard deviation (S.D.)

[b] Mean wind speed of the study area (35~37.5°N, 129~132°E) from QuikSCAT satellite data during each observation period, expressed as the mean ± S.D.

[c] Mean sea-air CO_2 fluxes based on the transfer coefficient of Wanninkhof (1992), expressed as the mean ± S.D. Positive values represent CO_2 emission from the sea to the atmosphere, while negative values represent CO_2 absorption from the atmosphere to the sea.

[d] Annual mean sea-air CO_2 flux was calculated from sigmoid function which has the least residuals as follows,

$$Flux = 6.82 \times \cos[(month-7.91)/1.8] - 6.55$$

where Flux is monthly mean sea-air CO_2 flux.

high surface Chl-*a* concentrations (up to 8.1 mg m^{-3}), which reinforced CO_2 uptake by photosynthesis. This strong biological activity probably offset the increase in surface fCO_2 from vertical mixing and led to the negative ΔfCO_2 in this region. SSTs in the western part were approximately 2.0°C lower in April 2008 than in May 2004, which also decreased the surface fCO_2 and led to negative ΔfCO_2 in this region. The areal mean ΔfCO_2 in April 2008 was almost two times lower than in May 2004, probably because of the differences in SST. The areal mean SST was higher by about 3.0°C in May 2004 than in April 2008, which would increase fCO_2 by 48 μatm in the study area considering the coefficient of 4.23% $°C^{-1}$ (Takahashi *et al*., 1993), which is rather similar to the difference (39 μatm) in the areal mean ΔfCO_2 between May 2004 and April 2008.

The two summer observations of sea-air ΔfCO_2 also differed. In July 2006, ΔfCO_2 was negative across the entire study area, except for the frontal area, but in August 2003 positive values were found in the eastern part (Fig. 3.15). In summer, the strong CO_2 sink in the western part was ascribed to low SSS in the region, as supported by previous observations of lower fCO_2 in less saline surface waters in the ECS during summer (Tsunogai *et al*., 1999; Wang *et al*., 2000; Shim *et al*., 2007; Chou *et al*., 2009; Zhai and Dai, 2009). In the study area, the less saline surface waters in summer were mainly originated from the Changjiang plume (Kim *et al*., 2009). The positive ΔfCO_2 in August 2003 may have been associated with high SSTs in the eastern part, which increased the surface fCO_2 and led to oversaturation with respect to atmospheric CO_2. In July 2006, negative ΔfCO_2 in

the eastern part was probably due to lower SSTs, which were approximately 4°C lower than in August 2003. The areal mean ΔfCO_2 was lower by 44 μatm in July 2006 than in August 2003, probably resulting from differences in SSTs. The areal mean SST was 2.9°C higher in August 2003 than in July 2006, which would increase fCO_2 by 46 μatm in the study area considering the coefficient of 4.23% $°C^{-1}$ (Takahashi *et al*., 1993).

The two autumn observations, while only a month apart, showed a slight difference in the sea-air ΔfCO_2 (Fig. 3.17). The areal mean ΔfCO_2 differed by only 7.8 μatm between the two autumn observations (Table 3.2). SST and SSS displayed some differences, especially in the western part of the study area. The areal mean SST and SSS were 2.3°C and 0.5 higher in October 2004 than in November 2005, respectively. Surface Chl-*a* and nitrate concentrations were higher in November 2005 than in October 2004. Lower SSTs and SSSs and higher surface Chl-*a* concentrations in November 2005 might have decreased the surface fCO_2 and led to the lower ΔfCO_2. However, higher surface nitrate concentrations may indicate more active vertical mixing with CO_2-enriched subsurface waters, which would increase the surface fCO_2 and offset the fCO_2 decrease by the lower SSTs and SSSs and higher surface Chl-*a* concentrations. Kim *et al.* (2009) suggested that the high surface nitrate concentrations in the northern ECS during autumn resulted from vertical mixing with nutrient-enriched subsurface waters.

4.2.2 Seasonal variation of sea-air ΔfCO_2

The sea-air ΔfCO_2 displayed unique seasonal variation in the northern ECS. In spring and autumn, ΔfCO_2 was positive in the western part and negative in the eastern part, whereas the opposite trend was found in summer. In spring and autumn, the water column was less stratified and thus vertical mixing was active, especially in the western part where water depths were less than 50 m (Figs. 4.2 and 4.3). In spring and autumn, therefore, the positive ΔfCO_2 in the western part resulted from active vertical mixing with the CO_2-enriched bottom waters. Shim *et al.* (2007) also attributed the high surface fCO_2 in the western part during spring and autumn to vertical mixing with CO_2-rich water masses. Tsunogai *et al*. (1999) found high surface fCO_2 levels, above atmospheric CO_2 levels, in the western ECS in November 1995 and suggested that this was caused by turbulent mixing of the surface water with CO_2-rich subsurface water. In the eastern part where water depths were relatively deep (~100 m), vertical mixing in spring and autumn was limited to the upper 50 m, where CO_2 was not fully enriched (Peng *et al.*, 1999). Therefore, the surface fCO_2 in the eastern part was not sufficiently increased by vertical mixing, and negative ΔfCO_2 was observed in spring and autumn.

In summer, the water column was strongly stratified (Fig. 4.2) and therefore surface fCO_2 was not affected by vertical mixing. The surface fCO_2 in the ECS during summer was mainly determined by SST and SSS (Tsunogai *et al*., 1999; Wang *et al*., 2000; Shim *et al*., 2007; Chou *et al*., 2009). In summer, both SST and SSS were much higher in the eastern part than in the western part, which led to

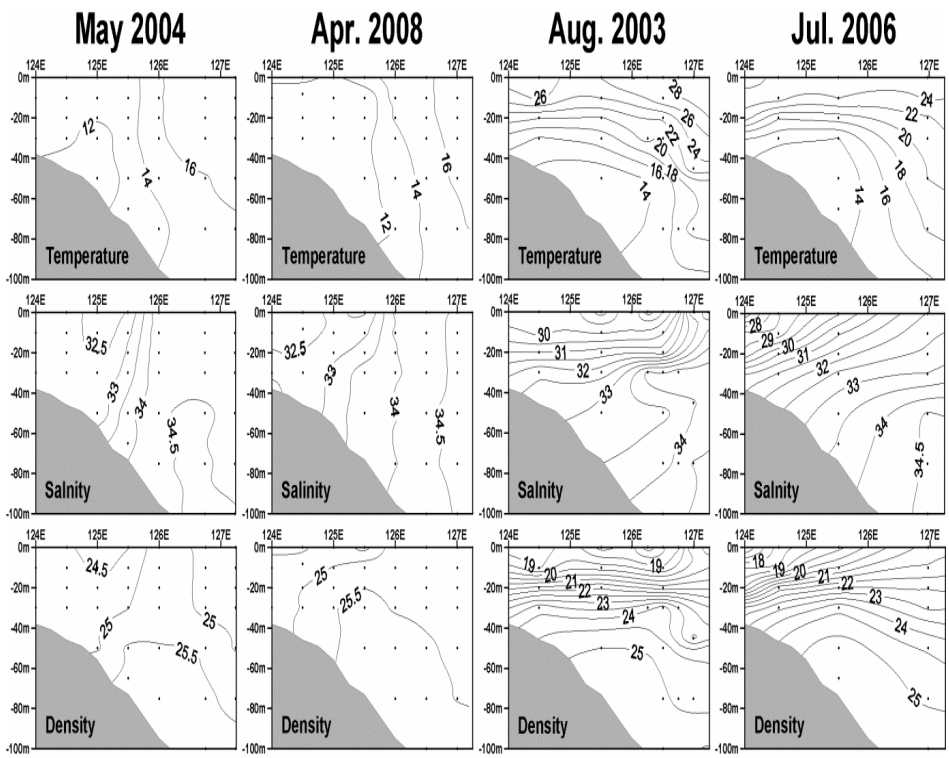

Figure 4.2. Vertical distributions of temperature, salinity, and density in the northern East China Sea in spring and summer. Data obtained in August 2003 and May 2004 are from Shim *et al*. (2007).

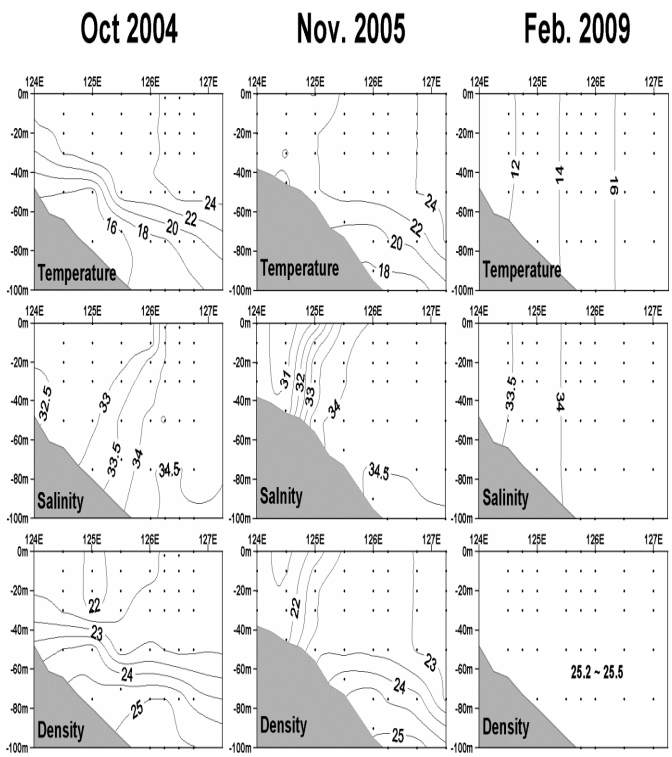

Figure 4.3. Vertical distributions of temperature, salinity, and density in the northern East China Sea in autumn and winter. Data obtained in October 2004 and November 2005 are from Shim *et al*. (2007).

positive ΔfCO_2 in the eastern part and negative ΔfCO_2 in the western part. The relatively high surface Chl-*a* concentrations in the western part may have been responsible for the negative ΔfCO_2 in this region. Tsunogai *et al.* (1999) also found that the Kuroshio water was oversaturated with respect to atmospheric CO_2, but the region off the Changjiang was undersaturated.

In winter, the water column in the study area was completely mixed from the surface to the bottom (Fig. 4.3). Although there was active vertical mixing, values of ΔfCO_2 were negative across the entire study area, presumably due to low SSTs and sea-air CO_2 exchange. In the two autumn observations, ΔfCO_2 values were positive in the western part, indicating CO_2 degassing to the atmosphere in this region. Continuous CO_2 degassing from October to January may have reduced surface fCO_2 to the atmospheric CO_2 level. In the northern ECS, wind speeds were highest in winter (Table 3.2), which accelerated the CO_2 degassing in this season. In addition, SSTs were about 10°C lower in winter than in autumn, which may have brought surface fCO_2 below the atmospheric CO_2 level. Zhai and Dai (2009) also reported that surface fCO_2 was lower than the atmospheric fCO_2 level in the outer Changjiang Estuary in winter.

The areal mean sea-air ΔfCO_2 showed large seasonal variation, with maxima in autumn and minima in spring (Table 3.2). The mean ΔfCO_2 in summer was rather similar to that in spring, which was somewhat lower than that in winter. The mean ΔfCO_2 was positive only in autumn and negative in the other seasons. In autumn, temperature gradients disappeared in the upper 40 m, but still had high

values, with a range of 21~25°C in this layer (Fig. 4.3). Thus, stratification was weakened in the surface layer and eventually vertical mixing actively occurred, especially in the western part where water depths were shallower than 50 m. Vertical mixing brought CO_2-enriched bottom waters to the surface and resulted in the positive ΔfCO_2 in autumn. In addition, high SSTs (21~25°C) also contributed to maintaining the positive ΔfCO_2. Zhai and Dai (2009) also reported that autumn was the only season when the outer Changjiang Estuary degassed CO_2 to the atmosphere. They suggested that hypoxic and CO_2-rich bottom waters mixed with surface waters in late autumn, and thus degassed CO_2 to the atmosphere.

4.3 The western North Pacific

- Factors influencing the temporal variability of surface fCO_2

SST is regarded as one of major factors to control the surface fCO_2 in the western NP (Fushimi, 1987; Inoue *et al*., 1995; Ishii *et al*., 2001). To elucidate the temporal variations of SST, we examined the differences between each areal mean SST and the whole areal mean. Though observations did not cover an entire year, there was no seasonality nor any trend of monthly SST changes (Fig. 4.4). There was El Nino as a global event that could arouse an interannual variability of SST especially in the low-latitude tropic Pacific. Figure 4.5 shows time-series of Oceanic Nino Index (ONI) from 2006 to 2010 with our five observation periods (ONI from http://www.cpc.ncep.noaa.gov/products/analysis_monitoring/ensostuff/ensoyears.s

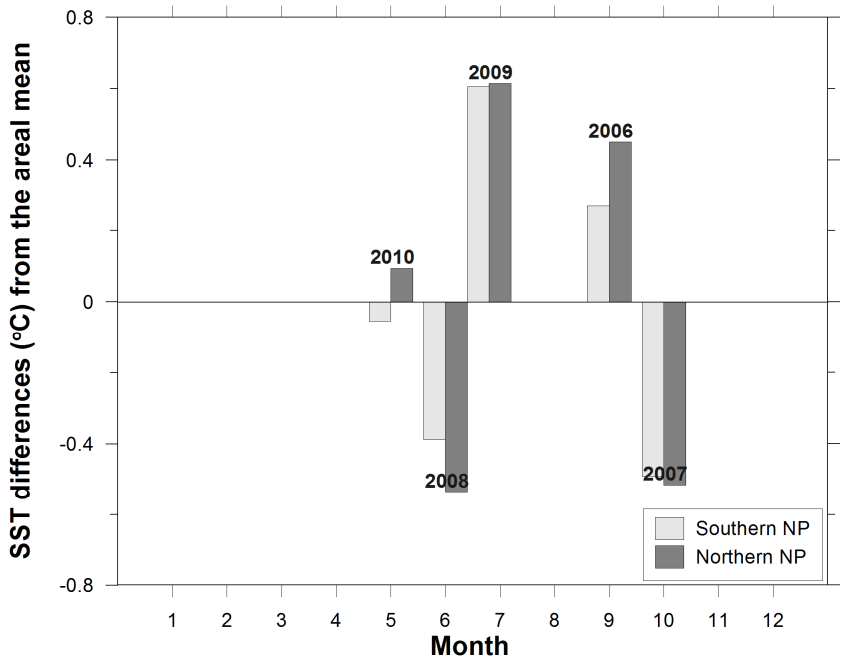

Figure 4.4. The differences between each areal mean sea surface temperature (SST) and the whole areal mean on month in the western North Pacific

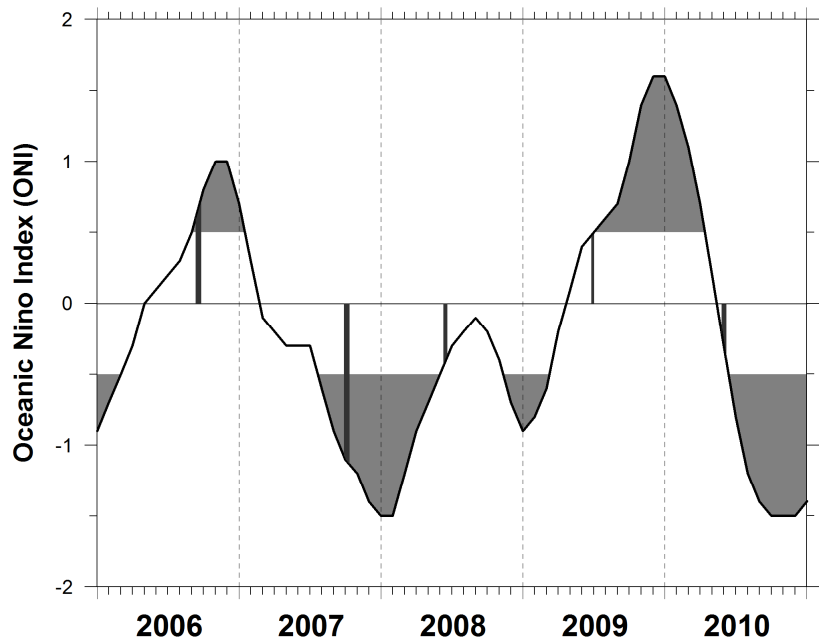

Figure 4.5. Oceanic Nino Index (ONI) from 2006 to 2010 with five observation periods in the western North Pacific (ONI from http://www.cpc.ncep.noaa.gov/products/analysis_monitoring/ensostuff/ensoyears.shtml). The vertical bars represent the observation periods.

html). September 2006 was in El Nino period, whereas October 2007 was in La Nina period. Other three observation periods, June 2008 and 2009 and May 2010, were neither in El Nino nor in La Nina. To examine the ONI effect on SST, relationship between each differences of areal mean SST from the whole areal mean and ONI was shown in Figure 4.6. SST differences from the whole areal mean had a good relationship with ONI (r^2=0.81, $p<0.04$) in both NEC (southern NP) and subtropical gyre (northern NP). Thus, variation of SST in the western NP was mainly controlled by ONI.

To examine the variations of surface fCO_2 by ONI, relationship between $TER_{temporal}$ of each observation and ONI was shown in Figure 4.7. $TER_{temporal}$ did not show a certain relationship with ONI. All of $TER_{temporal}$ were higher than 0.5 and then a half of it were between 0.65 and 0.8 without distinction of ONI. It meant that surface fCO_2 in the western NP was determined by SST and SSS about 65~80% except NEC in June 2008 and subtropical gyre in June 2009, etc. In the western NP, temporal and spatial variations of SST (from 25.8 to 31.6^oC) were larger than those of SSS (from 33.5 to 34.9) in all observation periods. Besides, variation of fCO_2 by thermodynamic changes on SST (4.23% $^oC^{-1}$; about 24.5% of surface fCO_2 changes when SST changes in 5.8 (=31.6-25.8) $^oC^{-1}$; Takahashi *et al*., 1993) is also larger than those on SSS ($(\sigma pCO_2/\sigma S)(S/pCO_2)$=0.94; about 3.8% of surface fCO_2 changes when SSS changes in 1.4 (=34.9-33.5); Takahashi *et al*., 1993). Thus, thermodynamic changes of surface fCO_2 could reflect those by SST changes rather than SSS changes in the western NP.

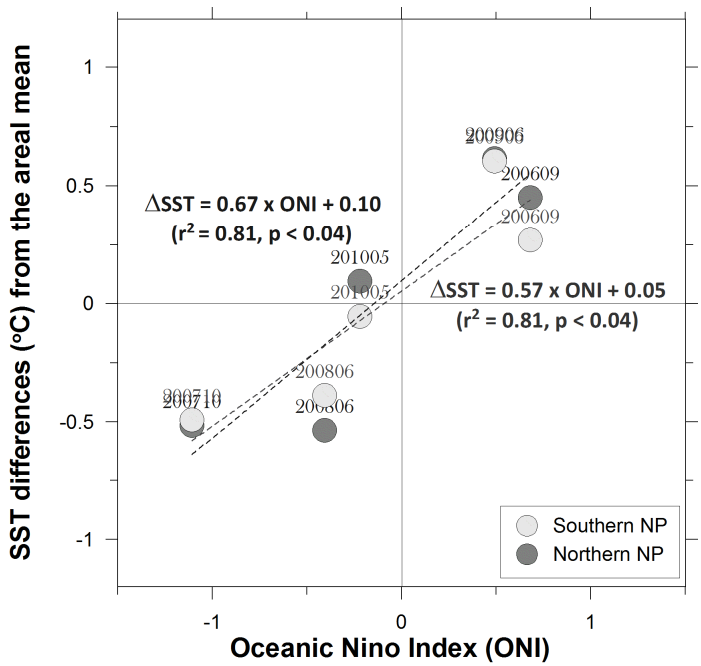

Figure 4.6. Relationship between sea surface temperature (SST) differences of each areal mean from the whole areal mean and Oceanic Nino Index (ONI) in the western North Pacific.

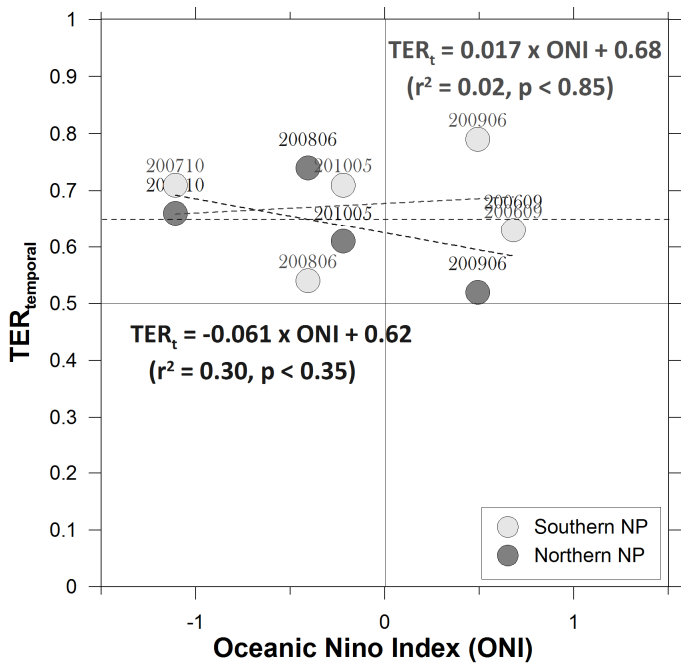

Figure 4.7. Relationship between $TER_{temporal}$ of each observation and Oceanic Nino Index (ONI) in the western North Pacific.

The western NP is one of oligotrophic area among global oceans in particular (Fig. 4.8). Nevertheless, biological activity is one of only a few processes to reduce the surface fCO_2. Chl-*a* concentrations of surface seawater were in a very low ranges from 0.040 to 0.070 mg m^{-3} (Noh *et al*., 2006, 2007, 2009, and 2010). However, due to the deep euphotic depth, primary productivity were not as low as surface Chl-*a*, ranging from 196.15 to 359.7 mg C m^{-2} day^{-1} (Noh *et al*., 2006, 2007, 2009, and 2010). Both surface Chl-*a* concentrations and primary productivity showed more or less negative correlation with ONI (Fig. 4.9). Biological activity in this area seemed to be influenced by inflow from the productive eastern equatorial Pacific. Biological activity might affect to reduce the surface fCO_2 in May 2010, while it might rarely in September 2006 and June 2009.

MLD is an important parameter to understand the surface fCO_2 variations. Generally deepening of MLD led to increase of surface fCO_2 by entrainment of CO_2-rich subsurface water to surface mixed layer. MLD during the observations were varied from 16.3 to 57.5 m (Fig. 4.10). Although it was known that MLD in winter was generally deeper than that in summer (Ishii *et al*., 2001), it was not clear in our results. MLD of NEC was deeper than that of subtropical gyre except May 2010. There were negative correlations in some degree between MLD in both areas and ONI (Fig. 4.11). It meant that MLD went deeper in La Nina periods. There were also less negative correlations between MLD and surface fCO_2 in both areas (Fig. 4.12). It indicated that deep MLD by stack up surface water during La Nina could not lead to increase surface fCO_2. During the observations, MLD did not act

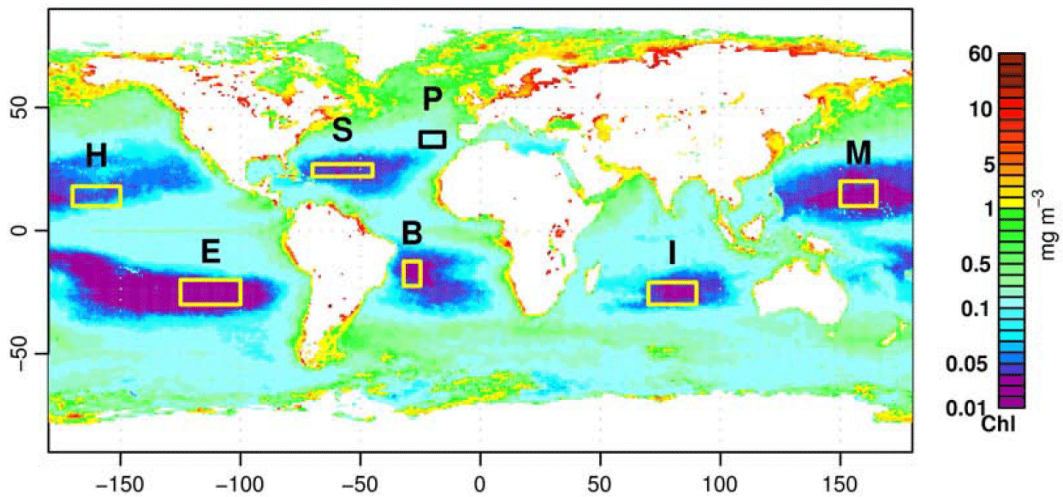

Figure 4.8. Annual composite (year 2006) of SeaWiFS chlorophyll concentration for the global ocean. The yellow boxes superimposed on the maps show the oligotrophic zones (from Morel *et al*., 2010; the quantities are provided and distributed by NASA).

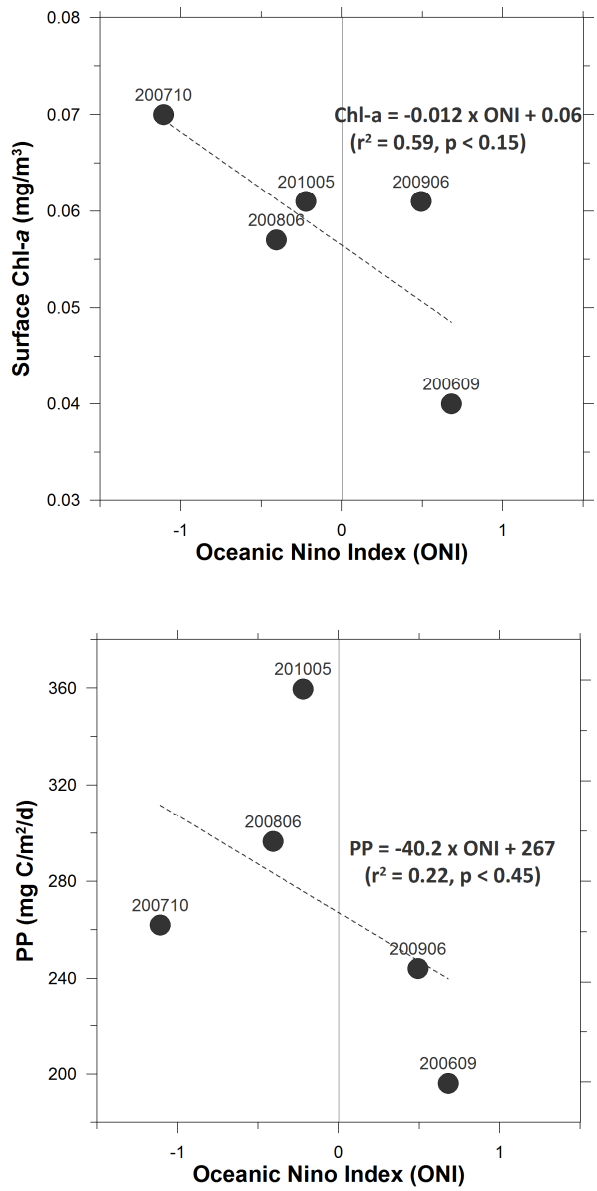

Figure 4.9. Relationship between (a) surface chlorophyll *a* (Chl-*a*) and Oceanic Nino Index (ONI), and (b) primary productivity (PP) and ONI in the western North Pacific.

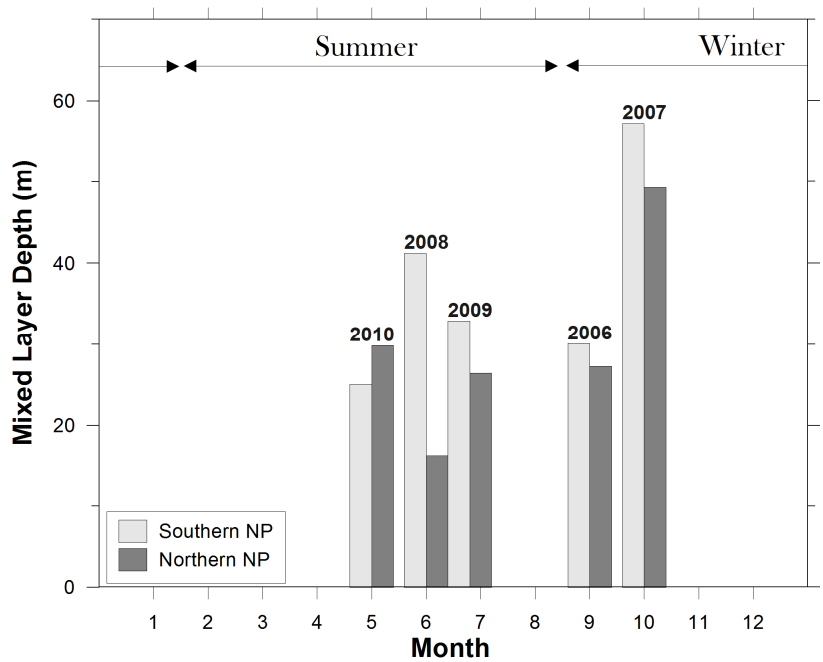

Figure 4.10. Mixed layer depth (MLD) of each area during five observations in the western North Pacific.

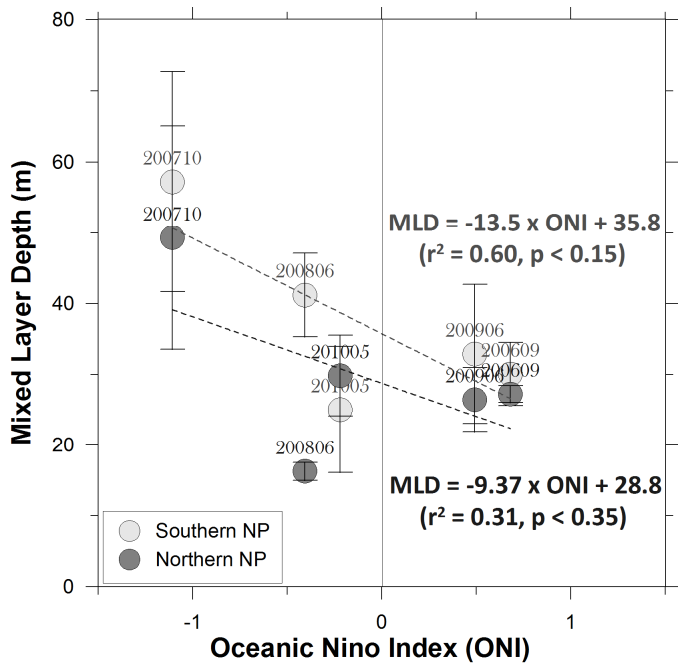

Figure 4.11. Relationship between mixed layer depth (MLD) of each observation period and Oceanic Nino Index (ONI) in the western North Pacific.

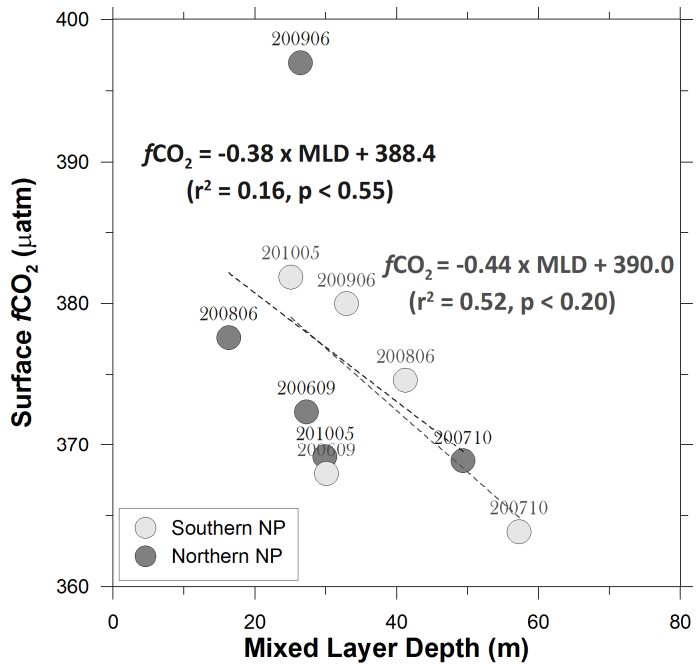

Figure 4.12. Relationship between surface fCO_2 of each observation period and mixed layer depth (MLD) in the western North Pacific.

as a factor to control the temporal variations of surface fCO_2.

Sea-air CO_2 flux through the sea surface could change the surface fCO_2 and reduce the $TER_{temporal}$ in each observation period. Figure 4.13 showed the relationship between $TER_{temporal}$ and absolute amounts of sea-air CO_2 flux in each period. There was a strong negative correlation between $TER_{temporal}$ and absolute amounts of sea-air CO_2 flux, which was over 0.5 mmol C m^{-2} day^{-1}. Thus, sea-air CO_2 flux over 0.5 mmol C m^{-2} day^{-1} induced decrements the variability of surface fCO_2.

4.4 Sea-air CO_2 Fluxes

4.4.1 The Ulleung Basin of the East Sea

Table 4.2 shows the averaged sea-air differences of CO_2 fugacity (ΔfCO_2), wind speeds, and calculated sea-air CO_2 fluxes for the four seasons. There are several kinds of parameterizations of gas exchange coefficient, k (Liss and Merlivat, 1968; Wanninkhof, 1992; Wanninkhof and McGillis, 1999; Naghtingale *et al*., 2000; and Ho *et al*., 2006). Hahm *et al*. (2003) compared 3 kinds of most popular k, k_{LM} by Liss and Merlivat (1986), k_W by Wanninkhof (1992), and k_{WM} by Wanninkhof and McGillis (1999), and reported that k_W was between k_{LM} (about 48~53% of k_W) and k_{WM} (about 110~127% of k_W) and had smallest difference by using long- and short-

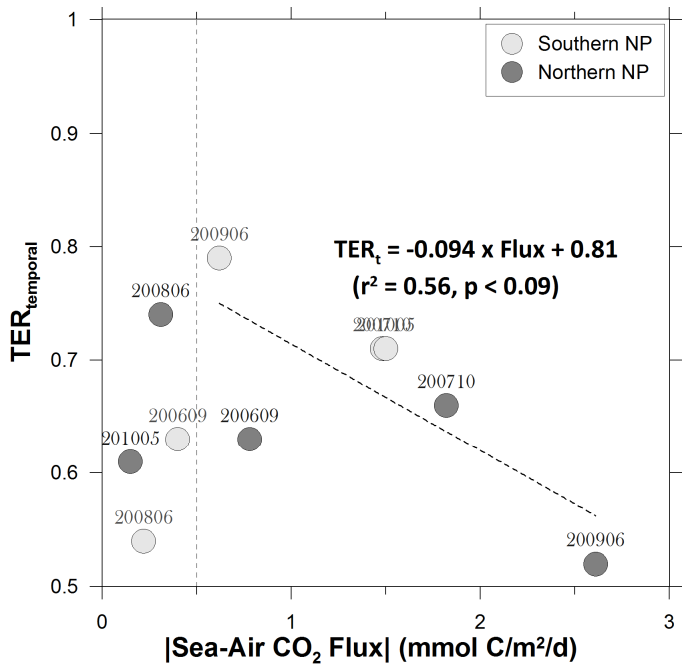

Figure 4.13. Relationship between $TER_{temporal}$ and absolute amounts of sea-air CO_2 flux of each observation period in the western North Pacific. The relationship between $TER_{temporal}$ and absolute amounts of sea-air CO_2 flux was obtained only for the sea-air CO_2 flux larger than 0.5 mmol C m^{-2} day^{-1}.

term wind speed in the East Sea. Thus, CO_2 fluxes were calculated using k_W. The CO_2 fluxes had large seasonal variation. The UB of the ES was a sink of atmospheric CO_2 in spring, autumn, and winter, but a small source of CO_2 to the atmosphere in summer.

In spring, the CO_2 influx (negative sign) was calculated to be 10.4 ± 5.43 mmol C m^{-2} day^{-1}. The lowest ΔfCO_2 was observed in spring among the four seasons, probably due to the spring phytoplankton bloom. Thus, the large CO_2 influx in spring resulted from high biological activities. The calculated CO_2 influx was somewhat higher than that (5.9 mmol C m^{-2} day^{-1}) calculated in the southern part of the ES during April (Oh, 1998).

In summer, the UB of the ES acted as a source of CO_2 to the atmosphere, with CO_2 flux of 0.26 ± 2.29 mmol C m^{-2} day^{-1}, which was almost the same as that (0.33 ± 2.48 mmol C m^{-2} day^{-1}) estimated in August 2005 (Choi *et al*., 2011). The CO_2 outflux was also rather similar to that (1.7 mmol C m^{-2} day^{-1}) calculated for the southern part of the ES in August (Oh, 1998).

In autumn, the CO_2 influx was calculated to be 3.83 ± 0.70 mmol C m^{-2} day^{-1}. The autumn ΔfCO_2 was similar to that in spring, but the autumn CO_2 influx was less than half that in spring due to the low wind speed (Table 4.2). The CO_2 influx was quite similar to that (2.9 mmol C m^{-2} day^{-1}) calculated in the southern ES in October (Oh, 1998).

The largest CO_2 influx (13.3 ± 3.62 mmol C m^{-2} day^{-1}) was estimated in winter (Table 4.2). This high CO_2 influx was mainly attributable to high wind

speeds in winter, because the winter ΔfCO_2 was higher than that in spring or autumn (Table 4.2). The winter CO_2 influx was somewhat lower than that (17.4 mmol C m^{-2} day^{-1}) calculated for the southern part of the ES in February (Oh, 1998).

The annual integrated sea-air CO_2 flux in the UB of the ES was -2.47 ± 1.26 mol C m^{-2} yr^{-1} (Table 4.2), quite similar to the previous estimate (-2.2 mol C m^{-2} yr^{-1}) for the southern ES (Oh, 1998). The annual CO_2 uptake rate in this study area was considerably larger than the estimate for worldwide continental shelves (-1.1 mol C m^{-2} yr^{-1}; Chen and Borges 2009) and the global mean (-0.51 mol C m^{-2} yr^{-1}; Takahashi *et al*., 2009). Kim *et al*. (2012) reported that the annual sea-air CO_2 flux in the northern ECS was -2.2 ± 2.1 mol C m^{-2} yr^{-1}, which is comparable to our result. Therefore, the UB of the ES, like the ECS, acts as a strong sink of atmospheric CO_2.The UB of the ES is much deeper basin than the northern ECS. But the CO_2 fluxes were similar magnitude because there is a certain degree of mixing barrier between warm surface waters flows into the UB of the ES through the Korea Strait and exiting subsurface waters.

4.4.2 The northern East China Sea

Table 3.2 displays the areal mean sea-air ΔfCO_2, monthly averaged wind speeds, and the calculated sea-air CO_2 fluxes for the seven expeditions. The calculated CO_2 flux results indicate that the northern ECS was a sink of atmospheric CO_2 in spring,

summer, and winter, but a small source of CO_2 to the atmosphere in autumn.

Spring CO_2 influxes (negative sign) were 5.1 ± 4.3 and 8.4 ± 1.9 mmol C m^{-2} day^{-1} in May 2004 and April 2008, respectively (Table 3.2). The higher CO_2 influx in April 2008 was presumably associated with the lower SSTs and higher biological activity compared with those of May 2004. The average CO_2 influx in spring was 6.8 ± 4.3 mmol C m^{-2} day^{-1}, which was somewhat lower than that (8.8 ± 5.8 mmol C m^{-2} day^{-1}) calculated for the outer Changjiang Estuary during spring (Zhai and Dai, 2009), but higher than that (5.8 ± 7.7 mmol C m^{-2} day^{-1}) estimated for the ECS during spring (Peng *et al*., 1999).

In summer, the two estimates of sea-air CO_2 flux did not differ much, despite the large difference in ΔfCO_2 (Table 3.2). The average CO_2 influx in summer was 6.6 ± 8.5 mmol C m^{-2} day^{-1}, rather similar to that in spring. The summer CO_2 influx was somewhat higher than that (4.9 ± 4.0 mmol C m^{-2} day^{-1}) for the outer Changjiang Estuary during summer (Zhai and Dai, 2009) and similar to that (6.3 ± 3.7 mmol C m^{-2} day^{-1}) estimated for the ECS during summer, excluding the coastal upwelling area that was the most important CO_2 source in the ECS (Chou *et al.*, 2009).

In autumn, the northern ECS emitted CO_2 to the atmosphere at a rate of 0.81 ± 7.3 mmol C m^{-2} day^{-1} (Table 3.2). Tsunogai *et al*. (1997) reported that the ECS was undersaturated with respect to atmospheric CO_2 in autumn, and thus absorbed CO_2 from the atmosphere. However, Tsunogai *et al.* (1999) found high surface fCO_2, above the atmospheric CO_2 level, at the continental shelf zone of the ECS in

November 1995. Zhai and Dai (2009) also reported that CO_2 was emitted at a rate of 2.9 ± 2.5 mmol C m^{-2} day^{-1}, more than three times our estimate, in the outer Changjiang Estuary during autumn.

The largest CO_2 influx (12 ± 4.1 mmol C m^{-2} day^{-1}) occurred in winter (Table 3.2). This high CO_2 influx can mainly be attributed to high wind speeds in winter, because the winter ΔfCO_2 in water was lower than those in spring and summer. Shim *et al*. (2007) assumed that the winter CO_2 flux in the northern ECS was an intermediate value (-2.3 mmol C m^{-2} day^{-1}) between spring and autumn; their estimate was about five times lower than our estimate. Zhai and Dai (2009) reported that CO_2 flux was -10 ± 2.3 mmol C m^{-2} day^{-1} in the outer Changjiang Estuary during winter, which was somewhat similar to our estimate.

The annually integrated sea-air CO_2 flux in the northern ECS was -2.2 ± 2.1 mol C m^{-2} yr^{-1} (Table 3.2), more than two times a previous estimate (-0.87 mol C m^{-2} yr^{-1}) for the northern ECS (Shim *et al*., 2007). This large difference was presumably responsible for the underestimation of winter CO_2 influx, which was assumed as an arithmetic mean of autumn and spring fluxes by Shim *et al*. (2007) and the large intraseasonal variation of CO_2 flux. High-resolution temporal observations are the only way to overcome misleading results caused by large intraseasonal variations. Our estimate was rather similar to previous estimates for the ECS (2.0~3.0 mol C m^{-2} yr^{-1}) (Tsunogai *et al*., 1997, 1999; Chen and Wang, 1999; Wang *et al*., 2000). Zhai and Dai (2009) estimated annually integrated CO_2 flux in the outer Changjiang Estuary to be 1.9 mol C m^{-2} yr^{-1} based on seven field

surveys, but this estimate was confined to the western part of the ECS where Kuroshio water was not observed. The annually integrated CO_2 flux for worldwide continental shelves was -1.1 mol C m^{-2} yr^{-1} on average (Chen and Borges, 2009), which was lower than the CO_2 influx estimated for the ECS. Therefore, the ECS acts as a strong sink for atmospheric CO_2 in comparison to other continental shelves.

4.4.3 The western North Pacific

Table 4.3 displays the areal mean SST, SSS, surface fCO_2, and the calculated sea-air CO_2 fluxes for the five observations. In May 2010, sea-air CO_2 fluxes were 1.50 ± 1.01 mmol C m^{-2} day^{-1} and -0.15 ± 0.78 mmol C m^{-2} day^{-1} in the NEC and subtropical gyre, respectively. In the NEC, ocean emitted CO_2 to the atmosphere, while, in the subtropical gyre, ocean absorbed CO_2 from the atmosphere. Reported CO_2 flux in May was rough ranges from -4 to 2 mmol C m^{-2} day^{-1} (Inoue *et al*., 1995) and from -3 to 3 mmol C m^{-2} day^{-1} (Ishii *et al*., 2001), positive in low latitudes and vice versa.

In June 2008 and 2009, all of the calculated CO_2 fluxes were positive outfluxes, i.e. ocean emitted CO_2 to the atmosphere. In the NEC, 0.22 ± 0.96 and 0.62 ± 0.39 mmol C m^{-2} day^{-1} in June 2008 and 2009, respectively (Table 4.3). In the subtropical gyre, 0.31 ± 0.80 and 2.61 ± 1.24 mmol C m^{-2} day^{-1} in June 2008 and 2009, respectively. The highest CO_2 outflux in June 2009 was presumably

Table 4.3. Sea surface Temperature (SST), sea surface salinity (SSS), surface fCO_2 and sea-air CO_2 flux in the western North Pacific during the five observations

Period		SST[a] (°C)	SSS[a]	fCO_2 [a] (μatm)	Sea-air CO_2 Flux [b] (mmol C m^{-2} day^{-1})
Sep. 2006	N	29.32±0.26	34.42±0.21	372.4±7.0	0.78±0.67
	S	30.05±0.34	34.05±0.15	368.0±7.2	0.40±0.59
Oct. 2007	N	28.35±0.34	34.34±0.16	368.9±3.5	-1.82±0.57
	S	29.28±0.42	33.85±0.13	363.9±4.2	-1.48±0.66
Jun. 2008	N	28.33±0.47	34.14±0.12	377.6±8.7	0.31±0.80
	S	29.39±0.23	34.17±0.09	374.6±7.3	0.22±0.96
June. 2009	N	29.48±0.60	34.28±0.17	397.0±16.4	2.61±1.24
	S	30.38±0.36	34.37±0.18	380.0±4.5	0.62±0.37
May 2010	N	28.96±0.76	34.62±0.12	386.0±6.5	-0.15±0.78
	S	29.72±0.48	34.70±0.14	396.5±12.5	1.50±1.01

[a] Mean SST, SSS and fCO_2 along the cruise tracks expressed as the mean ± standard deviation (S.D.)

[b] Mean sea-air CO_2 fluxes based on the transfer coefficient of Wanninkhof (1992), expressed as the mean ± S.D. Positive values represent CO_2 emission from the sea to the atmosphere, while negative values represent CO_2 absorption from the atmosphere to the sea.

associated with the higher SSTs and lower biological activity. Reported CO_2 flux of the western NP in June was wide ranges from -2 to 2 mmol C m^{-2} day^{-1} (Inoue *et al*., 1995) and from -3 to 3 mmol C m^{-2} day^{-1} (Ishii *et al*., 2001).

In September 2006, sea-air CO_2 fluxes were 0.40 ± 0.59 mmol C m^{-2} day^{-1} and 0.78 ± 0.67 mmol C m^{-2} day^{-1} in the NEC and subtropical gyre, respectively. Reported CO_2 flux in September was ranges from 0 to 2 mmol C m^{-2} day^{-1} (Inoue *et al*., 1995) and from 0 to 3 mmol C m^{-2} day^{-1} (Ishii *et al*., 2001).

In October 2007, sea-air CO_2 fluxes were both negative, -1.48 ± 0.66 and -1.82 ± 0.57 mmol C m^{-2} day^{-1} in the NEC and subtropical gyre, respectively. Whereas, reported CO_2 flux in October was ranges from 0 to 2 mmol C m^{-2} day^{-1} (Inoue *et al*., 1995) and from 0 to 3 mmol C m^{-2} day^{-1} (Ishii *et al*., 2001). The reversal of CO_2 fluxes might come from lower SST and higher biological activity induced by La Nina.

The calculated CO_2 flux results indicate that the NEC, the southern NP, was a source of atmospheric CO_2 except October 2007. In October, the NEC generally acted as a CO_2 source also. However, in 2007, when it was in La Nina, the NEC acted as a CO_2 sink. The subtropical gyre, the northern NP, was a source of CO_2 in June and September, but a sink of CO_2 to the atmosphere in May and October. La Nina also put the starting time of acting as a CO_2 sink forward to October.

4.5 Distinctions between the Korean marginal seas and the North Pacific

Chen and Borges (2009) reported that the temperate and high-latitude shelves are undersaturated with respect to atmospheric CO_2, while low-latitude shelves are oversaturated. Although the northern ECS belongs to a temperate shelf, it is slightly oversaturated with respect to atmospheric CO_2 in autumn. Even though seasonal processes such as riverine less saline water input in summer and vertical mixing from autumn to spring affected, surface fCO_2 was mainly controlled by SST and SSS, $TER_{seasonal}$ were between 0.62 and 0.94, in the northern ECS. The northern ECS acted as a strong sink of atmospheric CO_2 with annually integrated sea-air CO_2 flux, -2.2 ± 2.1 mol C m^{-2} yr^{-1} (-6.0 ± 5.8 mmol C m^{-2} day^{-1}).

ES is a typical marginal seas and the UB locates adjacent the shallow main entrance of the ES, the Korea Strait. The UB of the ES is slightly oversaturated with respect to atmospheric CO_2 only in summer. There were also some seasonal processes that affected surface fCO_2 such as biological uptake in spring, riverine less saline water input in summer and vertical mixing in autumn and winter. However, the major controlling factors of surface fCO_2 were still SST and SSS, $TER_{seasonal}$ were between 0.50 and 0.79, except in winter ($TER_{seasonal}$ in winter was 0.40). As the northern ECS, the UB of the ES acted as a strong sink of atmospheric CO_2 with annually integrated sea-air CO_2 flux, -2.5 ± 1.8 mol C m^{-2} yr^{-1} (-6.8 ± 5.0

mmol C m^{-2} day^{-1}).

The NP is a part of the largest open ocean on earth. The low-latitude ocean was oversaturated with respect to atmospheric CO_2 during most of the observation periods. Sea-air CO_2 fluxes and partially biological activities seemed to affect surface fCO_2 in the western NP. SST and SSS were also the major controlling factors of surface fCO_2, $TER_{temporal}$ were between 0.52 and 0.79. Sea-air CO_2 fluxes were between -1.8 to 2.6 mmol C m^{-2} day^{-1}. Though sea-air CO_2 fluxes varied both negative and positive ranges, the western NP was also a net CO_2 sink (Takahashi *et al*., 2009).

SST and SSS were the major controlling factors of surface fCO_2, irrespective of location and size of the sea. However, the extent of control was varied from 50 to 94%.

Chapter 5 Summary and Conclusions

Observations from four seasonal cruises showed that the UB of the ES acts as a strong sink for atmospheric CO_2. The sea-air CO_2 flux displayed large seasonal variation, with CO_2 emitted to the atmosphere in summer and absorbed from the atmosphere in other seasons. This finding is consistent with modeling results showing the ES emitting CO_2 into the atmosphere from June to September and absorbing CO_2 from October through May (Oh, 1998; Kang, 1999). In the UB of the ES, the seasonal variation of surface fCO_2 could not be explained solely by seasonal changes in SST and SSS. Considering only the temperature effect of 4.23% $^{o}C^{-1}$, the surface fCO_2 would show a difference of about 200 μatm between winter and summer, but the surface fCO_2 varied only by 62 μatm. The alleviated seasonal variability of surface fCO_2 was attributed to the high surface fCO_2 due to the active vertical mixing in winter, the lateral transport of water masses with the lower surface fCO_2 in summer, and the sea-air CO_2 exchange. The UB of the ES adsorbed atmospheric CO_2 at an annual rate of 2.47 ± 1.26 mol C m^{-2} yr^{-1}, which was comparable with the previous model result (-2.2 mol C m^{-2} yr^{-1}) for the southern ES (Oh, 1998). The annually integrated CO_2 flux for worldwide continental shelves was -1.1 mol C m^{-2} yr^{-1} (Chen and Borges, 2009), which was less than half the CO_2 influx estimated for the UB of the ES. Therefore, the UB of the ES acts as a strong sink for atmospheric CO_2 compared to other continental shelves.

Based on observations from seven research cruises with high temporal and spatial resolution, we showed that the northern ECS acts as an important sink for atmospheric CO_2. The sea-air CO_2 flux displayed large intraseasonal variation, especially in spring when phytoplankton blooms occasionally occurred. Furthermore, CO_2 flux exhibited large interseasonal variation, with CO_2 being emitted to the atmosphere in autumn and absorbed from the atmosphere in other seasons. The CO_2 degassing in autumn was attributable to vertical mixing with CO_2-enriched subsurface waters and relatively high SSTs in this season. In winter, CO_2 influx from the atmosphere was the highest among the four seasons owing to strong winds. The northern ECS adsorbed atmospheric CO_2 at an annual rate of 2.2 ± 2.1 mol C m^{-2}, which was more than double a previous estimate (-0.87 mol C m^{-2} yr^{-1}) for the northern ECS (Shim *et al*., 2007). This large difference probably resulted from underestimation of winter CO_2 influx by Shim *et al*. (2007) and the large interannual variation of CO_2 flux. This study corroborated the suggestion by Chen and Borges (2009) that high-resolution coverage, both temporal and spatial, could provide robust and unbiased estimates of sea-air CO_2 fluxes at continental shelves.

Based on observations from five observations along cruise tracks, we showed that the western NP acts as a CO_2 source to the atmosphere in June and September. Temporal SST variations were heavily associated with ONI. However, ONI was not the immediate cause of temporal variations of surface fCO_2. More than half of the temporal variations of surface fCO_2 were caused by thermodynamic

changes from SST and SSS variability. Up to 65~80% of temporal variations of surface fCO_2 could be explain by thermodynamic changes from SST and SSS variability in half of all the observations. Biological activity might affect to reduce the surface fCO_2 in May 2010, while it might rarely in September 2006 and June 2009. Though MLD was deepening with reversal ONI, deep MLD in La Nina could not lead to increase surface fCO_2. Sea-air CO_2 flux (over 0.5 mmol C m^{-2} day^{-1}) induced decrements the variability of surface fCO_2. The NEC, southern area, acted as a source of CO_2 to the atmosphere from May to September, 0.22 ~ 1.5 mmol C m^{-2} day^{-1}. In October, the NEC generally acted as a CO_2 source also. However, in 2007, when it was a La Nina, the NEC acted as a CO_2 sink, -1.48 mmol C m^{-2} day^{-1}. The subtropical gyre, southern area, acted as a CO_2 source from June to September, 0.31 ~ 2.61 mmol C m^{-2} day^{-1}. While it acted as a CO_2 sink in May and October, -1.82 ~ -0.15 mmol C m^{-2} day^{-1}. La Nina also put the starting time of acting as a CO_2 sink forward in October.

The annual CO_2 uptake rate would be 3.15 x 10^{-3} Pg C yr^{-1} and 2.96 x 10^{-3} Pg C yr^{-1} in the UB of the ES and the northern ECS, respectively. Those were 0.22% and 0.21% of global annual carbon uptake rate, while those were 0.033% and 0.034% of global ocean area. In the western NP, the annual CO_2 uptake rate would be 8.03 x 10^{-2} Pg C yr^{-1}, 5.6% of global carbon uptake rate whereas 8.1% of area (Takahashi *et al*., 2009). The marginal seas around the Korea Peninsula, the UB of the ES and northern ECS, are powerful atmospheric CO_2 sinks about seven times as strong as open ocean, the western NP.

References

Bearsley, R. C., Limeburner, R., Yu, H., Cannon, G. A., 1985. Discharge of the Changjiang (Yangtze River) into the East China Sea. *Cont. Shelf Res.*, **4**, 57–76.

Borges, A. V., Delille, B., Frankignoulle, M., 2005. Budgeting sinks and sources of CO_2 in the coastal ocean: diversity of ecosystems counts. *J. Geophy. Res*., **32**, L14601, doi:10.1029/ 2005GL023053.

Chang, K.-I., Hogg, N. G. ,Suk, M.-S., Byun, S.-K., Kim, Y.-G., Kim, K., 2002. Mean flow and variability in the southwestern East Sea. *Deep-Sea Res. I*, **49**, 2261-2279.

Chang, K.-I., Teague, W. J., Lyu, S. J., Perkins, H. T., Lee, D.-K., Watts, D. R., Kim, Y.-B., Mitchell, D. A., Lee, C. M., Kim, K., 2004. Circulation and currents in the southwestern East/Japan Sea: Overview and review. *Prog. in Oceanogr.,* **61**, 105-156.

Chen, C. T. A., Borges, A. V., 2009. Reconciling opposing views on carbon cycling in the coastal ocean: Continental shelves as sinks and near-shore ecosystems as sources of atmospheric CO_2. *Deep-Sea Res. II*, **56**, 578-590.

Chen, C. T. A., Wang, S. L., 1999. Carbon, alkalinity and nutrient budget on the East China Sea continental shelf. *J. Geophys. Res*., **104**, 20675-20686.

Chen, C., Zhu, J., Beardsley, R. C., Franks, P. J. S., 2003. Physical-biological sources for dense algal blooms near the Changjiang River. *J. Geophy. Res.,* **30**, 1515, doi:10.1029/2002GL016391.

Chern, C.-S., Wang, J., Wang, D.-P., 1990. The exchange of Kuroshio and East China Sea shelf water. *J. Geophys. Res.*, **93**, 16017–16023.

Choi, S.-H., Kim, D., Shim, J. H., Min, H. S., 2011. The spatial distribution of surface fCO_2 in the southwestern East Sea/Japan Sea during summer 2005. *Ocean Sci. J.,* **46**, 13-21.

Choi, S.-H., Kim, D., Shim, J. H., Kim, K. H., Min, H. S., Kim, K. R., 2012. Seasonal variations of surface fCO_2 and sea-air CO_2 fluxes in the Ulleung Basin of the East/Japan Sea. *Terr. Atmos. Ocean. Sci.,* **23**(3), 343-353.

Chou, W.-C., Gong, G.-C., Sheu, D. D., Hung, C.-C., Tseng, T.-F., 2009. Surface distribution of carbon chemistry parameters in the East China Sea in summer 2007. *J. Geophys. Res.*, **114**, C07026, doi:10.1029/ 2008JC005128.

Fushimi, K. 1987. Variation of carbon dioxide partial pressure in the western North Pacific surface water during the 1982/83 El Nino event. *Tellus*, **39B**, 214-227.

Gong, G.-C., Wen, Y.-H., Wang, B.-W., Liu, G.-J., 2003. Seasonal variation of chlorophyll a concentration, primary production and environmental conditions in the subtropical East China Sea. *Deep-Sea Res. II*, **50**, 1219-1236.

Hahm, D., Kim, K.-R., 2008. Observation of bottom water renewal and export production in the Japan Basin, East Sea using tritium and helium isotopes. *Ocean Sci. J.*, **43**(1), 39-48.

Hahm, D., Rhee, T. S., Kang, D.-J., Kim, K.-R., 2003. Influence of gas transfer velocity parameterization on air-sea CO_2 exchange in the East (Japan)

Sea. *J. Korean Soc. Oceanogr.*, **38**(3), 135-142.

Hickox, R., Belkin, I., Cornillon, P., Shan, Z., 2000. Climatology and seasonal variability of ocean fronts in the East China Sea, Yellow and Bohai Seas from satellite SST data. *Geophys. Res. Lett.*, **27** (18), 2945-2948.

Ho, D. T., Wanninkhof, R., Masters, J., Feely, R. A., Cosca, C. E., 1997. Measurement of underway fCO_2 in the eastern equatorial Pacific on NOAA ships Baldrige and Discoverer. NOAA Data Report, ERL AOML-30, 52 p.

Ho, D. T., Law, C. S., Smith, M. J., Schlosser, P., Harvey, M., Hill, P., 2006. Measurements of air-sea gas exchange at high wind speeds in the Southern Ocean: Implications for global parameterizations. *Geophy. Res. Lett.*, **33**, L16611. doi:10.1029/2006GL026817.

Hu, D., 1994. Some striking features of circulation in Huanghai Sea and East China Sea. In: Zhou, D., Liang, Y.-B., Zeng, C.-K. (Eds.), Oceanology of China Seas, Vol. 1. Kluwer Academic, Norwell, pp. 27–38.

Inoue, H., Matsueda, H., Ishii, M., Fushimi, K., Hirota, M., Asanuma, I., Takasugi, Y., 1995. Long-term trend of the partial pressure of carbon dioxide (pCO_2) in surface waters of the western North Pacific, 1984-1993. *Tellus*, **47**, 391-413.

IPCC. 2007. Climate Change 2007: The physical scientific basis: Contribution of working group I to the Fourth Assessment Report of the Intergovernmental Panel on Climate Change. ed. by S. Solomon, D. Qin, M. Manning, M. Marquis, K. Averyt, M. M. B. Tignor, H. L. Miller, Jr., and Z. Chen. Cambridge University Press, Cambridge, U.K. 996 p.

Ishii, M., Inoue, H., Matsueda, H., Saito, S., Sushimi, K., Nemoto, K., Yano, T., Nagai, H., Midorikawa, K., 2001. Seasonal variation in total inorganic carbon and its controlling processes in surface waters of the western North Pacific subtropical gyre. *Mar. Chem*., **75**, 17-32.

Kang, D.-J., 1999. A Study on the Carbon Cycle in the East Sea. Ph.D thesis, Seoul National University, 159 pp.

Kattner, G., 1999. Storage of dissolved inorganic nutrients in seawater: poisoning with mercuric chloride. *Mar. Chem.*, **67**, 61-66.

Keeling, C. D., 1968. Carbon dioxide in surface ocean waters. *J. Geophys. Res.*, **73**(14), 4543-4553.

Kim, D., Choi, S. H., Kim, K. H., Shim, J. H., Yoo, S., Kim, C.-H., 2009. Spatial and temporal variations in nutrient and chlorophyll-*a* concentrations in the northern East China Sea surrounding Cheju Island. *Cont. Shelf Res.*, **29**, 1426-1436.

Kim, D., Choi, S.-H., Shim, J. H., Kim, K.-H., Kim, C.-H., 2012. Seasonal variability of sea-air CO_2 fluxes in the northern East China Sea. *J. Mar. Syst.* (submitted).

Le, K., 1988. A preliminary study of the basic hydrographic features and the current structures off the Changjiang River mouth in the dry season. *Progr. in Oceanogr.*, **21**, 387–400.

Liss, P. S., Merlivat, L., 1986. Air–sea gas exchange rates: Introduction and synthesis, in The Role of Air–Sea Exchange in Geochemical Cycling. edited by P. Buat-Ménard, pp. 113-127, D. Reidel, Dordrecht.

Liu, K.-K., Iseki, K., Chao, S.-Y., 2000. Continental margin carbon fluxes. In: Hanson, R. B., H. W. Ducklow, and J. G. Field (Eds.), The Changing Ocean Carbon Cycle: A Midterm Synthesis of the Joint Global Ocean Flux Study. Cambridge University Press, Cambridge, 187−239.

Min, D.-H., Kim, K.-R., Weiss, R. F., 2002. Decadal-scale changes of ventilation rates in the East Sea (Sea of Japan): a study by the chlorofluorocarbons and a simple model. CREAMS/PICES Symposium, Seoul (available at http://www.utmsi.utexas.edu/staff/min).

Murata, A., Takizawa, T., 2003. Summertime CO_2 sinks in shelf and slope waters of the western Arctic Ocean. *Cont. Shelf Res*., **23**, 753-776.

Nightingale, P. D., Malin, G., Law, C. S., Watson, A. J., Liss, P. S., Liddicoat, M. I., Boutin, J., Upstill-Goddard, R. C., 2000. In situ evaluation of air-sea gas exchange parameterizations using novel conservative and volatile tracers. *Glob. Biogeochem. Cycle*, **14**, 373-387.

Noh, J. H., Choi, D. H., Kim, S. Y., 2006. Biological Oceanography, In: Pacific Ocean Study on Environment and Interactions between Deep Ocean and National seas, KORDI, Seoul, 101-137 (In Korean with English abstract).

Noh, J. H., Choi, D. H., Kim, S. Y., 2007. Biological Oceanography, In: Pacific Ocean Study on Environment and Interactions between Deep Ocean and National seas (POSEIDON), 135-166 (In Korean with English abstract).

Noh, J. H., Choi, D. H., Kim, S. H. 2009. Interrelation of ecosystem structure in the Kuroshio region and in the marginal seas, In: Northwestern Pacific

Ocean Study on Environment and Interactions between Deep Ocean and marginal seas (POSEIDON), 77-98 (In Korean with English abstract).

Noh, J. H., Choi, D. H., Kim, S. H., 2010. Interrelation of ecosystem structure between Kuroshio and marginal seas, In: Northwestern Pacific Ocean Study on Environment and Interactions between Deep Ocean and marginal seas (POSEIDON), 100-118 (In Korean with English abstract).

Noh, J. H., Yoo, S., Lee, J. A., Kim, H. C., Lee, J. H., 2005. Phytoplankton in the waters of the Ieodo Ocean Research Station determined by microscopy, flow cytometry, HPLC pigment data and remote sensing. *Ocean and Polar Res.*, **27**, 379-417 (in Korean, with English abstract).

Oh, D.-C., 1998. A Study on the Characteristics of fCO_2 Distributions and CO_2 Flux at the Air-sea Interface in the Seas around Korea. M.S. thesis, Seoul National University, 92pp.

Omar, A. M., Johannessen, T., Olsen, A., Kaltin, S., Rey, F., 2007. Seasonal and interannual variability of the air-sea CO_2 flux in the Atlantic sector of the Barents Sea. *Mar. Chem.*, **104**, 203-213.

Park, G.-H., Lee, K., Tishchenko, P., Min, D.-H., Warner, M. J., Talley, L. D., Kang, D.-J., Kim, K.-R., 2006. Large accumulation of anthropogenic CO_2 in the East (Japan) Sea and its significant impact on carbonate chemistry. *Global Biogeochem. Cycles,* **20**, GB4013, doi:10.1029/2005GB002676.

Peng, T.-H., Hung, J.-J., Wanninkhof, R., Millero, F., 1999. Carbon budget in the East China Sea in spring. *Tellus*, **51B**, 531-540.

Rios, A. F., Perez, F. F., Alvarez, M., Mintrop, L., Gonzalez-Davila, M., Santana Casiano, J. M., Lefevre, N., Watson, A. J., 2005. Seasonal sea-surface carbon dioxide in the Azores area. *Mar. Chem*., **96**, 35-51.

Sabine, C. L., Feely, R. A., Gruber, N., Key, R. M., Lee, K., Bullister, J. L., Wanninkhof, R., Wong, C. S., Wallace, D. W. R., Tilbrook, B., Millero, F. J., Peng, T.-H., Kozyr, A., Ono, T., Rios, A. F., 2004. The oceanic sink for anthropogenic CO_2. *Science*, **305**, 367-371.

Sarmiento, J. L., Gruber, N., 2002. Sinks for anthropogenic carbon. *Physics today*, **55**(8), 30-36.

Shim, J. H., Kang, Y. C., Kim, D., Choi, S.-H., 2006. Distribution of net community production and surface pCO_2 in the Scotia Sea, Antarctica, during austral spring 2001. *Mar. Chem.,* **101**, 68-84.

Shim, J. H., Kim, D., Kang, Y. C., Lee, J. H., Jang, S.-T., Kim, C.-H., 2007. Seasonal variations in pCO_2 and its controlling factors in surface seawater of the northern East China Sea. *Cont. Shelf Res*., **27**, 2623-2636.

Simpson, J. H., Hughes, D. G., Morris, N. C. G., 1977. The relation of seasonal stratification to tidal mixing on the continental shelf. In: Angel, M. (Ed.), Voyage of Discovery, 327–340.

Strickland, J. D. H., Parsons, T. R., 1972. A Practical Handbook of Seawater Analysis. Fisheries Research Board of Canada, Bulletin No. 167, 2nd edition.

Su, Y., Weng, X., 1994. Water masses in China Sea. In: Zhou, D., Liang, Y.-B., Zeng, C.K. (Eds.), Oceanology of China Sea. Kluwer Academic Publishers, Netherlands, pp. 3–16.

Sverdrup, K., Armbrust, E., 2008. An Introduction to the World's Oceans, 10th edition. McGraw-Hill Higher Education, Boston. 521 p.

Takahashi, T., Olafsson, J., Goddard, J., Chipman, D., Sutherland, S., 1993. Seasonal variations of CO_2 and nutrients in the high-latitude surface oceans: a comparative study. *Glob. Biogeochem. Cycles*, **7**, 843-878.

Takahashi, T., Sutherland, S. C., Wanninkhof, R., Sweeney, C., Feely, R. A., Chipman, D. W., Hales, B., Friederich, G., Chavez, F., Sabine, C., Watson, A., Bakker, D. C. E., Schuster, U., Metzl, N., Yoshikawa-Inoue, H., Ishii, M., Midorikawa, T., Nojiri, Y., Körtzinger, A., Steinhoff, T., Hoppema, M., Olafsson, J., Arnarson, T. S., Tilbrook, B., Johannessen, T., Olsen, A., Bellerby, R., Wong, C. S., Delille, B., Bates, N. R., de Baar, H. J. W., 2009. Climatological mean and decadal change in surface ocean pCO_2, and net sea-air CO_2 flux over the global oceans. *Deep-Sea Res.* II, **56**, 554-577, doi: 10.1016/j.dsr2.2008.12.009.

Thomas, H., Bozec, Y., Elkalay, K., de Baar, H. J. W., 2004. Enhanced open ocean storage of CO_2 from shelf sea pumping. *Science*, **304**, 1005-1008.

Tsunogai, S., Watanabe, S., Nakamura., J., Ono, T., Sato T., 1997. A preliminary study of carbon system in the East China Sea. *J. Oceanogr.*, **53**, 9-17.

Tsunogai, S., Watanabe, S., Sato, T., 1999. Is there a "continental shelf pump" for the absorption of atmospheric CO_2? *Tellus*, **51B**, 701-712.

Uda, M., 1934. Oceanographic conditions in the Japan Sea and its adjacent waters (the result of simultaneous oceanographical investigations in the Japan Sea and its adjacent water in May and June, 1932). *J. Imperial Fish. Expedition Station*, **5**, 57-190 (in Japanese with English abstract).

Wang, S.-L., Chen, C.-T. A., 1996. Comparison of seawater carbonate parameters in the East China Sea and the Sea of Japan. *La mer*, **34**: 131-136.

Wang, S.-L., Chen, C. T. A., Hong, G.-H., Chung, C.-S., 2000. Carbon oxide and related parameters in the East China Sea. *Cont. Shelf Res.*, **20**, 525-544.

Wanninkhof, R., 1992. Relationship between wind speed and gas exchange over the ocean. *J. Geophy. Res.*, **97**, 7373-7382.

Wanninkhof, R., McGillis, W. R., 1999. A cubic relationship between air-sea CO_2 exchange and wind speed, *Geophys. Res. Lett.*, **26**, 1889-1892.

Wanninkhof, R., Thoning, K., 1993. Measurement of fugacity of CO_2 in surface water using continuous and discrete sampling methods. *Mar. Chem.*, **44**, 189–204.

Watai, T., Harada, K., Gotoh, K., Murayama, S., Nakazawa, T., 1999. Latitudinal distribution of CO_2 fugacity along 175^{o}E in the North Pacific in 1992-1996. *J. Oceanogr.*, **55**, 655-665.

Weiss, R., 1974. Carbon dioxide in water and seawater: the solubility of a non-ideal gas. *Mar. Chem*., **2**, 203-205.

Weiss, R., 1981. Determinations of carbon dioxide and methane by dual catalyst flame ionization chromatography and nitrous oxide by electron capture chromatography. *J. Chem. Sci.*, **19**, 61–616.

Wong, G. T. F., Chao, S.-Y., Li, Y.-H., Shiah, F.-K., 2000. The Kuroshio edge exchange processes (KEEP) study – an introduction to hypotheses and highlight. *Cont. Shelf Res.*, **20**, 335-347.

Yamada, K., Ishizaka, J., Nagata, H., 2005. Spatial and temporal variability of satellite primary production in the Japan Sea from 1998 to 2002. *J. Oceanogr*., **61**, 857-869.

Yang, Z., Wang, H., Saito, Y., Milliman, J. D., Xu, K., Qiao, S., Shi, G., 2006. Dam impacts on the Changjiang (Yangtze) River sediment discharge to the sea: The past 55 years and after the Three Gorges Dam. *Water Resour. Res.*, **42**, W04407, doi:10.1029/2006WR003970.

Yeh, S.-W., Kug, J.-S., Dewitte, B., Kwon, M.-H., Kirtman, B. P., Jin, F.-F., 2009. El Nino in a changing climate. *Nature*, **461**, 511-514.

Yoo, S., Park, J., 2009. Why is the southwest the most productive region of the East Sea/Sea of Japan? *J. Mar. Syst.,* **78**, 301-315.

Zhai, W., Dai, M., 2009. On the seasonal variation of sir-sea CO_2 fluxes in the outer Changjiang (Yangtze River) Estuary, East China Sea. *Mar. Chem.*, **117**, 2-10.

Zhai, W., Dai, M., Cai, W.-J., Wang, Y., Hong, H., 2005. The partial pressure of carbon dioxide and air-sea fluxes in the northern South China Sea in spring, summer and autumn. *Mar. Chem*., **96**, 87-97.

요약문

대륙주변해와 대양의 표층 이산화탄소분압 분포와 그 조절요인, 해양-대기 이산탄소 교환량을 파악하기 위해 동해 울릉분지와 동중국해 북부해역, 북서태평양의 표층 이산화탄소를 분석했다.

동해 울릉분지의 표층수온과 염분, 엽록소 a, 이산화탄소분압을 계절에 따라 4 회 관측했다. 봄철 표층 이산화탄소분압 범위는 260 에서 356 μatm 로 큰 변화를 보였으며, 대기중 이산화탄분압에 비해 낮았다. 여름철 표층 이산화탄소분압은 316 에서 409 μatm 으로 관측 중 가장 높았다. 관측해역 중앙부는 대기 이산화탄소분압에 비해 표층해양이 낮은 불포화상태를 보인 반면, 동해안과 울릉분지 동쪽끝단에서는 대기보다 높은 과포화상태는 보였다. 가을철에는 관측해역 전역이 대기 이산화탄소분압에 비해 현저히 낮은 불포화상태를 나타냈다. 겨울철에는 가을에 비해 표층수온은 크게 낮아졌지만 표층 이산화탄소분압은 303 에서 371 μatm 으로 가을철과 유사했다. 표층 이산화탄소분압의 계절변동은 표층수온과 염분의 변화만으로는 설명되지 않는다. 수층의 수직혼합과 해수의 흐름, 해양-대기 이산화탄소 교환 등이 표층 이산화탄소분압의 계절변동에 영향을 미친다. 동해 울릉분지는 봄, 가을, 겨울에는 대기 이산화탄소를 흡수하는 소모원으로 작용하는 반면, 여름에는 대기로 이산화탄소를 약하게 방출하는 공급원으로 작용한다. 동해 울릉분지의 연간 해양-대기 이산화탄소 교환량은 -2.49 ± 1.84 mol C m^{-2} yr^{-1} 로 동해 남부해역에 대한 이전

연구결과 (-2.2 mol C m^{-2} yr^{-1}) 와 잘 일치한다. 이는 동해 울릉분지가 대기 이산화탄소를 흡수하는 강력한 소모원으로 작용함을 의미한다.

동중국해 북부해역에서 2003 년부터 2009 년까지 수온과 염분, 엽록소 a, 질산염, 표층해양과 대기의 이산화탄소분압을 7 회 관측했다. 표층해양과 대기의 이산화탄소분압 차이는 봄철과 여름철에 큰 계절내 변동을 보였다. 봄철 관측해역의 해양-대기 이산화탄소분압 차이는 2008 년 4 월이 2004 년 5 월에 비해 약 절반 가량으로 작았으며, 이는 표층수온 차이로 인한 것으로 보였다. 여름철 관측해역의 해양-대기 이산화탄소분압 차이는 2003 년 8 월이 2006 년 7 월에 비해 약 두배 가량 컸다. 해양-대기 이산화탄소분압 차이는 가을철에만 양의 값을 보였으며, 나머지 계절에는 모두 음의 값을 보였다. 가을철 이산화탄소분압 차이가 양의 값을 보인 것은 상대적으로 표층수온이 높고, 수층 수직혼합에 의해 이산화탄소 농도가 높은 저층수가 유입되었기 때문인 것으로 보였다. 동중국해 북부해역의 연간 해양-대기 이산화탄소 교환량은 -2.2 ± 2.1 mol C m^{-2} yr^{-1} 으로 해양이 대기의 이산화탄소를 흡수하는 것으로 나타났다. 동중국해 북부해역의 이산화탄소 흡수량은 전세계 대륙붕 해역 흡수량 추정치의 약 두배로, 동중국해 북부해역이 다른 대륙붕 해역에 비해 더 강한 대기 이산화탄소 소모원으로 작용함을 나타낸다.

북서태평양에서 2006 년부터 2010 년까지 수온과 염분, 표층 이산화탄소분압을 다섯차례 관측했다. 표층수온의 시간변동은 Oceanic Nino Index (ONI) 변화와 매우 잘 일치했다. 그러나 표층 이산화탄소분압의 시간변동은 ONI 변화가 일차요인은 아니었다. 관측자료의 절반 이상의

자료에서 표층 이산화탄소분압 변동의 65~80%는 표층수온과 염분에 의한 열역학적 변화로 설명할 수 있다. 생물활동은 2010 년 5 월 표층 이산화탄소분압을 낮추는데 기여했을 수 있지만, 2006 년 9 월과 2009 년 6 월에는 그럴 가능성이 매우 희박하다. 표면혼합층의 깊이는 ONI 와 반비례하여 깊어졌지만, 표면혼합층이 깊어진 La Nina 시기에 표층 이산화탄소분압은 증가하지 않았다. 0.5 mmol C m^{-2} day^{-1} 이상의 해양-대기 이산화탄소 교환량은 표층 이산화탄소분압의 변동을 줄이는데 기여했다. 관측해역의 남부에 위치한 북적도해류 (North Equatorial Current, NEC) 해역은 5 월에서 9 월까지 대기로 이산화탄소를 방출하는 공급원으로 작용했으며, 10 월에는 이산화탄소 흡수원으로 작용했다. 관측해역의 북부에 위치한 아열대순환해역은 6 월에서 9 월까지 이산화탄소 공급원으로 작용했으며, 5 월과 10 월에는 이산화탄소 흡수원으로 작용했다

동해 울릉분지와 동중국해 북부해역의 연간 이산화탄소 흡수량은 각각 3.17 x 10^{-3} Pg C yr^{-1}와 2.96 x 10^{-3} Pg C yr^{-1} 이다. 이는 연간 전지구 해양의 탄소흡수량의 0.22%와 0.21%에 해당하는 양으로, 전지구 해양에 대한 각각의 면적비율 0.033%와 0.034%에 비해 월등히 크다. 북서태평양의 연간 이산화탄소 흡수량은 8.03 x 10^{-2} Pg C yr^{-1}으로 전지구 해양 탄소흡수량의 5.6%로 면적비율 8.1%에 비해 작다 (Takahashi *et al.*, 2009). 동해 울릉분지와 동중국해 북부해역, 두 한반도 주변해는 북서태평양과 같은 대양에 비해 약 7배 가량 대기의 이산화탄소 흡수율이 높은 강력한 이산화탄소 소모원이다.

주요어: 표층 이산화탄소분압, 해양-대기 이산화탄소 교환량, 계절변동,
대륙주변해, 동해, 동중국해, 북서태평양

학 번: 95312-806

감사의 글

아직도 부끄럼움이 남는 논문이지만, 아주 오랜 시간 끝에 마무리하며 제게 도움을 주신 여러분들께 감사의 마음을 전하고 싶습니다. 지나온 오랜 시간만큼이나 도움을 주신 고마운 분들이 너무나도 많아 혹여 잠깐 놓치고 지나는 실수를 범할까 조심스럽습니다.

대학교 수업시간 학자의 모습을 보여주셔서 무지한 제가 화학 해양학에 관심을 갖게 해주시고, 우둔한 제자를 오랜동안 인내해 주신 지도교수 김경렬 교수님께 감사드립니다. 바쁘신 중에도 흔쾌히 논문심사를 해주시고 좋은 방향을 제시해 주신 허영숙 교수님과 이동섭 교수님, 강동진 박사님, 김동선 박사님께 감사드립니다.

대학을 입학한 이후 지금까지, 내 인생의 어느 순간을 함께하며 도움을 준 내 소중한 동기들과 선후배님들 모두에게 감사의 마음을 전합니다. 이제는 한국해양과학기술원으로 이름이 바뀐 연구원의 모든 분들께도 감사드립니다.

항상 믿음으로 지켜봐 주시고, 헌신적인 지원을 아끼지 않으시는 제 양가 부모님들과 가족 모두에게 고마움을 전합니다.

그리고, 내 영원한 친구이자 연인인 민홍식님께 감사의 마음과 사랑을 전합니다.

마지막으로 세상에 딱 셋뿐인 나의 보물들 형준이, 서연이, 형진이에게 사랑의 마음을 전합니다.